UNIVERSITY OF CANTERBURY

DOCTORAL THESIS

Cosmic Microwave Background Anisotropies in an Inhomogeneous Universe

Author:
Mohammad AHSAN Nazer

Supervisor:
Prof. David L. WILTSHIRE

Submitted in partial fulfilment of the requirements for the degree of Doctor of Philosophy, Department of Physics and Astronomy, University of Canterbury

February 2015

Declaration

I, Mohammad Ahsan Nazer, hereby certify that any content in this dissertation, 'Cosmic Microwave Background Anisotropies in an Inhomogeneous Universe' which is not my own work has been properly acknowledged. The contents of the research papers presented here have not been part of any previous dissertation by any other thesis student. The work presented in this dissertation is based on the following research articles to which I have made substantial contributions

- James A.G. Duley, M. Ahsan Nazer, David L. Wiltshire (2013). Timescape cosmology with radiation fluid. *Class. Quant. Grav.*, 30:175006. arXiv:1306.3208
- M. Ahsan Nazer, David L. Wiltshire (2015). Cosmic microwave background anisotropies in the timescape cosmology. *Phys. Rev. D.*, 91. in press. arXiv:1410.3470.

Abstract

Cosmic Microwave Background Anisotropies in an Inhomogeneous Universe

by Ahsan

The timescape cosmology represents a potentially viable alternative to the standard homogeneous and isotropic Friedmann–Lemaître–Robertson–Walker (FLRW) cosmology, without the need for dark energy. This thesis first extends the previous work on the timescape cosmology to include a radiation component in the evolution equations for the timescape cosmology and tests of the timescape model are then performed against the Cosmic Microwave Background (CMB) temperature anisotropies from the Planck satellite.

Although average cosmic evolution in the timescape scenario only differs substantially from that of FLRW cosmologies at relatively late epochs when the contribution from the energy density of radiation is negligible, a full solution of the Buchert equations to incorporate radiation is necessary to smoothly match parameters to the epoch of photon decoupling and to obtain constraints from CMB data. Here we have extended the matter-dominated solution found in earlier work to include radiation, providing series solutions at early times and an efficient numerical integration strategy for generating the complete solution.

To analyse the spectrum of CMB anisotropies in the timescape cosmology we exploit the fact that the timescape cosmology is extremely close to the standard cosmology at early epochs and adapt existing numerical codes to produce CMB anisotropy spectra. To find a FLRW model that matches as closely as possible the timescape expansion history, we have studied and compared a number of matching methods. We perform Markov Chain Monte Carlo analyses on the timescape model parameter space, and fit CMB multipoles $50 \leq l \leq 2500$ to the Planck satellite data. Parameter fits include a dressed Hubble constant, $H_0 = 61.0\,\mathrm{km\,s^{-1}\,Mpc^{-1}}$ ($\pm 1.3\%$ stat) ($\pm 8\%$ sys), and a present void volume fraction $f_{\mathrm{v}0} = 0.627$ ($\pm 2.3\%$ stat) ($\pm 13\%$ sys). In the timescape model this value of $f_{\mathrm{v}0}$ means that the galaxy/wall observer infers an accelerating universe, where the apparent acceleration is due to gravitational energy gradients and clock rate differences rather than some dark energy. We find best fit likelihoods which are comparable to that of the best fit ΛCDM cosmology in the same multipole range.

Acknowledgements

Here in New Zealand, I am grateful and indebted to my parents for their love and support, to my sister Hameeda for her friendship and to my six year old nephew Matin for our fights over the TV remote. Nearby in Sydney, Australia, I thank my brothers Hamid and Yasir. Back home in Kabul, I am grateful to my brother Asad for his vision. My sister Shukuria and the rest of the family in Kabul, my sister Shayma, my cousin Marzia Khanum and the rest of the family currently in Quetta, I thank you all, younger or older than myself, for your love and support.

No graduate student can succeed without the wisdom and support of an able supervisor. I am thankful to Professor David Wiltshire for his guidance over the years during the course of my studentship. I also thank Teppo Mattsson for discussions.

My friends Niaz and Raza (in alphabetical order) I am **** for the many conversations in the recent years and your friendships when we were all young but not much better looking. I am happy to have befriended Cheng-Yang Lee ever since I started my graduate studies and I thank him for reading the drafts of this thesis. I thank James McKay for thanking me in his thesis.

I acknowledge the financial support from Mardsen Fund Royal Society of New Zealand and the Department of Physics and Astronomy at the University of Canterbury.

I thank Pedro Ferreira for the hospitality on my six-week visit to Oxford University and Chris Gordon for supervising me during that period. I thank Henry Tillson and Thibaut Louis with whom I shared an office during my visit. I thank the organizers of the 2012 Cape Town cosmology summer school and in particular Alan Heavens.

I also thank all those whom I have contacted on technical matters over the years, including Julien Lesgourgues who is one of the authors of CLASS code and Benjamin Audren the author of Monte Python code. I have also made use of a number of other software packages; I am thankful to all those people who have made their works available for use to the wider scientific community.

For what it's worth, I dedicate this work to the people of Afghanistan.

Contents

List of Figures

List of Tables

Preface

I first layout the motivation for the work carried out in this thesis. The introduction contains a brief review of Modern cosmology from a perspective that relates it to the topic of inhomogeneity. Later in Chapters 2.4 and 3 I present the specific research carried out to understand the issues and answer the questions raised in the introduction. The single sentence that succinctly encapsulates the very crux of the problem at large that I have endeavoured to answer at some level would be "Is the universe homogeneous and isotropic?". In what follows all the investigations performed are ultimately to answer this question directly or indirectly.

Inhomogeneous cosmology is an active and wide field of research. There are many topics and problems in inhomogeneous cosmology that could be researched and likewise there are many choices for tools that could be used for carrying out the research into those problems. Here for the most part I use timescape cosmology proposed by Wiltshire [Wiltshire, 2007a]. In the timescape cosmology it is proposed that the present fraction of volume in voids can be used as a parameter to extract important cosmological information such as the age, matter and curvature energy content of the universe.

To test various timescape model predictions against observational data I first present the work carried out in [Duley et al., 2013] which extended the timescape cosmology to include radiation content. The work presented in Sec. 2.4 explains how to efficiently solve the timescape equations when provided with a set of model parameters. In Sec. 2.4.3 the recombination history in the timescape cosmology is studied. The procedure in this chapter could be used to study recombination in any inhomogeneous model.

In Chapter 3 the practical framework developed in Chapters 2 and 2.4.3 is put to use to test the timescape cosmology against data from the cosmic microwave background (CMB). The work in this chapter involved a large body of numerical code for solving the timescape equations and performing Bayesian analysis. These codes where mainly written in Fortran and Python but also use Cython as an interface to the CMB Boltzmann code [Lesgourgues, 2011] written in C. Unfortunately the Fortran code makes heavy use of the commercial Fortran library IMSL and cannot be publicly released.

In Chapter 4 we conclude with a discussion and presentation of the main results from this thesis.

Chapter 1

Introduction

1.1 Brief history of modern cosmology

Modern cosmology began almost 100 years ago when Einstein first applied general relativity to the universe as a whole [Einstein, 1917]. Since its birth modern cosmology has proceeded by a combination of model building based on simplifying assumptions, and by fitting observations to these models. It is unique among the sciences in that the scales of distance and time to which it applies are so vast that the raw data—angles, photon fluxes, wavelengths of light, number counts of galaxies—can often only be reduced to measures of distance, area and volume using model assumptions.

One of the most pervading assumptions has been the Copernican Principle—the very reasonable philosophical idea that we as observers should not occupy a privileged position in the universe. In the standard cosmology this has been translated into the Cosmological Principle; namely that the geometry of the universe is spatially homogeneous (independent of position) and spatially isotropic (independent of direction). Given that structure exists in the universe then the universe is not exactly homogeneous. The standard cosmology assumes nonetheless that the Cosmological Principle applies on sufficiently large scales.

Mathematically, the assumptions of exact spatial isotropy and homogeneity lead to a unique class of geometries, the Friedmann–Lemaître–Robertson–Walker (FLRW) cosmologies. The standard model of cosmology is based on a spatially flat FLRW geometry with a cosmological constant Λ and Cold Dark Matter (CDM) commonly referred to as the ΛCDM model.

If one entirely subscribes to the ΛCDM paradigm of cosmology then the universe is very close to spatially flat containing smooth pressureless dust, and a smooth dark energy

from a cosmological constant. One prominent consequence of the ΛCDM model is that the universe began a period of accelerated expansion in recent cosmological aeons and will continue to expand forever. Notwithstanding some unexplained problems deemed to be *anomalies*[1] that continue to persist, the ΛCDM model has also been very successful in explaining observations such as the tiny fluctuations seen in the cosmic microwave background (CMB) temperature [Ade et al., 2014a], the dimming of supernovae explosions [Perlmutter et al., 1999] and features of large scale structure of the universe [Eisenstein et al., 2005; Cole et al., 2005] among others. However, the successes of ΛCDM cosmology do not negate the validity of alternative theories and models that may also explain these data, and its failures do arouse the search for yet even better explanations.

Given the successes of the ΛCDM cosmology should we even consider alternatives to the ΛCDM model? Here I draw on a historical narrative to make the point that if history is anything to go by then it is more likely that our present theories of the universe will change than not. Some theories will evolve as they are continually adjusted to fit new observational data, others will be discarded. To say that we have already stumbled on to the ultimate cosmological theory is hard to fathom and would be at the very least quite pretentious.

The cosmologists' modus operandi in explaining and exploring the universe is to adopt a theoretical model and use it until it fails to fit new data. As new experiments are conducted and more data becomes available the model has to fit the new and old data simultaneously. If models fail, they essentially fail a self-consistency check, i.e., not fitting all data from diverse observations related to diverse physical phenomena. The same set of model parameters must fit all data sets. In this respect the status of a theoretical model always remains a conjecture, from the time when it is first proposed to when it is finally refuted. Subsequent tests of the model reaffirm or repudiate its validity but because the need to explain new phenomena is seemingly endless a theoretical model is forever a conjecture.

There are at least two problems that have in fact, emerged from cosmological studies with the FLRW cosmology as the model assumed for the universe. First, the value for cosmological constant from FLRW cosmology is many orders of magnitude smaller than simple estimates from theoretical particle physics. Second, the present cosmological constant energy density is about three times the energy density in matter in the FLRW model. Since for most of the expansion history of the universe these values are not comparable in magnitude to each other, we find ourselves living at a time when they are, leading to the so called *coincidence problem* [Zlatev et al., 1999].

[1] The statistical significance of unexpected correlations in large angle CMB multipoles is much debated on account of the effects of cosmic variance, see e.g., [Copi et al., 2010; Nadathur et al., 2012; Rassat et al., 2014; Ade et al., 2014c].

The cosmological constant is firmly entrenched in the standard model of cosmology, yet its status remains controversial. Its dynamical—or more accurately non-dynamical—nature is simple, it does not evolve with time but an understanding of its physical nature remains elusive. The existence of such a term which does not couple directly to the matter degrees of freedom presents a profound challenge to theories of gravity which seek a conceptual unification of the forces of nature. General relativity is based on the notion that spacetime is a relational structure between material objects. Yet the cosmological constant is separate from this relational structure. Some attempts to better understand the cosmological constant have involved consideration of scalar fields which possibly couple to matter, with a dynamically evolving vacuum expectation value as we will discuss later.

In fact, the cosmological constant and the controversy surrounding it predates the construction of the FLRW model. Two years after Albert Einstein put forward the general theory of relativity in 1915, he applied it to model the universe. His Einstein static universe [Einstein, 1917] required the cosmological constant energy density to be exactly half of the energy density in matter and to be spatially closed with a finely tuned positive scalar curvature. The controversy stemmed from the fact that the value of the cosmological constant had to be fine tuned relative to the matter density and that the equations describing the static Einstein universe were unstable[2]. A slight increase in matter content would mean the universe collapses under the gravitational force while a slight decrease would see the repulsive forces win, leading to an ever expanding universe. The cosmological constant as it was introduced in its primary form and purpose was no longer deemed necessary after the discovery[3] of the Hubble law [Lemaître, 1927; Hubble, 1929] pointed to an expanding universe. Hubble found that the recession velocity of distant nebulae increased proportional to their distance.

Although expanding universe solutions of the Einstein's equations had been found as early as 1922 by Friedmann [1922] they were not considered relevant to the real universe, thought to be static at the time. Friedmann considered the case of positive spatial curvature, with arbitrary values of the matter and cosmological constant energy densities and then extended this to the case of negative spatial curvature [Friedmann, 1924]. Lemaître [1927] derived these solutions independently and also extended them to include a radiation energy density. Lemaître was the first to take the expansion of the universe as a physical reality that could be tested. He wrote down Hubble's law for the first time, and derived a value of the Hubble constant using existing observational data. He was also the first to suggest an explosive beginning to the universe—the big bang —in

[2]Here I am taking advantage of hindsight and referring to the Einstein's static universe model as the limit of Friedmann's equatons with both the first and second time derivatives of the scale factor set to zero.

[3]For a thorough account of the historical events prior to Hubble's works see [Luminet, 2013]

his "primeval atom" theory [Lemaître, 1927]. Lemaître's work was virtually unkown until Arthur Eddington and Willem de Sitter drew attention to it in 1930 following Hubble's independent discovery. Subsequently Howard Robertson[4] [Robertson, 1935, 1936] and Arthur Walker [Walker, 1936] derived the Friedmann equations on the basis of homogeneity and isotropy alone. Today homogeneous and isotropic expanding universe models are widely referred to as FLRW[5] models.

By 1933 Lemaître [Lemaître, 1933] and 1934 Tolman [Tolman, 1934a] had extended the expanding universe models and incorporated inhomogeneity in the metric for the universe. What is now most often known as the Lemaître-Tolman-Bondi[6] solutions of the Einstein's equations contains pressureless matter known as dust with radial inhomogeneity distributed so as to preserve spherical symmetry around some origin. The dust FLRW and Einstein static universes are realized as particular cases of the LTB model.

It is interesting to note that the now almost ubiquitous assumption that the universe is homogeneous and isotropic was not generally accepted in the first decades of the advent of modern cosmology. In [Tolman, 1934b, pp. 363] Tolman regards the FLRW model as a working hypothesis. See also the discussion by Jim Peebles in [Peebles, 2012]. Both Tolman and Bondi [see Bondi, 1952, 1960, Chap. XIV] envisaged that more powerful telescopes would reveal an inhomogeneous universe, even though the FLRW model appealed to Bondi for philosophical reasons [see Bondi, 1952, 1960, Chap. VIII] because it embodies the cosmological principle.

In fact, Bondi together with Gold and Hoyle went on to formulate a "Perfect Cosmological Principle" in which observers should not occupy a privileged position in time. This was the basis of the Steady State model [Bondi and Gold, 1948; Hoyle, 1948] in which time extends infinitely to the past and future, and although the universe expands matter is continuously created so that on average the universe always looks the same establishing a *dynamic equilibrium*. The discovery of the CMB[7]—which had no natural explanation in the Steady State model and which had been anticipated 20 years earlier in the hot big bang model by Gamov and collaborators [Alpher et al., 1948]—was the final nail in the coffin for the Steady State cosmology.

[4] In his semi-popular book "The expanding Universe" first published in 1933 Eddington credits Roberston for independently discovering the expanding solutions for the third time. See page 47 in [Eddington, 1933].

[5] I here point out a fun fact that coincidently the increasing alphabetical order in which the acronym for the standard model is spelled, i.e., FLRW is in harmony with the temporal order in which each person worked on the expanding universe problem. Had Walker worked on the problem before the others we would have had to live with the acronym WFLR.

[6] The acronym LTB is used because of important work done later on by Bondi [1947] which also uses the metric in its modern day form.

[7] Lemaître, who originally formulated what is now called the big bang theory, died in 1966 a year after the discovery of the CMB in 1965. He would have been aware of [Dicke et al., 1965] which confirmed the big bang origin of the universe.

Observations have often been pivotal in overturning philosophical principles that appear elegant to one generation of physicists in describing the ultimate nature of space and time. To some extent the earlier intuition of Lemaître, Tolman and Bondi concerning inhomogeneity has been proved right by recent large scale structure surveys. The question before us is whether observations will ultimately overturn the Cosmological Principle also.

Although the cosmological constant had been included in the dynamical universe models investigated in the 1920s [Friedmann, 1922; Lemaître, 1927], once the evidence for the expanding universe [Hubble, 1929] began to be accepted, Einstein no longer saw a need to include this term, whose physical nature he had never found completely satisfactory. In 1932 Einstein and de Sitter published a paper [Einstein and de Sitter, 1932] in which they advocated a spatially flat cosmology, with pressureless dust as the only source of energy density, and no cosmological term. This came to be called the Einstein-de-Sitter model.

In the intervening years observational interest in the cosmological constant has waxed and waned. Astronomers, cosmologists and theorists alike have turned to it when ever the need arose to explain new observations with old tools. For example, in 1967 measurements of the then recently discovered quasar population appeared to favour models [Petrosian et al., 1967; Shklovskii, 1967; Kardashev, 1967; Zel'dovich, 1968] in which the universe underwent a "costing phase" during which the comic scale factor increased relatively slowly. This is possible with a cosmological constant but not in general. Astrophysical evidence for such a phase soon disappeared, however, as did interest in a cosmological constant.

Observational arguments about the cosmological constant went back and forth over the next few decades. By the early 1990s galaxy surveys favoured a matter density $\Omega_{\rm M} \approx 0.15$–$0.3$ [Estathiou et al., 1990], which meant either that the Universe was open with hyperbolic spatial sections or—as inflationary theorists preferred—some other smooth energy density was present to make $\Omega_{\rm tot} = 1$. Some actively considered the Λ–term [Fukugita et al., 1990; Hoell and Priester, 1991; Kochanek, 1995], while the majority of observers still took an $\Omega_{\rm M} = 1$ cosmology dominated by CDM as the standard. This was the case, for example, in fitting the CMB data [Smoot et al., 1992]. The 1998 discovery that supernovae were fainter [Riess et al., 1998; Perlmutter et al., 1999] than expected in FLRW models with homogeneous matter was the key observation that convinced the community to take the cosmological constant as physical reality. This way one could have $\Omega_{\rm M0} < 1$ in agreement with other observations, while having $\Omega_{\rm tot} = \Omega_{\rm M0} + \Omega_{\Lambda 0} = 1$.

In the last 25 years the pace of progress in observational cosmology has increased dramatically. The number of observations and their precision has exploded on a number of independent fronts.

- *Cosmic microwave background:* From the COBE satellite's [Mather et al., 1994] confirmation to high precison of the black body nature of the CMB and its measurements of the low multipole moments temperature anisotropy, WMAP's detection of the CMB acoustic peaks [Hinshaw et al., 2003] to Planck's high resolution CMB maps [Ade et al., 2014a,b] that probe angular scales down to 5 arcmin all experiments are consistent with a near to homogeneous and isotropic (one parts in a hundred thousand) early universe.

- *Supernovae:* Since the early work 15 years ago, there have been many major surveys [Riess et al., 2007; Wood-Vasey et al., 2007; Amanullah et al., 2010; Lampeitl et al., 2010]. These can be used to study the expansion history of the universe reliably to redshifts $z \leq 1.5$. Currently there are important systematic uncertainties in reducing the light curves, which can hopefully be resolved before future missions such as the Euclid survey [Amendola et al., 2013].

- *Gamma Ray Bursts (GRBs):* These have been used as standard candles in the redshift range $2 \leq z \leq 6$ [Gehrels et al., 2004]. These presently have very large systematic uncertainties, which makes their use as standard candles much more problematic. However, since they are observed in a range where Type Ia supernovae are not predominant, they could conceivably be an important cosmological tool in future.

- *Large Scale Structure:* Over the last 15 years galaxy surveys have probed deeper redshift depths with wider sky coverage and larger number of galaxies. Some prominent surveys have included [Cole et al., 2005; Skrutskie et al., 2006; Beutler et al., 2001; Scrimgeour et al., 2012; Anderson et al., 2013]. One very important measurement has been the detection of the baryon acoustic oscillation (BAO) scale [Eisenstein et al., 2005], namely a small excess of galaxies in the 2-point correlation function at a comoving distance scale which corresponds to the proper distance associated with the first acoustic peak in the CMB. More technically, it represents the scale of the sound horizon at the baryon drag epoch as will be discussed in Chap. 2.4.3 and 3.

  Measurement of the BAO scale now constitutes an important cosmological test in its own right [Beutler et al., 2001]. The BAO scale has also recently been detected in the Lyman-α absorption gas clouds of light from very distant quasars [Delubac et al., 2015]. This is an important technique at redshifts $z > 1.5$ which are too distant for current galaxy surveys.

These observational feats are permanent and future observations will build on and supplement the findings from past and present experiments.

On the theoretical frontier this progress has been matched with work on the FLRW cosmology. We are now aiming to constrain the Hubble constant in the FLRW model to better than a percent. If however future experiments turn out not to be fully compatible with a homogeneous and isotropic model than the theoretical progress can be undone. Thus this rapid progress tends to obscure the fact the the questions we ask and explore are not too different from those both asked and explored by the founders of modern cosmology. So long as general relativity is our theoretical medium of choice in one way or another we will be asking exactly the same question that Tolman [1929] and others asked nearly a century ago, i.e., "What is the line element of the universe?"

The discovery [Riess et al., 1998; Perlmutter et al., 1999] that distances to supernovae were larger than for the standard CDM model of the time sparked the search for the source of accelerated expansion. The answer in the context of ΛCDM model was the cosmological constant. However, theoretical models do not dictate the nature of physical reality they just help uncover it and frame the questions that we ask about it. A model may hypothesize phenomena that may or may not exist in reality. A variety of approaches have been adopted to explain the accelerated expansion. Here I briefly discuss some of them.

1.2 Explanations for cosmic acceleration

Here are some of the ways to tackle the problems that can not be solved with the standard model of cosmology:

1. Change the matter fields content by adding terms (scalar fields etc.) to the right hand side of Einstein's equations.

2. Modify the Einstein-Hilbert action of general relativity, thereby changing the l.h.s of Einstein's equations.

3. To seek solutions within the general relativistic framework and demand a stricter application of relativistic principles coupled with an abandonment of assumptions thought to be behind the problems in standard model (e.g., assuming homogeneity and isotropy leads to the introduction of the cosmological constant). This can involve the averaging of Einstein's equations to obtain a framework for an average homogeneous cosmic evolution. It therefore involves making changes to both sides

of the Einstein's equations. Broadly speaking Wiltshire's timescape cosmology falls in this category.

In the subsequent sections I review some of the approaches that are adopted to explain the cosmic acceleration in extensions of the FLRW model, modifications to general relativity and the inhomogeneous cosmology studies, particularly the timescape cosmology.

1.2.1 Dark energy and cosmic acceleration in homogeneous and isotropic models

1.2.1.1 Quintessence

Quintessence models are one among the many classes of dynamical dark energy models. In the simplest types of quintessence models the dark energy density and pressure are expressed in terms of a time dependent scalar field $\phi(t)$ [Rata and Peebles, 1988; Carroll, 1998; Zlatev et al., 1999] and its potential $V(\phi)$. On an FLRW background the scalar field density ρ_ϕ and pressure p_ϕ replace the cosmological constant density and pressure in the Friedmann equations (2.2), (2.3) and (2.4). Care has to be taken in choosing the scalar field potential so that certain conditions are met. For example, the scalar field should evolve in such a way that its density dominates at late times only with radiation density remaining dominant at early times. Generally the scalar field equation of state w_ϕ (pressure / density) has to satisfy

$$-1 \leq w_\phi < -\frac{1}{3}\,. \tag{1.1}$$

The upper bound[8] is a necessary condition for acceleration and the lower bound corresponds to the Dominant Energy Condition, which is that the speed of sound should not exceed the speed of light. Phantom energy scenarios which violate the condition Eq. (1.1) also have an acceleration which ultimately leads to infinite expansion in finite time [Caldwell et al., 2003]. Accelerated expansion becomes possibles once the potential term $V(\phi)$ of the scalar field dominates its kinetic (proportional to $\dot{\phi}$) term. The specific form for the scalar field potential and its equation of state determine the nature of accelerated expansion.

If the scalar field has scale dependence then the perturbed Einstein equations on an FLRW background couple the scalar field perturbations to perturbations in the matter and radiation via the metric gravitational potentials (2.11). In other generalizations of

[8] Fields with $w_\phi \geq -1/3$ satisfy the Strong Energy Condition (SEC) and focus light rays, which is why cosmic acceleration requires that the SEC is violated.

the quintessence models dark energy can also couple to one, some, or all other components of the energy momentum tensor via non gravitational interactions. Couplings between dark energy and matter (baryonic and nonbaryonic) can than directly impact structure formation in addition to any indirect influence through the expansion rate. These generalizations thus extend the role of the quintessence type models beyond just explaining the late time accelerated expansion [Copeland et al., 2006].

1.2.2 Modified gravity

One example of a modification to general relativity itself is provided by the $f(R)$ theories of gravity [Sotiriou and Faraoni, 2010]. The basic rationale in $f(R)$ theories is that gravity on cosmological scales may not be Einsteinian gravity. The field equations are derived by varying a modified Einstein-Hilbert action

$$S_{\rm EH} = \frac{c^4}{16\pi G}\int R\sqrt{\det(g_{\mu\nu})}\mathrm{d}^4x \quad \longrightarrow \quad S = \frac{c^4}{16\pi G}\int f(R)\sqrt{\det(g_{\mu\nu})}\mathrm{d}^4x\,, \tag{1.2}$$

where $f(R)$ is some generic function of the Ricci scalar R. To pin down an exact form for $f(R)$ certain criteria are imposed:

- Since general relativity is well tested on small scales $f(R)$ must reduce to Einstein gravity on relevant scales. This requirement then imposes conditions on the derivatives of $f(R)$ w.r.t R (f', f'', f''').
- The chronological order in which the acceleration source dominates the energy density in the universe must follow radiation and matter domination. This allows big bang nucleosynthesis during radiation domination and structure formation during matter domination to proceed as in the standard model. Even then $f(R)$ theories can be identified from the distinctive imprint they leave on CMB anisotropies.

On a flat FLRW background the generalized forms for the Friedmann equations (2.2) and (2.3) are given by

$$\left(\frac{\dot{a}}{a}\right)^2 = \frac{8\pi G}{3c^4}\frac{1}{f'}\left[\rho + \frac{Rf' - f}{2} - 3H\dot{R}f''\right] \tag{1.3}$$

$$2\frac{\ddot{a}}{a} + H^2 = -\frac{8\pi G}{3c^4}\frac{1}{f'}\left[p + (\dot{R})^2 f''' + 2H\dot{R}f'' + \ddot{R}f'' + \frac{1}{2}\left(f - Rf'\right)\right]\,. \tag{1.4}$$

More complicated forms for $f(R)$ in which contractions of the Ricci tensor $R_{\mu\nu}$ appear in $f(R^{\mu\nu}R_{\mu\nu})$ can also be constructed. The $f(R)$ theories have a number of problems including those that stem from higher derivatives of the metric (i.e. more than second order) apearing in the field equations. Nevertheless $f(R)$ theories are an alternative

approach to possibly solving the dark energy problem that is in stark contrast to the timescape approach. For further details see review of Clifton et al. [2012].

1.2.3 Brane cosmology

Relativity is based on a 4-dimensional manifold with Riemannian geometry. But Riemannian geometry is not just restricted to 4 dimensions so it is not entirely surprising that theorists seeking to unify gravity and Quantum theory make use[9] of 10 and even 11 dimensional spacetimes. This leads to modifications of general relativity in four dimensions that arise from considering the 4-dimensional universe to exist in a more fundamental higher-dimensional theory. One can either take the extra dimensions to be small and compact, giving rise to Kaluza-Klein cosmologies (see [Wiltshire, 1987] and references therein), or alternatively on can consider the four-dimensional universe to be a surface or "brane" living in a higher dimensional reality. See Brax et al. [2004] for a review.

As a simple example of the latter consider the 5-dimensional spacetime of Binetruy et al. [2000],

$$\mathrm{d}s^2 = g_{\mu\nu}\mathrm{d}x^\mu \mathrm{d}x^\nu + b^2 \mathrm{d}y^2 \,. \tag{1.5}$$

This example is pertinent to the discussion here because the authors manage to obtain an exact generalized Friedmann type solution of the 5-dimensional Einstein equations with an *effective*[10] cosmological constant. In (1.5) $g_{\mu\nu}$ is the metric of a 4-dimensional hypersurface called the brane that we live on and $b^2\mathrm{d}y^2$ characterizes the fifth dimension. In the exact solution obtained by Binetruy et al. the scale factor confined to the $y = 0$ hypersurface has a squared density term, ρ_b^2, from the brane[11] unlike Eq. (2.2) in which the energy density appears as a linear term. This brane cosmology model at late times has an accelerating phase sourced by the effective cosmological constant. This example shows that if our 4-dimensional universe is in fact part of a higher dimensional space time then the late time acceleration may possibly be explained as an inevitable consequence of such an embedding.

[9] It is beyond the scope of this thesis to give details for the reasons why specifically 10 and 11 dimensional space times are used.

[10] The identification of the cosmological constant is imposed and does not arise naturally.

[11] ρ_b is part of the 4-dimensional energy momentum tensor.

1.3 Inhomogeneous models, backreaction and cosmic acceleration

An approach which is more conservative—in the sense that it requires no modifications to the action of general relativity and no exotic fields—is to explain cosmic acceleration as an apparent effect in inhomogeneous models. In the standard model, the universe is assumed to have the same FLRW geometry on all scales larger than bound structures. In particular, increase of volume of a swarm of test particles is isotropic on all scales and preserves the same spatial curvature everywhere. Any deviations from this uniform expansion are treated by local boosts, or peculiar velocities of galaxies in the terminology of astronomers. In general inhomogeneous cosmologies, however, space may expand differentially with spatial curvature varying from region to region. This will give rise to differences in the distance–redshift relations. How infinitesimal distances add up to set distances on cosmological scales is dependent on the choice of metric on different scales. The line element is to general relativity what the cosmic distance ladder is to astronomy. An incorrect distance measure from an inappropriate line element may be the reason for the inference of accelerated expansion.

1.3.1 Non-Copernican exact solutions

Inhomogeneous cosmologies such as the dust LTB models admit exact analytical solutions to Einstein's equations. The LTB models permit the study of a nonlinear matter density evolution and light propagation in a non perturbative setting. However, the matter inhomogeneity in LTB models must preserve spherical symmetry about some origin. In these models one relinquishes the Copernican Principle and the condition that we as observers should not occupy a privileged position in the universe can no longer be met.

The reason LTB models have garnered considerable attention is because these models can fit the supernovae data and explain cosmic acceleration without a cosmological constant [Enqvist and Mattsson, 2007]. This was shown by Célérier [2000] and Tomita [2000] soon[12] after the discovery of the accelerated expansion in the context of FLRW

[12]The spherically symmetric Stephani model with inhomogeneous pressure was shown by Dabrowski and Hendry [1998] to fit the supernovae data from [Perlmutter et al., 1997]. Although the Dabrowski and Hendry [1998] study was not in the context of accelerated expansion, it showed Stephani models could fit the supernovae data and allow the age for the universe to be as high as 15 Gyr which was problematic for FLRW models at the time. No observational evidence exists to warrant models in which late time expansion of the universe is dominated by pressure gradients from some exotic fluid.

cosmologies. Typically in many LTB models the matter inhomogeneity is a void of size $\sim$ 1Gpc and the observer is confined to a location[13] close to the centre of the void.

The underlying reason LTB models can be used to explain cosmic acceleration is that supernovae and BAO data constrain the luminosity distance–redshift relation. In LTB models the luminosity–redshift relation is different from that in FLRW cosmologies. Therefore the deceleration parameter obtained from fits of LTB models to supernovae data can be made negative with parameter choices that include a zero cosmological constant term. The LTB model has two free functions, giving the freedom to fit many luminosity distance–redshift relations. One density profile that very closely matches the standard ΛCDM luminosity–distance relation in fact has an overdense hump near the origin, rather than a void [Célérier et al., 2010].

Szekeres [1975a] found exact solutions which are generalizations of the LTB models, in which the metric is no longer invariant under rotations. The matter inhomogeneity in the quasispherical Szekeres solutions [Szekeres, 1975b] forms nonconcentric shells around the origin. These are a subclass of Szekeres solutions with certain free functions fixed as constants. These models can also fit the supernovae data and explain acceleration without a dark energy [Bolejko and Célérier, 2010] but have been used in relatively fewer studies owing to their complexity.

1.3.2 The fitting problem, averaging and backreaction

In studying the actual inhomogeneous universe cosmologists use some idealized model such as the FLRW cosmology. It is understood that the idealized model is a good representation of the real universe only on large enough scales which in this study we take to be the homogeneity scale $\simeq 100\,h^{-1}\,$Mpc. The challenge then is to identify and quantify how different the actual universe is from our idealized model. This is referred to as the *fitting problem* by Ellis [1984]; Ellis and Stoeger [1987].

If we can construct equations that describe the average evolution of our universe then we can make some headway in addressing the fitting problem by comparing the smoothed universe to our idealized model. Procedures that take averages of the Einstein's equations forge a connection between the fitting problem and what is called *backreaction*, which we describe shortly. A widely used averaging procedure is the Buchert scheme [Buchert, 2000, 2001] which takes volume averages of scalars on constant time hypersurfaces.

[13] A large number of studies choose to place the observer at the centre of inhomogeneity because radial null geodesics are simpler to study. The null geodesics for an off centre observer acquire a dependence on polar angle which is an additional complication.

The Buchert averaging formalism has been applied to both completely general metrics in the synchronous gauge and to exact inhomogeneous solutions of the Einstein equations. A number of researchers have argued that backreaction of inhomogeneities neglected in FLRW models may be the source of acceleration and not some mysterious dark energy [Räsänen, 2006; Wiltshire, 2007a; Clarkson et al., 2009, 2011]. The term backreaction refers to the property that initially small perturbations can modify the background to the extent that average evolution changes. In the context of cosmology this means that when density contrasts become large, $|\delta\rho/\rho| > 0.1$, then the FLRW approximation breaks down and the dynamical equations from such a perfectly smooth background can no longer apply to the real universe.

1.3.2.1 Buchert averaging formalism

The Buchert averaging scheme is the result of work by Thomas Buchert and collaborators in the 1990s. Buchert and Ehlers [1997] first studied the averaging problem in Newtonian cosmologies, which ultimately culminated to the averaging procedure [Buchert, 2000] in which volume averages of scalars are taken in a general relativistic setting. The initial work applied to dust cosmologies only, and in subsequent work [Buchert, 2001] the averaging procedure was extended to perfect fluid cosmologies with radiation. Since the averaging procedure can only be applied to scalars, information about the average evolution of the universe can only be gleaned from the scalar parts of Einstein's equations. We defer a derivation of the Buchert equations to Sec. 2.3.

The Buchert averaging formalism has its drawbacks. The volume averages in the Buchert scheme only apply to scalars but not tensors. There have been attempts at averaging tensors such as the Zalaletdinov averaging formalism [Zalaletdinov, 1997] but the method requires complicated additional mathematical structures and assumptions, and does not easily lend itself to being used for actual numerical computations. Another frequent criticism of the Buchert formalism is that it is not covariant. The scheme relies on a foliation of the 4-dimensional spacetime into space and time. A comoving observer is assumed to be synchronous with constant time hypersurfaces. Such dependence on foliation is unwelcome[14] because in general relativity physical effects should be independent of spacetime foliation.

[14] Although the FLRW metric in the standard model of cosmology is also foliated into constant time hypersurfaces, the foliation in that case is somewhat natural because each spacelike hypersurface is homogeneous and isotropic. The constant time foliation complements the inherent symmetries of the spacetime metric. This would not be the case if some other foliation such as constant mean extrinsic curvature hypersurfaces is chosen.

1.3.2.2 Covariant averages

Averaged Einstein equations derived from averaging procedures that drop some of the assumptions made in the Buchert scheme can be derived but increased generality is accompanied by increased complexity in calculations. One is ultimately forced to study particular cases such as dust solutions with no spatial curvature in perturbed FLRW models. Larena [2009] defines an averaging procedure (which is also gauge dependent) that takes a 3-dimensional volume integral similar to the Buchert scheme but with the Jacobian of the spatial 3-metric being replaced with the Jacobian of a projection operator that projects quantities onto hypersurfaces orthogonal to observer 4-velocities. The assumption that observers are comoving with the matter field is dropped which adds extra terms to the averaged Raychaudhuri Eq. (2.51) and Hamiltonian constraint Eq. (2.56), discussed in Sec. 2.3.

The Buchert equations are obtained by first transforming the metric to a specific form namely by setting the shift vector to zero (see Sec. 2.2). An extension of the Buchert scheme is developed by Gasperini et al. [2010] which they claim to be fully covariant and is derived without fixing the form of the metric. In their work the 3-dimensional spatial volume averaging integral Eq. (2.44) becomes a 4-dimensional integral and acquires dependence on a general spacelike hypersurface $\Sigma(S(x))$; unlike the Buchert formalism in which the $S = const$ and its 4-gradient remains timelike for all time. Similarly $\Sigma(S(x))$ also appears in the extensions to the commutation relation Eq. (2.49), the averaged Raychaudhuri Eq. (2.51) and Hamiltonian constraint Eq. (2.56) but remarkably no extra terms are introduced and $\Sigma(S(x))$ appears only inside the averaging operator.

In taking averages of the Einstein's equations the aim is to study the macroscopic properties and evolution of spacetime without having to keep track of the finer details on scales smaller than the averaging domain. The Buchert averaging scheme allows just this but only for the scalar components of Einstein's equations. Averaging the full Einstein's equations requires covariant averaging of its tensor components. In Zalaletdinov's *macroscopic gravity* [Zalaletdinov, 1992a,b, 1997] a covariant approach for averaging tensors is developed. Averaging a tensor entails comparing the tensor at different locations in spacetime for which Zalaletdinov defines bi-vector operators that act on the tensor which is then integrated over some 4-dimensional volume.

For a tensor $T^{\mu}{}_{\nu}(x)$ and bi-vector operator $\mathcal{A}^{\mu}{}_{\alpha}(x,x')$ then

$$T^{\mu}{}_{\nu}(x,x') = \mathcal{A}^{\mu}{}_{\alpha'}(x,x')\mathcal{A}^{\beta'}{}_{\nu}(x,x')T^{\alpha'}{}_{\beta'}(x') \tag{1.6}$$

is defined as the bi-vector tensor extension of $T^{\mu}{}_{\nu}$ at spacetime locations x and x'. An averaged tensor for $T^{\mu}{}_{\nu}$ is then constructed as

$$\bar{T}^{\mu}_{\nu}(x) = \frac{\int_{x' \in \Sigma_x} T^{\mu}{}_{\nu}(x, x') \sqrt{-g(x')} \mathrm{d}^4 x'}{\int_{x' \in \Sigma_x} \sqrt{-g(x')} \mathrm{d}^4 x'} \ , \tag{1.7}$$

where $\Sigma \subset \mathcal{M}$ in the spacetime manifold, $\mathcal{M}$, and g is the metric determinant. Because of its complexity very few studies [Coley et al., 2005; Paranjape and Singh, 2007; van den Hoogen, 2009] have used the Zalaletdinov formalism. Compare this to the Buchert formalism and it becomes evident why the Buchert scheme has been widely used in backreaction studies. In Buchert formalism with an appropriate ansatz[15] for either the backreaction or the average spatial curvature term the Buchert dynamical equations become closed, and can then be solved on their own without reference to the form of the spacetime metric.

1.3.2.3 Structure formation and backreaction

We deduce whether the actual universe is homogeneous or not by observing the presence of matter or lack thereof in the local universe. Naturally this leads to an examination of structure formation. The fact that the beginning of accelerated expansion roughly coincides with the onset of structure formation has also been investigated to see if there is a deeper connection between them.

Räsänen [2006] argued that gravitational collapse and structure formation can give rise to accelerated average expansion. Räsänen is careful to distinguish between local expansion and global average expansion and interprets the nonaveraged scalar components of the Einstein's equations (see (2.39)–(2.43)) as equations that describe the local expansion. Räsänen then points out that the shear σ^2 term in the Raychaudhuri equation is negative and decreases the local expansion rate. He then refers to the backreaction term Eq. (2.53) and argues that it causes acceleration in the Buchert equations Eq. (2.55) and (2.56).

This gives rise to a seemingly paradoxical situation in which the local expansion rate decelerates everywhere but the average expansion overall accelerates. The physical explanation for this is that the volume sampled on our past light cone changes as structure grows. Initially the fraction of voids is tiny; however, their expansion decelerates much less than that of the denser regions and so the volume of the faster expanding voids eventually outpace that of collapsing regions, giving rise to the accelerated expansion. Räsänen associates structure formation which increases the difference in expansion rate

[15] See, e.g., the section titled "Exact scaling solutions" in [Larena et al., 2009].

between locally collapsing regions and expanding void regions, thereby increasing the variance and backreaction, to ultimately be the cause of accelerated average expansion.

In the timescape scenario the argument given by Räsänen is said to be qualitatively correct but quantitatively impossible given reasonable initial conditions, if all time measurements are referred to the same volume–average clock. Wiltshire argues that volume–average clocks must be recalibrated relative to the local clocks of observers in collapsing regions, and this is necessary to make apparent acceleration phenomenologically viable.

1.3.2.4 Perturbative approach and backreaction

The definition of statistical homogeneity is complex in general. In the standard model one usually assumes that the FLRW geometry applies at all scales and that if the density contrast $\delta\rho/\rho$ is measured in boxes of equal size R at any instant on the surfaces of homogeneity then $\delta\rho/\rho \to 0$ as R is increased. The homogeneity scale is then the smallest scale at which this is reached [Gabrielli et al., 2005].

Given these assumptions then based on intuitive reasoning one is forced to conclude that there must be a connection between the scale of (statistical) homogeneity and the linearly perturbed regime. In prescribing a scale of statistical homogeneity of $\sim 100\,h^{-1}\,\mathrm{Mpc}$ one is also implicitly setting a lower bound on the scale above which the linear regime in perturbation theory should be applicable. This is because as long as we are in the linear regime departures from homogeneity must be small.

Is linear perturbation theory sufficient to study variations in the average expansion and quantify backreaction effects? Ishibashi and Wald [2005] answer this question affirmatively and the authors concluded that backreaction is negligible overall. Ishibashi and Wald [2005] argued that as long as the perturbed gravitational potentials (see Eq. (2.11)) to the FLRW metric remain small $\Psi \ll 1$ and the time variation in the potential is smaller than its spatial gradient

$$\left|\frac{\partial\Psi}{\partial t}\right|^2 \ll \frac{1}{a^2}\partial^i\Psi\partial_i\Psi\ , \tag{1.8}$$

then nonlinear density contrast no matter how large has no bearing on the average expansion rate. However Räsänen [2010] pointed out that the conclusion drawn by Ishibashi and Wald [2005] was based on an inconsistent use of first order perturbation theory. Räsänen argues that even when we only work with first order perturbations, quantities involving the laplacian of the potential $\Psi\nabla^2\Psi$ are not necessarily much smaller then pure first order terms and thus all perturbations should be taken to second order.

From Räsänen's work it emerges that it is necessary to keep second order terms to avoid consistency problems which can result by truncating to first order terms. It is however, not clear if second order perturbation theory is both necessary and sufficient. It is conceivable that third or higher order terms may not remain small when second order terms become important.

Green and Wald [2011, 2014] refined the arguments of Ishibashi and Wald [2005] by developing a particular approximation scheme in which the metric remains close to a background metric but allows arbitrarily large stress-energy fluctuations on small scales. If their arguments are correct, however, they only show that the ΛCDM cosmology is self-consistent. The assumption that the average evolution of the universe is exactly a solution of Einstein's equations with prescribed dust is still made from the outset.

In contrast, in the Buchert approach in general and in the timescape cosmology in particular the average evolution is not an exact solution of Einstein's equations. Once density perturbations become nonlinear then the background evolution, and perturbations on that background are no longer applicable. In the timescape model perturbation theory at the present epoch is not used to make predictions about the model. However, linear perturbation theory before the time of matter and radiation decoupling is assumed to be justified and used in calculations of CMB anisotropies (See Chap 3).

N-body simulations have also been used to test the regime of validity of the linear theory in the standard model but are themselves subject to criticism. In N-body simulations one starts with some initial conditions, and particles positions, and velocities are numerically evolved [Bertschinger, 1998]. The reason results from these simulations are questioned is that the Poisson equation used in N-body simulations is intrinsically Newtonian, and hence it cannot account for general relativistic effects that are bound to impact structure formation.

There have also been studies that have aimed to quantify the importance of backreaction on perturbed FLRW cosmologies. Clarkson et al. [2009] applied the averaging procedure of Larena [2009] to an Einstein-de Sitter universe which is perturbed to second order in the Newtonian gauge. Unsurprisingly, in their study the effect of backreaction on the averaged Hubble expansion is dependent on the size of the averaging domain with changes in the Hubble rate roughly of order 10^{-1} to 10^{-5}. This is an outcome of the fact that quantities from volume averages are only representative of some global average if the averaging domain is large enough compared to the scale of homogeneity. Furthermore, the variations in expansion rate are also dependent on the definition chosen for the *effective* averaged Hubble expansion. This is symptomatic of the wider issues relating to averaging and backreaction, i.e., once we deal with averaged notions there is ambiguity in relating averaged quantities to actual observables.

In another such study Umeh et al. [2011] apply both the averaging methods of Gasperini et al. [2010] and Larena [2009] to the FLRW model perturbed to second order in the Newtonian gauge with a conclusion, similar to above, that changes in the Hubble expansion from backreaction are less than a percent. Their study was aimed at checking the agreement between the averaging schemes and they report consistency (limited to second order perturbations) between results obtained from these different prescriptions. Their study also underscores the difficulties in studying backreaction effects from first principles even in the context of the standard model of cosmology. In calculating averaged scalar quantities they use the transfer functions of Eisenstein and Hu [1998] which are obtained by solving strictly first order equations; yet all backreaction averages are of second order. Strictly speaking this is the not same as starting from some Gaussian random initial conditions and then numerically evolving the spatially averaged second order perturbed equations and the final results are bound to be affected.

1.4 Overview of the timescape cosmology

The conceptual basis and mathematical formalism for the timescape cosmology was first provided by Wiltshire [2007a], where he argued that cosmic acceleration could be explained as a purely apparent effect. A key physical ingredient of Wiltshire's argument is that we mistakenly ascribe aspects of gravitational energy gradients to dark energy. The inference that the expansion appears to be accelerating arises from attempting to fit an FLRW model to an average evolution which is no longer close to a FLRW evolution at late epochs. For the most recent comprehensive review of timescape cosmology and philosophy see [Wiltshire, 2015].

Gravitational energy is a difficult concept in general relativity which is only well defined in spacetimes that possess a timelike Killing vector. However, the universe described by the FLRW metric does not possess a time symmetry. The scale factor in the FLRW metric has explicit time dependence and therefore there are no timelike killing vectors. Thus, what is the notion of gravitational energy referred to by Wiltshire? Here I give an overview of the ideas central to timescape cosmology including gravitational energy.

1.4.1 Fundamental concepts of the timescape cosmology

The timescape cosmology describes the average evolution of the universe and relies on the Buchert evaraging formalism [Buchert, 2000, 2001]. Wiltshire argues that the time parameter in the Buchert equations (2.53)–(2.59) is a statistical volume–average parameter, and is not the time observers bound in a cosmic structure (such as ourselves)

would measure. The statistical Buchert time parameter is not interpreted as a quantity that is measured by any observer, but that measured by fiducial observers in voids; where regional spatial curvature happens to match the volume–average (negative) spatial curvature over the horizon volume at any epoch.

Wiltshire is also cautious in applying the Buchert formalism to the Einstein equations

$$G^{\mu}{}_{\nu} = \frac{8\pi G}{c^4} T^{\mu}{}_{\nu} \,, \tag{1.9}$$

and points out the oversights made in cosmological models when using Eq. (1.9). In particular, the issues of coarse–graining the fluid on the right hand side, and the associated scale dependence of the metric on the left hand side of Eq. (1.9) are usually neglected in comparing local observations with statistical average quantities in cosmology. These oversights which include neglecting to define the scale of fluid "particles" on the r.h.s of Eq. (1.9) and the scale relevant to $g_{\mu\nu}$ on the l.h.s of Eq. (1.9) have important physical ramifications such as comic acceleration.

1.4.1.1 What is meant by "comoving with the dust"?

The energy momentum tensor approximates the constituents making up the universe as a fluid, with a perfect fluid equation of state assumed for each matter component in the standard model. In the standard interpretation of the FLRW model it is assumed that the observers making measurements, and stars/supernovae or galaxies which are the source of any emitted light are "comoving with the fluid", i.e., that these sources have a statistically random distribution on the surfaces of average homogeneity. At present day radiation content in the energy momentum tensor has negligible impact on the evolution of the universe. However, impact of pressureless matter called dust on expansion rate is sizeable and a fluid particle inevitably means a particle of dust.

Prior to recombination, subatomic particles such as electrons, protons, photons, neutrinos, dark matter particles together with hydrogen and helium nuclei constitute the most complex distinct entities in the universe. Post recombination gravitational collapse leads to the formation of stars, galaxies and galaxy clusters. Furthermore, voids and wall regions form which expand at different rates. Thus the matter content in the universe undergoes a transition from an era when subatomic particles form a fluid element to an era when stars and galaxies can be regarded as fluid elements or particles of "dust". In the face of such a stark contrast as to what is meant by a particle of dust, one can ask, how can then a single energy momentum tensor be used for all times?

The definition of an appropriate energy momentum tensor involves coarse–graining. For example, in going from a fluid description of the interior of a star to describing it as single particle we coarse–grain over the degrees of freedom described by the electromagnetic and nuclear forces.

A key ingredient of the timescape cosmology is to recognize that in coarse–graining over galaxies to make galaxy clusters, and over galaxy clusters to make filaments and sheets, we are now coarse–graining gravitational degrees of freedom that normally appear on the left hand side of the Einstein equations. This complicates the understanding of what is meant by "comoving", as we can no longer describe physics by one single Riemannian geometry and local Lorentz boosts.

One must think carefully about the definition of an average fluid element, since we must coarse–grain over the largest structures before we arrive at a smoothed fluid. Effectively, this means a hierarchy of coarse–graining as shown in Eq. (1.10) (see [Wiltshire, 2015] for further details).

$$g_{\mu\nu}^{\rm stellar} \to g_{\mu\nu}^{\rm galaxy} \to g_{\mu\nu}^{\rm cluster} \to \left.\begin{array}{r} g_{\mu\nu}^{\rm wall} \\ \vdots \\ g_{\mu\nu}^{\rm void} \end{array}\right\} \to g_{\mu\nu}^{\rm universe} \tag{1.10}$$

For most of the 20th century it was assumed that galaxies can be treated as "particles of dust". However, the existence of filaments, sheets and voids means that they are not randomly distributed. In the timescape cosmology it is therefore assumed that rather than having simple compact objects as particles of dust, fluid cells coarse–grained at the $100\,h^{-1}$ Mpc statistical homogeneity length scale are to be treated as the pressureless elementary entities with an equation of state. Only at this scale does a fluid element have a comoving energy density which does not vary significantly over the course of cosmic evolution from early times to the present.

The notion of what is meant by "comoving" with the cosmic fluid is left undefined in the Buchert formalism. The timescape cosmology provides an interpretational framework for the Buchert formalism; matching regional geometry on small scales to the statistical volume–average parameters that constitute the collective degrees of freedom of a $100\,h^{-1}$ Mpc average fluid cell. Such an interpretational framework requires physical principles which we will now discuss.

1.4.1.2 Cosmological Equivalence Principle (CEP)

The Strong Equivalence Principle (SEP) states that it is always possible to choose a local inertial (non accelerating) frame in a sufficiently small spacetime neighbourhood in which the laws of nature take their forms as in special relativity (Minkowski spacetime). In [Wiltshire, 2008] it is argued that the largest scale on which (SEP) can be applied has not been addressed. Wiltshire therefore proposes the CEP to extend the SEP and apply it on cosmological scales to relate regional geometry to the average statistical geometry of the entire universe. The CEP states:

In cosmological averages it is always possible to choose a suitably defined spacetime region, the cosmological inertial region (CIR), on whose boundary average motions (timelike and null) can be described by geodesics in a geometry which is Minkowski up to some time-dependent conformal transformation,

$$\mathrm{d}s^2_{\mathrm{CIF}} = a^2(\eta)\left[-\mathrm{d}\eta^2 + \mathrm{d}r^2 + r^2\mathrm{d}\Omega^2\right] \ . \tag{1.11}$$

In underdense regions (voids) the CIR is smaller than the scalar curvature scale, and near overdensities it is the finite infinity scale defined in Sec. 1.4.1.3, $2\,h^{-1}$–$10\,h^{-1}$ Mpc, depending on whether one is dealing with a small group of galaxies such as our own Local Group or a rich cluster of galaxies. The CEP embodies the idea that there is a scale over which radial motion of particles in a static spacetime cannot be distinguished from the case of particles at rest in an expanding volume in a dynamic spacetime.

In the early universe, or in those regions of a void where structures have never collapsed, then the CEP is equivalent to the SEP over short periods of time. In the timescape model one assumes that collapsing regions can always be surrounded by bounding surfaces on which (1.11) holds over long periods of time. The geometry (1.11) represents an effective asymptotic geometry for observers in bound systems.The CEP construct is used in building timescape model phenomenology, see Sec. 1.4.2.

1.4.1.3 Finite Infinity regions

A finite infinity region is a timelike surface taken to be a lower bound for the size of a CIR that bounds any overdensity. Finite infinity regions are on average spatially flat and can be $2\,h^{-1}$–$10\,h^{-1}$ Mpc in size for galaxy clusters, see Sec. 2.4 in Wiltshire [2015]. See Fig. 1.1 for a schematic illustration of this concept. Finite infinity separates external expanding void regions from an inner region which has zero average expansion. The innermost region is virialized which means at the inner boundary expansion is negative as matter is attracted towards the inner virialized region. This means one needs a shell,

which is underdense and expanding just outside the margins of the collapsing region. In order that the expanding, collapsing and virialized regions together on average have zero expansion. In Fig. 1.1 we see the boundary between this inner expanding and outer expanding region is shown by the dashed line as the finite infinity scale.

When we come to define statistical averages in the Buchert formalism, then the horizon volume that defines the volume average scale factor Eq. (2.67) in timescape cosmology is a disjoint union of void and wall regions. It is these finite infinity regions that together form a wall region and thus Eq. (2.67) shows the operational importance of this concept.

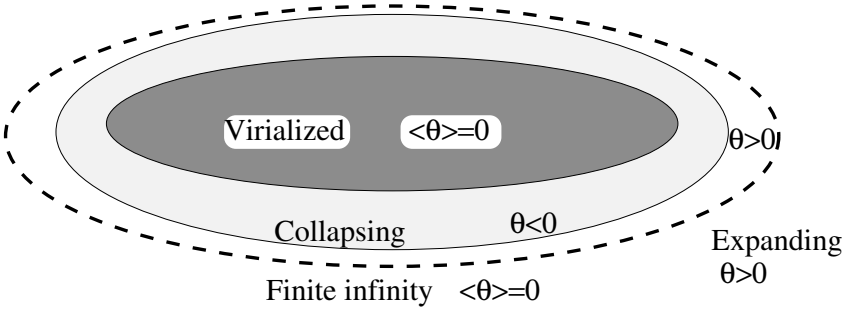

FIGURE 1.1: A schematic diagram of finite infinity region is shown. The dashed boundary separates the external expanding void regions from the inner region which has zero net expansion.

1.4.1.4 Gravitational energy

On account of the SEP the first derivatives of the metric can be set to zero at a point. To put this in colloquial terms we can always get rid of gravity at a point. Therefore all definitions of gravitational energy are nonlocal. Many energy definitions deal with the asymptotically flat case. As an example, consider the ADM energy [Arnowitt et al., 1962]

$$E = \oint \mathrm{d}S_i \left(\partial_j g_{ij} - \partial_i g_{jj}\right) \ , \tag{1.12}$$

where $\mathrm{d}S_i$ is a two-dimensional surface element at spatial infinity. However, since the actual universe is expanding it is not asymptotically flat. In a general situation, the best one can do is to define "quasilocal energy" by integrating a Hamiltonian density on an appropriate closed 2-surface within a spacelike hypersurface. See Szabados [2004] for a review of energy definitions in general relativity.

To date the timescape cosmology has not used any existing quasilocal energy expressions nor have any new definitions been given. Rather effects from gravitational energy

gradients are incorporated in the model phenomenologically based on a chain of physical arguments.

The quasilocal energy problem as treated in the literature [Szabados, 2004] thus far deals exclusively with internal energy of bound systems possibly including binding energy. The coarse–graining hierarchy (1.10) involves several steps that include binding energy of stars in galaxies, galaxies in clusters and the "thermal" energy of galaxies moving within clusters. These aspects of gravitational energy are qualitatively different to those that involve expanding regions of different density. In coarse–graining over finite infinity regions Wiltshire's intention is to only consider the problem of the relative kinetic energy of expansion.

Ultimately the timescape cosmology requires a rigorous formalism for relating regional geometry to the volume–average statistical geometry. Thus far Wiltshire has built a phenomenological model which incorporates the CEP. In particular, by conducting a series of thought experiments [Wiltshire, 2008] he reasons that below the scale of statistical homogeneity one can always make a "gauge choice" in which the Hubble parameter is regionally uniform at the expense of recalibrating clocks in the presence of spatial curvature gradients. Effectively, the relative regionally isotropic volume deceleration is treated as a physically relevant parameter in the calibration of asymptotic clocks. There is a gravitational energy cost associated with each spatial curvature gradient.

What are viewed as "constant time hypersurfaces" in the Buchert approach are viewed more as "thin sandwiches" in which each $100\,h^{-1}$ Mpc cell can be associated with different time parameters related to the regions of different spatial scalar curvature within each cell.

The Hubble parameter, which involves first derivatives of the statistical metric, is related to the connection on this geometry. There is freedom in choosing the Hubble parameter of regional observer. Wiltshire demands in particular that a uniform quasilocal Hubble flow gauge can be found, which might be viewed as a coarse–grained version of the uniform Hubble flow gauge of Bardeen [1980], or similar gauges [Katz et al., 2006] in perturbative approaches to FLRW cosmology.

1.4.2 Timescape model phenomenology

We as observers in a galaxy are located within a wall region that is part of the local distribution of matter. This local distribution of matter is an important aspect that needs to be considered when interpreting measurements made on our past light cone. In the timescape cosmology we begin with a local average metric (1.13) and extend it to obtain

a dressed global metric, the essential idea being that there is no single geometry that describes the entire universe and that "cosmological parameters are dressed" [Buchert and Carfora, 2002, 2003].

Our starting point for putting the timescape cosmology on a mathematical framework is the finite infinity regions with local metric

$$\mathrm{d}s^2_{\rm fi} = -\mathrm{d}\tau_{\rm w}^2 + a_{\rm w}^2(\tau_{\rm w})\left[\mathrm{d}\eta_{\rm w}^2 + \eta_{\rm w}^2\mathrm{d}\Omega^2\right] \ , \tag{1.13}$$

which constitute walls (subscript w refers to walls). Now consider a general spherically symmetric geometry

$$\mathrm{d}\bar{s}^2 = -\mathrm{d}t^2 + \bar{a}^2(t)\mathrm{d}\bar{\eta}^2 + \mathcal{A}(\bar{\eta},t)\mathrm{d}\Omega^2 \ , \tag{1.14}$$

with a spatial volume scaling $\bar{a}^3(t)$, which is relevant because cosmological information is obtained by radial spherically symmetric averages on our past light cone. Writing the metric (1.14) in terms of the wall time, $\tau_{\rm w}$, of finite infinity observers we get

$$\mathrm{d}\bar{s}^2 = -\bar{\gamma}_{\rm w}^2(\tau_{\rm w})\mathrm{d}\tau_{\rm w}^2 + \bar{a}^2(\tau_{\rm w})\mathrm{d}\bar{\eta}^2 + \mathcal{A}(\bar{\eta},\tau_{\rm w})\mathrm{d}\Omega^2 \ , \tag{1.15}$$

where $\bar{\gamma}_{\rm w} \equiv \mathrm{d}t/\mathrm{d}\tau_{\rm w}$. Although spherically symmetric this metric is not an LTB geometry because it is not a solution of the Einstein equations. Rather (1.15) is an effective radial metric related to a solution of the Buchert equations (2.61)–(2.65) in which $\bar{a}^3$ is the average spatial volume. Since the universe is dominated in volume by negatively curved voids the geometry (1.15) has negative spatial curvature.

In general relativity based on the Einstein Field Equations (EFE) with a single geometry one conventionally joins different metrics by applying the Israel–Wilson junction conditions. That is that the metric and its first derivatives, along with those of matter fields in $T_{\mu\nu}$, should be continuous. In the timescape model it is assumed that when we coarse–grain then different effective metrics apply on different scales and so standard junction conditions are not applicable.

Instead Wiltshire [2007a] assumes that light propagates on average on the null geodesics of (1.15). These are matched to those of the finite infinity geometry (1.13) by conformally equating the radial null sections; null geodesics being unaffected by an overall conformal scaling. One should stress that the metrics (1.13) and (1.15) have different spatial curvature and therefore represent different geometries; this matching procedure is not an isometry. The conformal factor encodes the difference in regional volume expansion between the wall geometry (1.13) and the average geometry (1.15). Phenomenologically it represents the term associated with differences in the kinetic energy of expansion of wall regions and the average.

In terms of the wall fraction $f_{\rm w} = f_{\rm wi}\,(a_{\rm w}/\bar{a})^3$ (see Eq. (2.67)) we write (1.13) as

$$\mathrm{d}s^2_{\rm fi} = -\mathrm{d}\tau^2_{\rm w} + \frac{(1-f_{\rm v})^{2/3}\,\bar{a}^2}{f^{2/3}_{\rm wi}}\left[\mathrm{d}\eta^2_{\rm w} + \eta^2_{\rm w}\mathrm{d}\Omega^2\right] \ . \tag{1.16}$$

The conformal matching of the radial sections leads to

$$\mathrm{d}\eta_{\rm w} = \frac{f^{1/3}_{\rm wi}}{\bar{\gamma}_{\rm w}\,(1-f_{\rm v})^{1/3}} \ . \tag{1.17}$$

We now extend the metric (1.13) beyond wall regions to obtain a dressed global metric,

$$\begin{aligned}\mathrm{d}s^2 &= -\mathrm{d}\tau^2_{\rm w} + \frac{\bar{a}^2}{\bar{\gamma}^2_{\rm w}}\mathrm{d}\bar{\eta}^2 + \frac{\bar{a}^2\,(1-f_{\rm v})^{2/3}}{f^{2/3}_{\rm wi}}\eta^2_{\rm w}\,(\bar{\eta},\tau_{\rm w})\,\mathrm{d}\Omega^2 \ , \\ &= -\mathrm{d}\tau^2_{\rm w} + a^2(\tau_{\rm w})\left[\mathrm{d}\bar{\eta}^2 + r^2_{\rm w}\,(\bar{\eta},\tau_{\rm w})\right] \ . \end{aligned} \tag{1.18}$$

Here $a \equiv \bar{\gamma}_{\rm w}\bar{a}$ is an effective scale factor and

$$r_{\rm w} \equiv \bar{\gamma}_{\rm w}\,(1-f_{\rm v})^{1/3}\,f^{-1/3}_{\rm wi}\eta_{\rm w}\,(\bar{\eta},\tau_{\rm w}) \ , \tag{1.19}$$

is an effective comoving distance in the average geometry (1.18) taken to be applicable on cosmological scales. This is the best fit global average metric that a wall observer assigns to the universe if they make a mistake—as we do—of assuming that our local spatially flat geometry extends globally and all fiducial observers have clocks synchronized with ours.

The dressed matter and radiation densities $\Omega_{\rm M}$, $\Omega_{\rm R}$ and expansion rate H from the geometry (1.18) can be related to volume average parameters in the Buchert equations (2.61)–(2.65) with the the following ansatz

$$\Omega_{\rm M} \equiv \bar{\gamma}^3_{\rm w}\bar{\Omega}_{\rm M} \ , \tag{1.20}$$

$$\Omega_{\rm R} \equiv \bar{\gamma}^4_{\rm w}\bar{\Omega}_{\rm R} \ , \tag{1.21}$$

$$\begin{aligned} H &\equiv \frac{1}{a}\frac{\mathrm{d}a}{\mathrm{d}\tau_{\rm w}} = \frac{1}{\bar{a}}\frac{\mathrm{d}\bar{a}}{\mathrm{d}\tau_{\rm w}} - \frac{1}{\bar{\gamma}_{\rm w}}\frac{\mathrm{d}\bar{\gamma}_{\rm w}}{\mathrm{d}\tau_{\rm w}} \ , \\ &= \frac{1}{\bar{a}}\frac{\mathrm{d}\bar{a}}{\mathrm{d}t}\frac{\mathrm{d}t}{\mathrm{d}\tau_{\rm w}} - \frac{1}{\bar{\gamma}_{\rm w}}\frac{\mathrm{d}\bar{\gamma}_{\rm w}}{\mathrm{d}\tau_{\rm w}} \ . \end{aligned} \tag{1.22}$$

The previously discussed quasilocal uniform Hubble flow gauge is implemented by assuming that

$$\bar{H} \equiv \frac{1}{\bar{a}}\frac{\mathrm{d}\bar{a}}{\mathrm{d}t} = \bar{\gamma}_{\mathrm{w}} H_{\mathrm{w}} = \bar{\gamma}_{\mathrm{v}} H_{\mathrm{v}} \tag{1.23}$$

$$H_{\mathrm{w}} \equiv \frac{1}{a_{\mathrm{w}}}\frac{\mathrm{d}a_{\mathrm{w}}}{\mathrm{d}t}\,, \qquad H_{\mathrm{v}} \equiv \frac{1}{a_{\mathrm{v}}}\frac{\mathrm{d}a_{\mathrm{v}}}{\mathrm{d}t}, \tag{1.24}$$

$$\bar{\gamma}_{\mathrm{w}} \equiv \frac{\mathrm{d}t}{\mathrm{d}\tau_{\mathrm{w}}}\,, \qquad \bar{\gamma}_{\mathrm{v}} \equiv \frac{\mathrm{d}t}{\mathrm{d}\tau_{\mathrm{v}}}\,, \tag{1.25}$$

and τ_{w} and τ_{v} are proper times in walls and voids respectively. These equations can be used to relate the dressed expansion rate H to the expansion rate within walls and voids H_{w}, H_{v}, and to the volume–average (bare) rate $\bar{H}$.

The framework in this section provides the mathematical basis which will be used for the physical interpretation of the solutions to the Buchert equations in the following chapters.

1.4.2.1 Apparent acceleration in the timescape scenario

The volume–average deceleration parameter is defined in the usual manner [Wiltshire, 2007a]

$$\bar{q} \equiv \frac{-1}{\bar{H}^2\bar{a}}\frac{\mathrm{d}^2\bar{a}}{\mathrm{d}t^2}\,, \tag{1.26}$$

where it is understood that the expansion rate, $\bar{H}$, and time parameter, t, are those relevant to the volume–average observer. The dressed deceleration parameter is defined as [Wiltshire, 2007a]

$$q \equiv \frac{-1}{H^2 a}\frac{\mathrm{d}^2 a}{\mathrm{d}\tau_{\mathrm{w}}^2}\,, \tag{1.27}$$

where the dressed expansion rate, H, and wall time parameter, τ_{w}, are those relevant to the wall/galaxy observer and the dressed global geometry in (1.18). In the timescape model with matter and radiation to a very good approximation

$$q \approx \frac{-(1-f_{\mathrm{v}0})(8f_{\mathrm{v}0}^3 + 39f_{\mathrm{v}0}^2 - 12f_{\mathrm{v}0} - 8)}{(4 + f_{\mathrm{v}0} + 4f_{\mathrm{v}0}^2)^2}\,, \tag{1.28}$$

where $f_{\mathrm{v}0}$ is the present void fraction and we have used the tracker matter only solution from Wiltshire [2007b].

From the outset it bas been realised that for realistic parameter values in the timescape cosmology [Wiltshire, 2007a,b] the volume–average deceleration parameter is always positive, $\bar{q} > 0$, and therefore the volume–average observer always infers a decelerating universe. However, the galaxy/wall observer may ($q < 0$) or may not ($q \geq 0$) infer an

accelerating universe. Thus far the best fit parameters as a result of tests against supernovae and gamma ray bursts data [Smale and Wiltshire, 2011; Smale, 2011] show that indeed the galaxy/wall observer infers acceleration, $q < 0$. In the timescape model this forms the premise of the argument that the inferred acceleration is apparent acceleration.

Chapter 2

The universe: rethinking the standard approach to cosmology

In this chapter we briefly revisit the standard model of cosmology and introduce its background and linearly perturbed metrics. We then introduce the 3+1 decomposition of the EFE in the ADM-gauge as a framework that allows us to study a general line element. To make the resulting equations more tractable whilst simultaneously capturing the essence of inhomogeneity and anisotropy we take spatial average of the Einstein's equations according to the Buchert scheme [Buchert, 2000, 2001]. We then present our original work in Sec. 2.4 which extends the matter only solution by Wiltshire [2007b] to include matter and radiation. The content in Sec. 2.4 was published in the research article of Duley et al. [2013], where the timescape model with matter and radiation was presented as a viable cosmological model that solves the Buchert equations for the averaged expansion of the Universe.

2.1 ΛCDM model of cosmology

The ΛCDM model of cosmology is based on the Cosmological Principle (CP) that "the universe is spatially homogeneous: there are no special locations, and spatially isotropic: there are no special directions". In general relativity the CP means that the metric of spacetime is left unchanged under spatial rotations and translations. The FLRW metric describing a homogeneous and isotropic expanding or contracting universe in spherical polar coordinates has the form

$$ds^2 = c^2dt^2 - a^2(t)\left[\frac{dr^2}{1-Kr^2} + r^2d\theta^2 + r^2\sin^2\theta d\phi^2\right], \tag{2.1}$$

where the scale factor $a(t)$ has dimension of length, the coordinate r is dimensionless and the spatial curvature parameter K is normalized to $K = +1, 0, -1$. The spacetime singularity when $K = +1$ and $\psi = \pi/2$ is a coordinate singularity, not a physical singularity. In the spatially curved cases, the parameter r may be related to angular or hyperbolic coordinates with $r = \sin\psi$ if $K = +1$, and $r = \sinh\psi$ if $K = -1$. The spacetime dynamics are described by the Friedmann equations relating the scale factor and its time derivative to the components of the energy momentum tensor via

$$H^2 \equiv \left(\frac{1}{a}\frac{\mathrm{d}a}{\mathrm{d}t}\right)^2 = -\frac{c^2K}{a^2} + \frac{8\pi G}{3}\rho + \frac{1}{3}\Lambda c^2 \,, \tag{2.2}$$

$$\frac{1}{a}\frac{\mathrm{d}^2a}{\mathrm{d}t^2} = -\frac{4\pi G}{3}\left(\rho + \frac{3p}{c^2}\right) \,. \tag{2.3}$$

where ρ and p includes both matter and radiation density and pressure respectively and Λ is the cosmological constant. The energy density conservation equation

$$\frac{\mathrm{d}\rho}{\mathrm{d}t} = -3H\left(\rho + \frac{p}{c^2}\right) \,, \tag{2.4}$$

is also useful but is not independent from Eq. (2.2) and (2.3). The standard ΛCDM model is taken to be the $K = 0$, spatially flat FLRW metric.

The real universe is not perfectly homogeneous and isotropic as is evident by the existence of stars, galaxies, clusters of galaxies, wall and voids. In the standard paradigm it is assumed that deviations from near homogeneity and isotropy have been small in the past and continue to be small on large scales even today. It is deemed adequate to study such departures from smoothness with linear perturbation theory. Only at the very small scales matter fluctuations are presumed nonlinear[1] but their effects on the overall average evolution of the universe are thought to be negligible. The homogeneous and isotropic metric is appended with an inhomogeneous, albeit small perturbation

$$g_{\mu\nu} = \bar{g}_{\mu\nu} + h_{\mu\nu}, \tag{2.5}$$

where $\bar{g}_{\mu\nu}$ is the metric of Eq. (2.1), and

$$h_{00} = -E \,, \tag{2.6}$$

$$h_{i0} = a(t)\left[\frac{F}{\partial x^i} + G_i\right] \,, \tag{2.7}$$

$$h_{ij} = a^2(t)\left[A\delta_{ij} + \frac{\partial^2 B}{\partial x^i \partial x^j} + \frac{\partial C_i}{\partial x^j} + \frac{\partial C_j}{\partial x^i} + D_{ij}\right] \,, \tag{2.8}$$

[1] Roukema et al. [2014] claim to have measured a 6% compression of the BAO scale across superclusters, for example.

where all the perturbation variables depend both on time and position. The given form for $h_{\mu\nu}$ is chosen to facilitate a classification of the perturbations into scalar, vector and tensor parts and requires that

$$\frac{\partial C_i}{\partial x^i} = \frac{\partial G_i}{\partial x^i} = 0\,, \qquad \frac{\partial D_{ij}}{\partial x^i} = 0\,, \qquad D_{ii} = 0\,. \tag{2.9}$$

This classification makes it possible to decompose the Einstein's equations into scalar, vector and tensor parts that to first order in perturbations do not interfere with each other. The scalar perturbations primarily source inhomogeneities; the vector perturbations quickly decay and are irrelevant today; and tensor perturbations generate gravitational waves but have not been detected as yet. In Sec. 2.3 , we will see that the Buchert averaging scheme is applicable only to the scalar parts of the Einstein's equations. Thus in the timescape model we study the averaged expansion of the universe sourced by the evolution of spatially averaged scalar quantities, i.e., the nonpropagating degrees of freedom. Cosmology based on averaged tensor quantities is outside the scope of this work.

Einstein's equations derived from the general metric $g_{\mu\nu}$ when solved include both physical and non-physical solutions. The non-physical solutions which correspond to a coordinate transformation of the background FLRW metric (a gauge choice) are removed by fixing a coordinate system. Two commonly used gauges are the Newtonian gauge

$$B = 0, \quad F = 0, \quad E = 2\Phi(x^\mu)\,, \quad A = -2\Psi(x^\mu)\,, \tag{2.10}$$

$$g_{00} = -1 - 2\Phi\,, \quad g_{0i} = 0\,, \quad g_{ij} = a^2\delta_{ij}\left[1 - 2\Psi\right]\,, \tag{2.11}$$

and the synchronous gauge

$$E = 0\,, \quad F = 0\,, \tag{2.12}$$

$$g_{00} = -1\,, \quad g_{0i} = 0\,, \quad g_{ij} = a^2\left[(1+A)\delta_{ij} + \frac{\partial^2 B}{\partial x^i \partial x^j}\right]\,. \tag{2.13}$$

In subsequent sections we will find that the phenomenological lapse function of timescape model quantifies clock rate differences between a galaxy/wall observer and an average observer analogous to the manner whereby $\Phi(t, x^i)$ in the Newtonian gauge quantifies clock rate differences between two observers at spatial coordinates x^i_1 and x^i_2. Contributions to the phenomenological lapse function are not limited to linear perturbations and we show that this leads to a significant recalibration of the inferred cosmological parameters. In the next section we present the $3+1$ decomposition of Einstein's equations which will enable us to introduce the Buchert averaging formalism from which the timescape equations are derived.

2.2 The 3+1 decomposition of Einstein's equations

Historically, the 3+1 decomposition of Einstein's equations was used in the Hamiltonian formulation of general relativity with the ultimate aim of developing a quantum theory of gravity. More recently, the availability of modern day computing power made it possible to numerically solve Einstein's equations which have no analytical solutions. In numerical relativity the gravitational field is evolved forward in time starting from some initial conditions, i.e., general relativity is posed as a Cauchy problem. In cosmology it is desirable to have an averaged metric that takes into effect the inhomogeneous distribution of matter in the universe. One way to model a lumpy universe is to take the spatial average of the Einstein field equations. In both numerical relativity and inhomogeneous cosmology a break down of spacetime in to space and time is required.

A general spacelike hypersurface $\Sigma(A)$ can be specified by holding a scalar field $A(x^\mu)$ constant. The unit future-pointing timelike normal to this hypersurface is given by

$$n_\mu = -\alpha \partial_\mu A \,, \quad \alpha = \frac{1}{\sqrt{-g^{\alpha\beta}\partial_\alpha A \partial_\beta A}} \,, \quad n_\mu n^\mu = -1 \tag{2.14}$$

This normal vector induces a spatial metric $P_{\mu\nu}$ on the 3-dimensional hypersurfaces Σ,

$$P_{\mu\nu} = g_{\mu\nu} + n_\nu n_\mu \,. \tag{2.15}$$

In fact, one can also define a projection (2.15) in the case that, n^ν, are tangents to a congruence of worldlines not necessarily orthogonal to any hypersurface.

The expansion tensor is defined as

$$\theta_{\mu\nu} = P_\mu{}^\rho P_\nu{}^\sigma \nabla_{(\rho} n_{\sigma)} \,, \tag{2.16}$$

and its trace θ describes the change in volume of a sphere of test particles centered on n^ν. The rotation tensor is taken to be the antisymmetric part of the projection of the gradient of the normal vector

$$\omega_{\mu\nu} = P_\mu{}^\rho P_\nu{}^\sigma \nabla_{[\rho} n_{\sigma]} \,. \tag{2.17}$$

By Frobenius' theorem a necessary and sufficient condition for the vector field, n^ν, to be normal to some hypersurface Σ is that the rotation tensor—or vorticity —vanishes. The normal vector is then the gradient of some scalar function as above, in Eq. (2.14). This is the case that will be considered here. The projector operator (2.15) then serves to project geometric objects onto the hypersurface.

The Einstein equations

$$G_{\mu\nu} \equiv R_{\mu\nu} - \frac{1}{2} R g_{\mu\nu} = 8\pi G T_{\mu\nu}, \tag{2.18}$$

can then be projected to the 3+1 form

$$G_{\mu\nu} n^\mu n^\nu = T_{\mu\nu} n^\mu n^\nu \equiv \varepsilon \,, \tag{2.19}$$

$$G_{\mu\nu} n^\mu P^\nu{}_\rho = T_{\mu\nu} n^\mu P^\nu{}_\rho \equiv J_\rho \,, \tag{2.20}$$

$$R_{\mu\nu} P^\mu{}_\rho P^\nu{}_\sigma = T_{\mu\nu} P^\mu{}_\rho P^\nu{}_\sigma - \frac{1}{2} h_{\rho\sigma} T \equiv S_{\rho\sigma} - \frac{1}{2} P_{\rho\sigma} T \,. \tag{2.21}$$

These equations, though covariant, are complicated, and can be simplified with a choice of coordinate system that reflects our 3+1 split of spacetime. In the Arnowitt-Deser-Misner (ADM) gauge the scalar field $A(x^\mu)$ is homogeneous and the normal vector n_μ takes the form

$$n_\mu = N(-1, 0, 0, 0) \,, \quad n^\mu = \frac{1}{N}(1, -N^i) \,, \tag{2.22}$$

where $N(x^\mu)$ is called the lapse function and N^i the shift vector

$$N = \frac{1}{\sqrt{-g^{00}}} \,, \quad N^i = g^{0i} N^2 \,, \tag{2.23}$$

and the projection tensor takes the simpler form

$$P^\mu{}_i = \delta^\mu{}_i \,, \quad P^0{}_0 = 0 \,, \quad P_{ij} = g_{ij} \,. \tag{2.24}$$

In terms of lapse function and shift vector the metric and its inverse can be expressed as

$$g_{\mu\nu} = \begin{pmatrix} -N^2 + N_i N^i & N_i \\ N_j & P_{ij} \end{pmatrix} \,, \quad g^{\mu\nu} = \begin{pmatrix} -N^{-2} & N^{-2} N^i \\ N^{-2} N^i & P^{ij} - N^{-2} N^i N^j \end{pmatrix} \,. \tag{2.25}$$

The normal vector n^μ apart from specifying the hypersurface and the projection operator also appears in the definitions of other key geometrical quantities. The extrinsic curvature, also called the second fundamental form is defined as the negative of the expansion tensor and measures the rate of change of the spatial metric $P_{\mu\nu}$ along the normal vector.

$$\begin{aligned} K_{\mu\nu} \equiv -P_\mu{}^\rho P_\nu{}^\sigma \nabla_\rho n_\sigma &= -\frac{1}{2} \mathcal{L}_{\mathbf{n}} P_{\mu\nu} \,, \\ &= -\nabla_\mu n_\nu - n_\mu a_\nu \,, \quad a_\nu \equiv n^\rho \nabla_\rho n_\nu \,, \end{aligned} \tag{2.26}$$

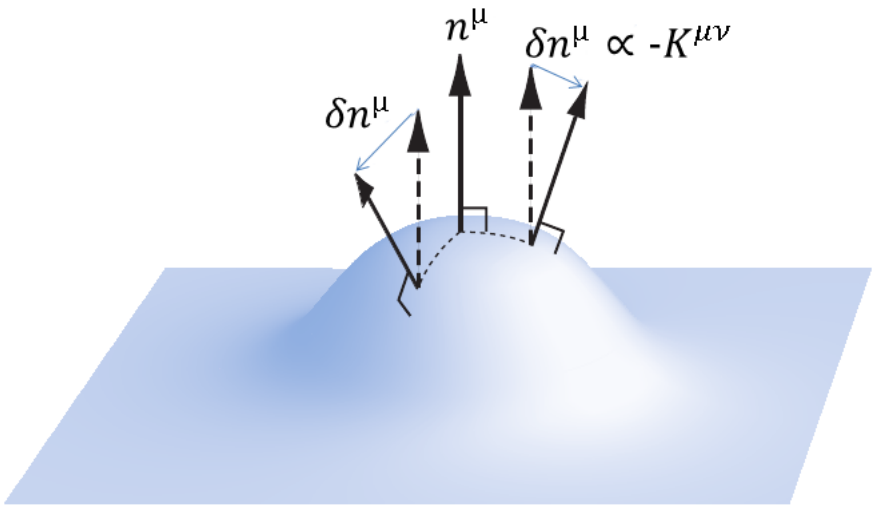

FIGURE 2.1: The extrinsic curvature is a measure of how much normal vectors to the hypersurface at neighbouring points are different to normal at the point under consideration. This image is a modified version of Figure 2.2 in Baumgarte and Shapiro [2010]

where $\mathcal{L}$ is the Lie derivative operator. Our choice of the normal vector n_μ in equation (2.22) implies that the expression for extrinsic curvature on the hypersurface Σ simplifies to

$$K_{ij} = -\nabla_i n_j \,. \tag{2.27}$$

The symmetric expansion tensor ($\Theta_{ij} = -K_{ij}$) is further decomposed in to a trace-free symmetric part called the shear tensor

$$\sigma_{ij} = \sigma_{\mu\nu} P^\mu{}_i P^\nu{}_j \,, \quad \sigma^i{}_i = 0 \,, \quad \sigma_{\mu\nu} n^\nu = 0 \,, \tag{2.28}$$

and its trace, the expansion tensor $\theta = \nabla_\mu n^\mu$, i.e.

$$-K_{ij} = \Theta_{ij} = \sigma_{ij} + \frac{1}{3}\theta g_{ij} \,, \quad -K = \theta \,. \tag{2.29}$$

The shear tensor is also defined from the expansion (2.16) in the general case even when $\omega_{\mu\nu} \neq 0$. The shear tensor represents a symmetric distortion about any spatial coordinate axis (e.g. the x-axis) in the shape of an initial sphere of test particles. Analogous to the two scalars associated with the trace and determinant of the expansion tensor we have the trace of extrinsic curvature and the rate of shear

$$K = -\theta \,, \quad \sigma^2 = \frac{1}{2}\sigma^i{}_j \sigma^j{}_i \,. \tag{2.30}$$

In the ADM gauge the 3+1 form of the Einstein's equations (2.19)–(2.21) are decomposed into constraint and evolution equations for the spatial metric, extrinsic curvature and

their derivatives. Explicitly we have the Hamiltonian constraint:

$$\mathcal{R} - K^i{}_j K^j{}_i + K^2 = 16\pi G\varepsilon\,, \tag{2.31}$$

where $\mathcal{R}$ is the Ricci scalar of the intrinsic metric, g_{ij}, on the hypersurface, and the momentum constraints:

$$K^i{}_{j||} - K_{||j} = 8\pi G J_j\,. \tag{2.32}$$

Here double vertical slash denotes covariant derivative with respect to the three metric g_{ij} , also called the first fundamental form. The evolution equation for the spatial metric is given by

$$\frac{1}{N}\partial_t g_{ij} = -2K_{ij} + \frac{1}{N}\left(N_{i||j} + N_{j||i}\right)\,, \tag{2.33}$$

and the evolution equation for the second fundamental form is given by

$$\begin{aligned}\frac{1}{N}\partial_t K^i{}_j =& \mathcal{R}^i{}_j + KK^i{}_j - \frac{1}{N}N^{||i}{}_{||j} + \frac{1}{N}\left(K^i{}_k N^k{}_{||j} - K^k{}_j N^i{}_{||k} + N^k K^i{}_{j||k}\right)\\ &- 8\pi G\left(S^i{}_j + \frac{1}{2}\delta^i_j\left(\varepsilon - S^k{}_k\right)\right)\,.\end{aligned} \tag{2.34}$$

In the next section we take the energy momentum tensor to be that of a perfect fluid and impose coordinate conditions which considerably simplify Eq. (2.31)–(2.34) . The end result is Eq. (2.39)–(2.42) , the scalar parts of Einstein's equations in the form used in the Buchert averaging formalism.

2.3 Spatial average of Einstein's equations

We take the normal vector n^μ orthogonal to the hypersufaces in (2.15) to be the 4-velocity field u^μ in the energy momentum tensor for a perfect fluid pervading the entire spacetime

$$n^\mu = u^\mu\,, \quad T_{\mu\nu} = \varepsilon u_\mu u_\nu + pP_{\mu\nu}\,, \tag{2.35}$$

where $p = p(x^\mu)$ is the fluid pressure and ε the fluid energy density. We further impose coordinate conditions by setting the shift vector to zero

$$N^i = 0\,, \tag{2.36}$$

so that all the spacetime features are hidden in the remaining lapse function N. In these coordinates the metric (2.25) becomes

$$ds^2 = -N^2 dt^2 + g_{ij}dX^i dX^j\,. \tag{2.37}$$

Using the relations

$$N_{i||j} = 0\,, \quad \frac{1}{N}N^{||i}{}_{||j} = a^i{}_{||j} + a^i a_j\,, \quad K^2 - K^i{}_j K^j{}_i = \frac{1}{3}\theta^2 - \sigma^2\,,$$

$$S^i{}_j = P^i{}_\mu P^\nu{}_j T^\mu{}_\nu = p\delta^i{}_j\,, \tag{2.38}$$

the equations (2.31)–(2.34) simplify to

$$\mathcal{R} + K^2 - K^i{}_j K^j{}_i = 16\pi G\varepsilon\,, \tag{2.39}$$

$$K^i{}_{j||i} - K_{|j} = 0\,, \tag{2.40}$$

$$\frac{1}{N}\partial_t g_{ij} = -2g_{ij}K^k{}_j\,, \tag{2.41}$$

$$\frac{1}{N}\partial_t K^i{}_j = KK^i{}_j + \mathcal{R}^i{}_j - 4\pi G\delta^i{}_j(\varepsilon - p) - (a^i{}_{||j} + a^i a_j)\,. \tag{2.42}$$

Taking the trace of (2.39) and inserting this in (2.42) gives an evolution equation for the expansion called the Raychaudhuri equation

$$\frac{1}{N}\partial_t\theta = -4\pi G(\varepsilon + 3p) + a^i{}_{||i} + a^i a_i - \frac{1}{3}\theta^2 - 2\sigma^2\,. \tag{2.43}$$

We are finally in a position to apply the Buchert formalism [Buchert, 2001] to Eq. (2.39) and the Raychaudhuri equation to study the dynamics of an averaged expanding universe. In the Buchert formalism the spatial average of a scalar field Υ is taken as

$$\langle\Upsilon\rangle := \frac{1}{V_\mathcal{D}}\int_\mathcal{D}\Upsilon J d^3X\,, \quad J := \sqrt{\det(g_{ij})}\,, \tag{2.44}$$

where $V_\mathcal{D}(t) := \int_\mathcal{D} J d^3X$. From the normalized volume we introduce a dimensionless scale factor

$$a_\mathcal{D}(t) := \left(\frac{V_\mathcal{D}}{V_{\mathcal{D}_0}}\right)^{1/3}\,, \tag{2.45}$$

for some initial volume $V_{\mathcal{D}_0}$ over a domain $\mathcal{D}_0$. And using the identity

$$\frac{1}{N}\partial_t J = \theta J\,, \tag{2.46}$$

we can relate the fractional rate of change of volume to the spatial average of the expansion θ,

$$\frac{\partial_t V_\mathcal{D}(t)}{V_\mathcal{D}(t)} = \frac{1}{V_\mathcal{D}(t)}\int_\mathcal{D}\partial_t J d^3X = \frac{1}{V_\mathcal{D}(t)}\int_\mathcal{D} N\theta J d^3X = \langle N\theta\rangle_\mathcal{D}\,. \tag{2.47}$$

By using the definition for the effective Hubble function

$$\langle N\theta\rangle = \frac{\partial_t V_\mathcal{D}(t)}{V_\mathcal{D}(t)} = 3\frac{\partial_t a_\mathcal{D}}{a_\mathcal{D}} =: 3\tilde{H}_\mathcal{D}\,, \tag{2.48}$$

and Eq. (2.44) we can derive the commutation rule

$$\partial_t\langle\Upsilon\rangle_{\mathcal{D}} - \langle\partial_t\Upsilon\rangle_{\mathcal{D}} = \langle\Upsilon N\theta\rangle_{\mathcal{D}} - \langle\Upsilon\rangle_{\mathcal{D}}\langle N\theta\rangle_{\mathcal{D}}\,. \tag{2.49}$$

We note that the commutation rule applied to the derivative of the effective Hubble function yields

$$\langle\partial_t N\theta\rangle = 3\frac{\partial_t^2 a_{\mathcal{D}}}{a_{\mathcal{D}}} + \frac{2}{3}\langle N\theta\rangle^2 - \langle N^2\theta^2\rangle\,. \tag{2.50}$$

From Eq. (2.43) we find that the averaged Raychaudhuri equation is

$$3\frac{\partial_t^2 a_{\mathcal{D}}}{a_{\mathcal{D}}} = -\frac{2}{3}\langle N\theta\rangle^2 + \frac{2}{3}\langle N^2\theta^2\rangle + \langle\theta\partial_t N\rangle - 2\langle N^2\sigma^2\rangle - 4\pi G\langle N^2(\varepsilon+3p)\rangle + \langle N^2\mathcal{A}\rangle\,, \tag{2.51}$$

where we used Eq. (2.50) and the identity

$$N\partial_t\theta = \partial_t(N\theta) - \theta\partial_t N\,. \tag{2.52}$$

By introducing kinematical and dynamical backreaction terms the averaged Raychaudhuri equation can be put in to a form analogous to the Friedmann equation of FLRW cosmology,

$$\tilde{\mathcal{Q}}_{\mathcal{D}} := \frac{2}{3}\langle(N\theta - \langle N\theta\rangle_{\mathcal{D}})^2\rangle_{\mathcal{D}} - 2\langle N^2\sigma^2\rangle_{\mathcal{D}}\,, \tag{2.53}$$

$$\tilde{\mathcal{P}}_{\mathcal{D}} := \langle N^2\mathcal{A}\rangle_{\mathcal{D}} + \langle\theta\partial_t N\rangle_{\mathcal{D}}\,, \tag{2.54}$$

$$3\frac{\partial_t^2 a_{\mathcal{D}}}{a_{\mathcal{D}}} + 4\pi G\langle N^2\varepsilon + 3N^2 p\rangle_{\mathcal{D}} \;=\; \tilde{\mathcal{Q}}_{\mathcal{D}} + \tilde{\mathcal{P}}_{\mathcal{D}}\,. \tag{2.55}$$

The averaged Hamiltonian constraint then takes the form

$$6\tilde{H}_{\mathcal{D}}^2 - 16\pi G\langle N^2\varepsilon\rangle_{\mathcal{D}} \;=\; -\left(\tilde{\mathcal{Q}}_{\mathcal{D}} + \langle\tilde{\mathcal{R}}\rangle_{\mathcal{D}}\right)\,. \tag{2.56}$$

For energy to be conserved the covariant derivative of the energy momentum tensor must vanish $\nabla_\mu T^{\mu\nu} = 0$. For a comoving observer with 4-velocity u^μ we have

$$u_\mu\nabla_\nu T^{\mu\nu} = 0 \Leftrightarrow \dot{\varepsilon} = -\theta\,(\varepsilon + p) \tag{2.57}$$

and its spatially averaged form

$$\partial_t\langle\varepsilon\rangle_{\mathcal{D}} + 3\tilde{H}_{\mathcal{D}}\langle\varepsilon + p\rangle = \langle\partial_t p\rangle_{\mathcal{D}} - \partial_t\langle p\rangle_{\mathcal{D}}\,. \tag{2.58}$$

We can think of Eq. (2.56) and (2.55) as generalized average cosmic evolution equations, analogous to the Friedmann equations, if Eq. (2.56) is differentiated with respect to t

and Eq. (2.55) is realized. This is the case if the integrability condition

$$\partial_t \tilde{\mathcal{Q}}_{\mathcal{D}} + 6\tilde{H}_{\mathcal{D}}\tilde{\mathcal{Q}}_{\mathcal{D}} + \partial_t\langle\tilde{R}\rangle_{\mathcal{D}} + 2\tilde{H}_{\mathcal{D}}\langle R\rangle_{\mathcal{D}} + 4\tilde{H}_{\mathcal{D}}\tilde{\mathcal{P}}_{\mathcal{D}} \\ -16\pi G\left[\partial_t\langle\tilde{\varepsilon}\rangle_{\mathcal{D}} + 3\tilde{H}\langle\tilde{\varepsilon}+\tilde{p}\rangle_{\mathcal{D}}\right] = 0\,, \tag{2.59}$$

is imposed.

In the Buchert formalism Eq. (2.55) and (2.56) are supplemented by the energy-momentum conservation equation (2.58) and the integrability condition (2.59) to obtain a mathematical model for studying cosmology in an averaged universe.

In the next section we present the Buchert–timescape equations for a matter and radiation fluid with their numerical solution—getting one step further towards building timescape into a full-fledged cosmological model.

2.4 Timescape cosmology with matter and radiation

The timescape model is based on the Buchert scheme for statistical averages of a fully inhomogeneous geometry, while maintaining a statistical Copernican principle. Since the Buchert scheme involves statistical quantities, additional physical assumptions are required to relate its average parameters to cosmological observables [Buchert and Carfora, 2002, 2003]. In timescape it is postulated that the relevant physical assumptions relate to gravitational energy, which provides a measure of the relative kinetic energy of regional expansion [Wiltshire, 2007a, 2008]. It is postulated that in describing the statistical cosmological geometry one can always choose a uniform Hubble flow slicing in which the effects of regional scalar spatial curvature are compensated by the choice of the canonical time coordinate of "cosmological inertial frames", namely expanding regions whose spatial extent is smaller than the (negative) curvature scale but larger than bound systems [Wiltshire, 2008].

In the ΛCDM cosmology the cosmological constant Λ, a form of dark-energy, causes the recent accelerated expansion. The physical explanation of apparent cosmic acceleration in the timescape scenario relies on the backreaction of inhomogeneities which define the average cosmic evolution, but even more on the differences of gravitational energy manifest in the canonical clocks of observers in galaxies as compared to observers in voids, where the spatial curvature is negative. These differences are insignificant in the early universe which is close to homogeneous, but grow cumulatively and become especially large when voids come to dominate the volume of the universe.

We will see that apart from the presence of the backreaction term, $\bar{\Omega}_{\mathcal{Q}}$, one key difference from the FLRW model is that the curvature parameter $\bar{\Omega}_{\rm K}$ does not scale simply in proportion to $(\bar{a}\bar{H})^{-2}$; i.e., cosmic expansion does not preserve average spatial curvature. This leads to important phenomenological differences from the FLRW models, both in the timescape scenario [Wiltshire, 2007a]–[Duley et al., 2013] and in other approaches [Roukema et al., 2013]–[Roukema et al., 2014] to backreaction. The nonrigid evolution of the average spatial curvature is subject to a cosmological test [Clarkson et al., 2008], for which current observationbal bounds [Sapone et al., 2014] are consistent with the timescape scenatio.

In the timescape cosmology we do not use the full Buchert equations (2.53)–(2.59) with inhomogeneous radiation content, rather we assume that variations in the radiation energy density and pressure are small and do not contribute to the backreaction term,

$$\partial_t \langle p_{\rm R} \rangle - \partial_t \langle p_{\rm R} \rangle = \langle p_{\rm R} \theta \rangle - \langle p_{\rm R} \rangle \langle \theta \rangle = 0 \, . \tag{2.60}$$

This assumption is justified given that fluctuations in the CMB temperature today are of the order 10^{-4} and were even smaller in the past. With homogeneous radiation the Buchert equations in the form that are used in the timescape model are:

$$\frac{3\dot{\bar{a}}^2}{\bar{a}^2} = 8\pi G \left(\langle \rho_{\rm M} \rangle + \langle \rho_{\rm R} \rangle - \frac{1}{2} \langle \mathcal{R} \rangle \right) - \frac{1}{2} \mathcal{Q} \, , \tag{2.61}$$

$$\frac{3\ddot{\bar{a}}}{\bar{a}} = -4\pi G \left(\langle \rho_{\rm M} \rangle + 2 \langle \rho_{\rm R} \rangle \right) + \mathcal{Q}, \tag{2.62}$$

$$\partial_t \langle \rho_{\rm M} \rangle + 3 \frac{\dot{\bar{a}}}{\bar{a}} \langle \rho_{\rm M} \rangle = 0 \, , \tag{2.63}$$

$$\partial_t \langle \rho_{\rm R} \rangle + 4 \frac{\dot{\bar{a}}}{\bar{a}} \langle \rho_{\rm R} \rangle = 0 \, , \tag{2.64}$$

$$\partial_t \left(\bar{a}^6 \mathcal{Q} \right) + \bar{a}^4 \partial_t \left(\bar{a}^2 \langle \mathcal{R} \rangle \right) = 0 \, . \tag{2.65}$$

The equations (2.61)–(2.65) in general do not form a complete closed system because the integrability condition, Eq. (2.65) can be used to fix just one of the two unknowns $\mathcal{Q}$ and $\langle \mathcal{R} \rangle$. The timescape model provides a physical interpretation of the Buchert time parameter, a description of the size of the averaging domain and a two-scale approach which ensure a complete set of closed differential equations. In the two-scale approach a collection of walls and voids constitute the averaging domain and the horizon volume, $\mathcal{V} = \mathcal{V}_i \bar{a}^3$. A void is constructed to have negative spatial curvature on average

$$\langle \mathcal{R}_{\rm v} \rangle = \frac{6 k_{\rm v}}{a_{\rm v}^2} \, , \tag{2.66}$$

where $a_{\rm v}$ is the scale factor with which the void evolves and $k_{\rm v} < 0$ is the Gaussian spatial curvature. A wall region evolves with a scale factor $a_{\rm w}$ and is assumed to be

spatially flat, $\langle \mathcal{R}_{\rm w} \rangle = 0$. The combined average spatial curvature is then simply from the voids $\langle \mathcal{R} \rangle = \langle \mathcal{R}_{\rm v} \rangle$. In the timescape model the scale factor appearing in the Buchert equations, which we call the volume–average scale factor, is related to wall and void scale factors by

$$\bar{a}^3 = f_{\rm vi} a_{\rm v}^3 + f_{\rm wi} a_{\rm w}^3 \,. \tag{2.67}$$

This equation sum the volumes in voids and walls to obtain $\mathcal{V} = \mathcal{V}_i \bar{a}^3$, the total horizon volume. If we rearrange Eq. (2.67) to

$$1 = f_{\rm vi} \frac{a_{\rm v}^3}{\bar{a}^3} + f_{\rm wi} \frac{a_{\rm w}^3}{\bar{a}^3} \,, \tag{2.68}$$

then we can define $f_{\rm v}(t) \equiv f_{\rm vi} \, (a_{\rm v}/\bar{a})^3$, $f_{\rm w}(t) \equiv f_{\rm wi} \, (a_{\rm w}/\bar{a})^3$ as the fraction of total volume in voids and walls respectively. This fixes $f_{\rm vi}$ and $f_{\rm wi}$ as the void and wall fractions at some initial time. From Eq. (2.67) the volume–average expansion is found to be

$$\bar{H} = \frac{1}{3} \langle \theta \rangle = f_{\rm w} H_{\rm w} + f_{\rm v} H_{\rm v} \,, \tag{2.69}$$

where

$$H_{\rm w} = \frac{1}{a_{\rm w}} \frac{{\rm d}a_{\rm w}}{{\rm d}t} \,, \quad H_{\rm v} = \frac{1}{a_{\rm v}} \frac{{\rm d}a_{\rm v}}{{\rm d}t} \tag{2.70}$$

are the expansion rates in walls and voids respectively.

In the timescape model we are able to get a closed system of differential equations because the kinematical backreaction $\mathcal{Q}$, i.e., the variance in the expansion rate is taken to be due to differences in expansion rates of walls and voids

$$\mathcal{Q} \equiv 6 f_{\rm v} f_{\rm w} \, (H_{\rm v} - H_{\rm w})^2 = \frac{2}{3} \frac{\dot{f_{\rm v}}^2}{f_{\rm v} \, (1 - f_{\rm v})} \,. \tag{2.71}$$

This extra physical assumption connects the two unknowns $\mathcal{Q}$ and $\langle \mathcal{R} \rangle$ with each other through the void fraction and its derivatives in the integrability condition Eq. (2.65) .

In the timescape model it is assumed that cosmic shear can be neglected on the scale of horizon volume averages. The Buchert equations neglect vorticity, and the effects of shear and vorticity are of the opposite sign in the generalized Raychaudhuri equation. Threfore they may be largely self-cancelling and in any case second order as compared to the variance in average expansion given in (2.71)

From the conservation equations (2.63) and (2.64) it follows that $\langle \rho_M \rangle = \bar{\rho}_{M0} \, (\bar{a}/\bar{a}_0)^{-3}$ and $\langle \rho_R \rangle = \bar{\rho}_{R0} \, (\bar{a}/\bar{a}_0)^{-4}$ are fixed at the present epoch and we can write the complete

Buchert-timescape equations as

$$\frac{\dot{\bar{a}}^2}{\bar{a}^2} + \frac{\dot{f_{\rm v}}^2}{9f_{\rm v}\left(1-f_{\rm v}\right)} - \frac{\alpha^2 f_{\rm v}^{1/3}}{\bar{a}^2} = \frac{8\pi G}{3}\left(\bar{\rho}_{\rm M0}\frac{\bar{a}_0^3}{\bar{a}^3} + \bar{\rho}_{\rm R0}\frac{\bar{a}_0^4}{\bar{a}^4}\right) , \tag{2.72}$$

$$\frac{\ddot{\bar{a}}}{\bar{a}} = \frac{2\dot{f_{\rm v}}^2}{9f_{\rm v}\left(1-f_{\rm v}\right)} - \frac{4\pi G}{3}\frac{\bar{a}_0^3}{\bar{a}^3}\left[\bar{\rho}_{\rm M0} + 2\bar{\rho}_{\rm R0}\frac{\bar{a}_0}{\bar{a}}\right] , \tag{2.73}$$

$$\ddot{f}_{\rm v} + \frac{\dot{f_{\rm v}}^2\left(2f_{\rm v}-1\right)}{2f_{\rm v}\left(1-f_{\rm v}\right)} + 3\frac{\dot{\bar{a}}}{a}\dot{f}_{\rm v} - \frac{3\alpha^2 f_{\rm v}^{1/3}\left(1-f_{\rm v}\right)}{2\bar{a}^2} = 0 , \tag{2.74}$$

$$\langle\mathcal{R}\rangle \equiv \frac{6k_{\rm v}f_{\rm vi}^{2/3}f_{\rm v}^{1/3}}{\bar{a}^2} , \qquad \mathcal{Q} \equiv \frac{2\dot{f_{\rm v}}^2}{3f_{\rm v}\left(1-f_{\rm v}\right)} , \tag{2.75}$$

$$\bar{H} \equiv \frac{\dot{\bar{a}}}{\bar{a}} = f_{\rm w}H_{\rm w} + f_{\rm v}H_{\rm v} , \tag{2.76}$$

where we have defined $\alpha^2 \equiv -k_v f_{\rm vi}^{2/3}$ to make it conspicuous that the spatial curvature in void regions is negative. Here Eq. (2.72) is the analogue of Friedmann's equation obtained from the Hamiltonian constraint, Eq. (2.31), and (2.73) is Raychaudhuri's Eq. (2.43). Equation (2.74) is the integrability condition in the timescape model written in terms of the volume–average scale factor and the void fraction.

The timescape equations can also be written in terms of the wall and void scale factors $a_{\rm w}$, $a_{\rm v}$ but the representation (2.72)–(2.76) is the most concise in form. To make the comparison with the Friedmann equations clear Eq. (2.72) can be written as

$$\bar{\Omega}_{\rm M} + \bar{\Omega}_{\rm R} + \bar{\Omega}_{\rm K} + \bar{\Omega}_{\mathcal{Q}} = 1 , \tag{2.77}$$

where

$$\bar{\Omega}_{\rm M} = \frac{8\pi G\bar{\rho}_{\rm M0}\bar{a}_0^3}{3\bar{H}^2\bar{a}^3} , \tag{2.78}$$

$$\bar{\Omega}_{\rm R} = \frac{8\pi G\bar{\rho}_{\rm R0}\bar{a}_0^4}{3\bar{H}^2\bar{a}^4} , \tag{2.79}$$

$$\bar{\Omega}_{\rm K} = \frac{\alpha^2 f_{\rm v}^{1/3}}{\bar{a}^2\bar{H}^2} , \tag{2.80}$$

$$\bar{\Omega}_{\mathcal{Q}} = \frac{-\dot{f_{\rm v}}^2}{9f_{\rm v}\left(1-f_{\rm v}\right)\bar{H}^2} = \frac{-\left(1-f_{\rm v}\right)\left(1-\bar{\gamma}\right)^2}{f_{\rm v}\bar{\gamma}^2} , \tag{2.81}$$

are the bare matter, radiation, spatial curvature and backreaction energy densities respectively. The backreaction density parameter does not have a standard model counterpart but the remaining density parameters are defined analogous to the standard model densities. In standard model spatial curvature is constant; here, however, the spatial curvature is not constant, and the time dependent factor $f_{\rm v}(t)^{1/3}$ appears in the spatial curvature energy density. In other words, space does not expand rigidly.

We provide series solutions to the system (2.72)–(2.76) at early times and an efficient numerical integrability strategy for generating the complete solution for all times in Sec. 2.4.1 and 2.4.2 . The work extends the matter only analytical solution from [Wiltshire, 2007b] to include radiation.

2.4.1 Early time series solution and numerical integration strategy

In the case of purely nonrelativistic matter, $\bar{\rho}_{\rm R} = 0$, an analytic solution of the timescape equations is readily found [Wiltshire, 2007b, 2009]. In the present case, we have not been able to find an analytical solution of the system (2.72)–(2.74) and here we present the results from a numerical solution. The issues that arise in getting a numerical solution require a modus for setting the initial conditions and a suitable integration strategy that avoids fixing the density parameters $(f_{\rm v0}, \bar{\Omega}_{\rm M0}, \bar{\Omega}_{\rm R0}, \bar{\Omega}_{\rm K0})$ independently from each other. Here we present series solutions, which naturally fix the initial conditions, and the numerical integration strategy that was adopted by Duley et al. [2013].

Observations provide a test for any cosmological model by constraining its parameters with experimental values measured at the present time. For example, the CMB temperature $T_0 = 2.7255$K at present fixes the radiation energy density parameter, $\Omega_{\rm R0}$, and number counts of galaxies set the present baryon density, $\Omega_{\rm B0}$. In the standard model of cosmology the present values of density parameters $\Omega_{\rm M0} = \Omega_{\rm CDM0} + \Omega_{\rm B0}$, $\Omega_{\rm R0}$, $\Omega_{\rm K0}$ and $\Omega_{\Lambda 0} = 1 - \Omega_{\rm M0} - \Omega_{\rm R0} - \Omega_{\rm K0}$ are enough to uniquely fix the relation between time and scale factor $x = a/a_0$ at any redshift via the integral

$$t(z) = \frac{1}{H_0} \int_0^{1/(1+z)} \frac{dx}{x\sqrt{\Omega_{\Lambda 0} + \Omega_{\rm K0} x^{-2} + \Omega_{\rm M0} x^{-3} + \Omega_{\rm R0} x^{-4}}} \,. \tag{2.82}$$

In timescape with scale factor $x = \bar{a}/\bar{a}_0$ the corresponding time integral is

$$t(\bar{z}) = \frac{1}{\bar{H}_0} \int_0^{1/(1+\bar{z})} \frac{dx}{x\sqrt{\bar{\Omega}_{\rm K0} f_{\rm v0}^{-1/3} f_{\rm v}^{1/3} x^{-2} + \bar{\Omega}_{\rm M0} x^{-3} + \bar{\Omega}_{\rm R0} x^{-4}}} \times \frac{}{\sqrt{1 + \left(\frac{df_{\rm v}}{dx}\right)^2 \frac{x^2}{9 f_{\rm v}\,(1 - f_{\rm v})}}} \,, \tag{2.83}$$

and $f_{\rm v}(x)$, $df_{\rm v}/dx$ have to be specified in addition to the present values for $f_{\rm v0}$, $\bar{\Omega}_{\rm M0} = \bar{\Omega}_{\rm CDM0} + \bar{\Omega}_{\rm B0}$, $\bar{\Omega}_{\rm R0}$ and $\bar{\Omega}_{\rm K0}$. Consequently a mere knowledge of the magnitudes of the parameters today is not sufficient and the coupled system of differential equations (2.72)–(2.74) have to be solved. Provided we know the initial values for

$$\bar{a}(t_{\rm init}) \,, \quad \left.\frac{d\bar{a}}{dt}\right|_{t_{\rm init}} \,, \quad f_{\rm v}(t_{\rm init}) \,, \quad \left.\frac{df_{\rm v}}{dt}\right|_{t_{\rm init}} \tag{2.84}$$

at some initial time $t_{\rm init}$ deep in the radiation dominated era the equations can be evolved forward in time once $\bar{\Omega}_{\rm M0}$, $\bar{\Omega}_{\rm R0}$, $\bar{\Omega}_{\rm K0}$ are fixed.

Let us assume that backreaction is negligible in the radiation dominated era then $\bar{a}(t_{\rm init}) \propto t_{\rm init}^{1/2}$ and $\dot{\bar{a}}(t_{\rm init}) \propto t_{\rm init}^{-1/2}$ but there is no way to assign $f_{\rm v}(t_{\rm init})$ and $\dot{f}_{\rm v}(t_{\rm init})$ a $t_{\rm init}$ dependence. Rather than beginning from $t_{\rm init}$ and evolving forward in time, one could start the integration at the present epoch $x = 1$, and evolve backwards in time. This requires assuming a value for the age of the universe and $\dot{f}_{\rm v}|_{x=1}$ has to be set from a constraint on the deceleration parameter $\bar{q} \equiv -\ddot{\bar{a}}/\left(\bar{H}^2\bar{a}\right)$ by using Eq. (2.62) in the form

$$\bar{q}_0 = -\frac{2}{9f_{\rm v0}\left(1-f_{\rm v0}\right)}\left[\left.\frac{df_{\rm v}}{dt}\right|_{x=1}\right]^2 + \frac{1}{2}\bar{\Omega}_{\rm M0} + \bar{\Omega}_{\rm R0}\,, \tag{2.85}$$

and would seemingly get rid of the problem of having to know $f_{\rm v}(t_{\rm init})$ as an initial condition. This method is undesirable because of the assumptions one would have to make on the parameters and in practice the method fails because the system of ODEs is numerically unstable when integrated backwards in time.

To resolve the initial value problem we found the following series solutions for $f_{\rm v}(t)$, and $\bar{a}(t)$, in powers of $\left(\bar{H}_0 t^{1/2}\right)$,

$$\begin{aligned}
\frac{\bar{a}}{\bar{a}_0} &= \sqrt{2}\bar{\Omega}_{\rm R0}^{1/4}\left(\bar{H}_0 t\right)^{1/2} + \frac{\bar{\Omega}_{\rm M0}\left(\bar{H}_0 t\right)}{3\bar{\Omega}_{\rm R0}} - \frac{7\bar{\Omega}_{\rm M0}\left(\bar{H}_0 t\right)^{3/2}}{72\sqrt{2}\bar{\Omega}_{\rm R0}^{5/4}} \\
&\quad + \left(\frac{5\bar{\Omega}_{\rm M0}^3}{216\bar{\Omega}_{\rm R0}^{3/2}} + \frac{8\bar{\alpha}^3}{25\sqrt{5}}\right)\frac{\left(\bar{H}_0 t\right)^2}{\bar{\Omega}_{\rm R0}^{1/2}} - \left(\frac{91\bar{\Omega}_{\rm M0}^3}{6912\sqrt{2}\bar{\Omega}_{\rm R0}^{3/2}} + \frac{7\sqrt{2}\bar{\alpha}^3}{75\sqrt{5}}\right)\frac{\bar{\Omega}_{\rm M0}\left(\bar{H}_0 t\right)^{5/2}}{\Omega_{\rm R0}^{5/4}} \\
&\quad + \left(\frac{\bar{\Omega}_{\rm M0}^3}{243\bar{\Omega}_{\rm R0}^{3/2}} + \frac{604\bar{\alpha}^3}{89925\sqrt{5}}\right)\frac{\Omega_{\rm M0}^2\left(\bar{H}_0 t\right)^3}{\bar{\Omega}_{\rm R0}^2} + \cdots
\end{aligned} \tag{2.86}$$

$$\begin{aligned}
\frac{f_{\rm v}}{\bar{\alpha}^3} &= \frac{2\sqrt{2}\left(\bar{H}_0 t\right)^{3/2}}{5\sqrt{5}\bar{\Omega}_{\rm R0}^{3/4}} - \frac{8\bar{\Omega}_{\rm M0}\left(\bar{H}0t\right)^2}{25\sqrt{5}\bar{\Omega}_{\rm R0}^{3/2}} + \frac{6617\bar{\Omega}_{\rm M0}^2\left(\bar{H}_0 t\right)^{5/2}}{25500\sqrt{10}\bar{\Omega}_{\rm R0}^{9/4}} \\
&\quad - \left(\frac{127\sqrt{5}\bar{\Omega}_{\rm M0}^3}{5967\bar{\Omega}_{\rm R0}^{3/2}} + \frac{576\bar{\alpha}^3}{8125}\right)\frac{\left(\bar{H}_0 t\right)^3}{\bar{\Omega}_{\rm R0}^{3/2}} \\
&\quad + \left(\frac{8811748927\bar{\Omega}_{\rm M0}^3}{100086480000\sqrt{10}\bar{\Omega}_{\rm R0}^{3/2}} + \frac{88522\sqrt{2}\bar{\alpha}^3}{1503125}\right)\frac{\bar{\Omega}_{\rm M0}\left(\bar{H}_0 t\right)^{7/2}}{\bar{\Omega}_{\rm R0}^{9/4}} + \cdots
\end{aligned} \tag{2.87}$$

where $\bar{\alpha} \equiv \alpha/\left(\bar{a}_0\bar{H}_0\right) = \bar{\Omega}_{\rm K0}^{1/2} f_{\rm v0}^{-1/6}$. It is instructive to compare Eq. (2.86) with the series for the FLRW scale factor. The FLRW model with matter and radiation has the solution

$$H_0 t = \frac{2}{3}\frac{\sqrt{\Omega_{\rm M0}a(t)/a_0 + \Omega_{\rm R0}}\left(\Omega_{\rm M0}a(t)/a_0 - 2\Omega_{\rm R0}\right)}{\Omega_{\rm M0}^2} + \frac{4}{3}\frac{\Omega_{\rm R0}^{3/2}}{\Omega_{\rm M0}}\,. \tag{2.88}$$

When expanded as a power series in t the solution takes the form

$$\frac{a}{a_0} = \sqrt{2}\Omega_{\rm R0}^{1/4}\left(H_0 t\right)^{1/2} + \frac{\Omega_{\rm M0}\left(H_0 t\right)}{3\Omega_{\rm R0}} - \frac{7\Omega_{\rm M0}\left(H_0 t\right)^{3/2}}{72\sqrt{2}\Omega_{\rm R0}^{5/4}} + \frac{5\Omega_{\rm M0}^3}{216\Omega_{\rm R0}^2}\left(H_0 t\right)^2 - \frac{91\Omega_{\rm M0}^4}{6912\sqrt{2}\Omega_{\rm R0}^{11/4}}\left(H_0 t\right)^{5/2} + \frac{\Omega_{\rm M0}^5\left(H_0 t\right)^3}{243\Omega_{\rm R0}^{7/2}} + \cdots \tag{2.89}$$

The differences between Eq. (2.86) and (2.89) appear in $O\left(\left(\bar{H}_0 t\right)^2\right)$ and higher order terms. The $\bar{a}$ series has the spatial curvature parameter $\bar{\alpha}^3$ terms superimposed on an FLRW like series for the scale factor. If $\bar{\alpha} = 0$ then $f_{\rm v} = 0$ and the correspondence between $\bar{a}$ and a_{FLRW} series becomes exact. The timescape model evolves like a spatially flat FLRW universe with matter and radiation at early times. We later on use this fact in our analysis of the CMB power spectrum in the timescape model.

The series Eq. (2.86) and (2.87) can be used to obtain series solutions for the void and wall scale factors given in Eq. (2.90) and (2.91) . Whereas in the matter only case [Wiltshire, 2009] walls evolve as an Einstein-de Sitter universe

$$\frac{a_{\rm w}(t)}{\bar{a}_0} = \left(\frac{3}{2}\sqrt{\frac{\Omega_{\rm M0}}{f_{\rm wi}}}\bar{H}_0 t\right)^{2/3},$$

and at late times voids expand as empty Milne universes $a_{\rm v}(t) = a_{v0}t$, the series for $a_{\rm v}$, $a_{\rm w}$ here show a more complex behaviour. In the timescape cosmology with radiation voids are no longer devoid of matter content although to leading order the evolution remains Milne like,

$$\begin{aligned} f_{\rm v0}^{1/3}\frac{a_{\rm v}}{a_{\rm v0}} &= \frac{2}{\sqrt{5}}\left(\bar{H}_0 t\right) + \frac{\sqrt{2}\bar{\Omega}_{\rm M0}}{15\sqrt{5}\bar{\Omega}_{\rm R0}^{3/4}}\left(\bar{H}_0 t\right)^{3/2} - \frac{209\bar{\Omega}_{\rm M0}^2}{5100\sqrt{5}\bar{\Omega}_{\rm R0}^{3/2}}\left(\bar{H}_0 t\right)^2 \\ &\quad + \left(\frac{53621\sqrt{2}\bar{\Omega}_{\rm M0}^3}{3978000\sqrt{5}\bar{\Omega}_{\rm R0}^{3/2}} + \frac{8\sqrt{2\bar{\alpha}^3}}{1625}\right)\frac{\left(\bar{H}_0 t\right)^{5/2}}{\bar{\Omega}_{\rm R0}^{3/4}} \\ &\quad - \left(\frac{261638807\Omega_{\rm M0}^3}{28149322500\sqrt{5}\Omega_{\rm R0}^{3/2}} + \frac{6716\bar{\alpha}^3}{901875\sqrt{5}}\right)\frac{\bar{\Omega}_{\rm M0}\bar{\alpha}\left(\bar{H}_0 t\right)^3}{\bar{\Omega}_{\rm R0}^{3/2}} + \cdots \end{aligned} \tag{2.90}$$

$$\begin{aligned} f_{\rm w0}^{1/3}\frac{a_{\rm w}}{a_{\rm w0}} &= \sqrt{2}\bar{\Omega}_{\rm R0}^{1/4}\left(\bar{H}_0 t\right)^{1/2} + \frac{\bar{\Omega}_{\rm M0}\left(\bar{H}_0 t\right)}{3\bar{\Omega}_{\rm R0}^{1/2}} - \frac{7\bar{\Omega}_{\rm M0}^2\left(\bar{H}_0 t\right)^{3/2}}{72\sqrt{2}\bar{\Omega}_{\rm R0}^{5/4}} \\ &\quad + \left(\frac{5\Omega_{\rm M0}^3}{216\Omega_{\rm R0}^{3/2}} + \frac{4\bar{\alpha}^3}{75\sqrt{5}}\right)\frac{\left(\bar{H}_0 t\right)^2}{\Omega_{\rm R0}^{1/2}} - \left(\frac{91\Omega_{\rm M0}^3}{6912\sqrt{2}\Omega_{\rm R0}^{3/2}} + \frac{7\sqrt{2}\bar{\alpha}^3}{225\sqrt{5}}\right)\frac{\bar{\Omega}_{\rm M0}\left(\bar{H}_0 t\right)^{5/2}}{\bar{\Omega}_{\rm R0}^{5/4}} \\ &\quad + \left(\frac{\Omega_{\rm M0}^3}{243\Omega_{\rm R0}^{3/2}} + \frac{11927\bar{\alpha}^3}{401625\sqrt{5}}\right)\frac{\bar{\Omega}_{\rm M0}^2\left(\bar{H}_0 t\right)^3}{\bar{\Omega}_{\rm R0}^2} + \cdots \end{aligned} \tag{2.91}$$

Here $a_{\rm v0} = a_{\rm v}(t_0)$ and $a_{\rm w0} = a_{\rm w}(t_0)$ and we used $a_{\rm v} = \bar{a} f_{\rm v}^{1/3} f_{\rm vi}^{-1/3} = (\bar{a}/\bar{a}_0)(f_{\rm v}/f_{\rm v0})^{1/3} a_{\rm v0}$

and $a_{\rm w} = \bar{a} f_{\rm w}^{1/3} f_{\rm wi}^{-1/3} = (\bar{a}/\bar{a}_0)(f_{\rm w}/f_{\rm w0})^{1/3} a_{\rm w0}$. We note that the power series for $\bar{a}$ and $a_{\rm w}$ have the same form with differences appearing at $O\left(\left(\bar{H}_0 t\right)^2\right)$ from the coefficients of $\bar{\alpha}$.

In the two scale model the Hubble expansion rate in voids is always larger than in walls when referred to any one set of clocks, $h_{\rm r} \equiv H_w/H_v < 1$. The series Eq. (2.92) shows that the relative expansion rate of walls and voids remains well defined in the $t \to 0$ limit. The relative expansion rate increases with time eventually approaching the value $h_r = 2/3$ of the matter only solution [Wiltshire, 2009]. Equation (2.93) for the phenomenological lapse function $\bar{\gamma} \equiv H_w/\bar{H}$ shows that the clock of volume–average and wall observers tick at the same rate when the universe is young and dominated in volume by walls:

$$h_r = \frac{1}{2} + \frac{3\bar{\Omega}_{\rm M0}\left(\bar{H}_0 t\right)^{1/2}}{20\sqrt{2}\bar{\Omega}_{\rm R0}^{3/4}} - \frac{463\bar{\Omega}_{\rm M0}^2\left(\bar{H}_0 t\right)}{6800\bar{\Omega}_{\rm R0}^{3/2}} + \left(\frac{332167\bar{\Omega}_{\rm M0}^3}{5304000\sqrt{2}\Omega_{\rm R0}^{3/2}} + \frac{\bar{\alpha}^3}{65\sqrt{5}}\right)\frac{\left(\bar{H}_0 t\right)^{3/2}}{\bar{\Omega}_{\rm R0}^{3/4}}$$
$$- \left(\frac{1452551123\bar{\Omega}_{\rm M0}^3}{50043240000\bar{\Omega}_{\rm R0}^{3/2}} + \frac{7329\bar{\alpha}^3}{120250\sqrt{5}}\right)\frac{\bar{\Omega}_{\rm M0}\left(\bar{H}_0 t\right)^2}{\bar{\Omega}_{\rm R0}^{3/2}} + \cdots \tag{2.92}$$

$$\bar{\gamma} = 1 + \frac{2\sqrt{2}\bar{\alpha}^3}{5\sqrt{5}\bar{\Omega}_{\rm R0}^{3/4}}\left(\bar{H}_0 t\right)^{3/2} - \frac{14\bar{\Omega}_{\rm M0}\bar{\alpha}^3}{25\sqrt{5}\bar{\Omega}_{\rm R0}^{3/2}}\left(\bar{H}_0 t\right)^2 + \frac{3781\bar{\Omega}_{\rm M0}^2\bar{\alpha}^3}{5100\sqrt{10}\bar{\Omega}_{\rm R0}^{9/4}}\left(\bar{H}_0 t\right)^{5/2}$$
$$- \left(\frac{142189\bar{\Omega}_{\rm M0}^3}{298350\sqrt{5}\bar{\Omega}_{\rm R0}^{3/2}} + \frac{736\bar{\alpha}^3}{8125}\right)\frac{\bar{\alpha}^3\left(\bar{H}_0 t\right)^3}{\bar{\Omega}_{\rm R0}^{3/2}} + \cdots \tag{2.93}$$

The above series solutions can be used to set the initial values for $f_{\rm v}$ and $\bar{a}$, but we must be careful in choosing the density parameters because they may not be independent. This is evident in the matter only case where the analytical solution found by Wiltshire [2009] shows the dependence of the parameters on void fraction.

$$\bar{\Omega}_{\rm M} = \frac{4(1-f_{\rm v})}{(2+f_{\rm v})^2} \tag{2.94}$$

$$\bar{\Omega}_{\rm K} = \frac{9f_{\rm v}}{(2+f_{\rm v})^2} = \frac{9}{2}\frac{\left(-\bar{\Omega}_{\rm M} - 1 + \sqrt{3\bar{\Omega}_{\rm M}+1}\right)\bar{\Omega}_{\rm M}}{\left(-1+\sqrt{3\bar{\Omega}_{\rm M}+1}\right)^2} \tag{2.95}$$

$$\bar{\Omega}_{\mathcal{Q}} = \frac{-f_{\rm v}(1-f_{\rm v})}{(2+f_{\rm v})^2} = \frac{\left(\bar{\Omega}_{\rm M} - 1 + \sqrt{3\bar{\Omega}_{\rm M}+1}\right)\left(-3\bar{\Omega}_{\rm M} - 2 + 2\sqrt{3\bar{\Omega}_{\rm M}+1}\right)}{2\left(-1+\sqrt{3\bar{\Omega}_{\rm M}+1}\right)^2} \tag{2.96}$$

$$\bar{\gamma} = \frac{1}{2}(2+f_{\rm v}) \tag{2.97}$$

$$H = \frac{(4f_{\rm v}^2 + f_{\rm v} + 4)}{2(2+f_{\rm v})}\bar{H}\ . \tag{2.98}$$

We anticipate that in the solution with radiation $\bar{\Omega}_{\rm M0}$ and $\bar{\Omega}_{\rm K0}$ cannot be set independently from $f_{\rm v0}$. We perform the numerical integration in units in which $\bar{\alpha}\bar{H}_0 t$ and $f_{\rm v}$

are treated as the dependent variables and $x \equiv \bar{a}/\bar{a}_0$ is the independent variable. It is then only necessary to prescribe just two parameter combinations $\alpha_{\rm M0} \equiv \bar{\alpha}^{-2}\bar{\Omega}_{\rm M0}$ and $\alpha_{\rm R0} \equiv \bar{\alpha}^{-2}\bar{\Omega}_{\rm R0}$, as discussed in Appendix A.

2.4.2 Numerical solutions and results

In figures 2.2 and 2.3 the void fraction $f_{\rm v}$ and bare time $\bar{H}_0 t$ are shown along with a comparison of the numerical and series solutions Eq. (A.6)–(A.7). In both instances the series solutions are in very good agreement with the exact numerical solutions up until matter–radiation equality. An important conceptual question arises about the operational interpretation of void and wall fractions at very early epochs when $f_{\rm v}(t) \ll 1$ and $f_{\rm w}(t) \approx 1$. This is because up until the time when growth of structure (chronologically much later than matter and radiation equality) causes a clear demarcation between those regions where gravitationally collapsed structures are concentrated and other regions which are largely devoid of matter content, $f_{\rm v}(t)$ and $f_{\rm w}(t)$ cannot be related to any structural entities. Before *finite infinity*[2] regions are defined, Wiltshire interprets $f_{\rm v}(t)$ as that fraction of the present horizon volume in which underdense density perturbations are not compensated by overdense density perturbations. In the series for bare scale factor, (2.86), and for the void fraction, (2.87), in the $t \to 0$ limit $\bar{a} \to 0$ and $f_{\rm v} \to 0$, but $f_{\rm v}$ approaches zero at a faster rate. Thus the perturbative interpretation of $f_{\rm v}$ remains valid even as we near the big bang singularity, $\bar{a} = 0$.

A comparison of the numerical solutions for $\bar{a}$, $a_{\rm w}$ and $a_{\rm v}$ displayed in figure 2.4 shows that at early times $\bar{a}$ grows like $a_{\rm w}$ with $a_{\rm v}$ contributing negligibly to the bare expansion. We note that in figure 2.4 the graph for $\bar{x}$ lies in between $a_{\rm w}/a_{\rm w0}$ and $a_{\rm v}/a_{\rm v0}$ because the bare scale factor

$$\bar{x}^3 \equiv \left(\frac{\bar{a}}{\bar{a}_0}\right)^3 = f_{\rm v0}\left(\frac{a_{\rm v}}{a_{\rm v0}}\right)^3 + f_{\rm w0}\left(\frac{a_{\rm w}}{a_{\rm w0}}\right)^3 , \tag{2.99}$$

is a weighted averaged of the void and wall scale factors. Equation (2.99) is a rearrangement of Eq. (2.67) in terms of the present values of wall $f_{\rm w0} = 1 - f_{\rm v0}$ and void $f_{\rm v0}$ fractions, which can take values in the range $0.50 \leq f_{\rm v0} \leq 0.8$ for realistic cosmological models. The spike in the ratio of numerical to series solutions for $a_{\rm v}$ is insignificant because the series solutions with a finite number of terms eventually break down. In practice the series solutions are never used at the relatively late times where the spike appears in figure 2.4.

An other important idea in the timescape model is that we as observers are located in a wall region. Our local metric is spatially flat and that we measure invariants

[2]See last paragraph of the section "Voids and walls" in [Wiltshire, 2009].

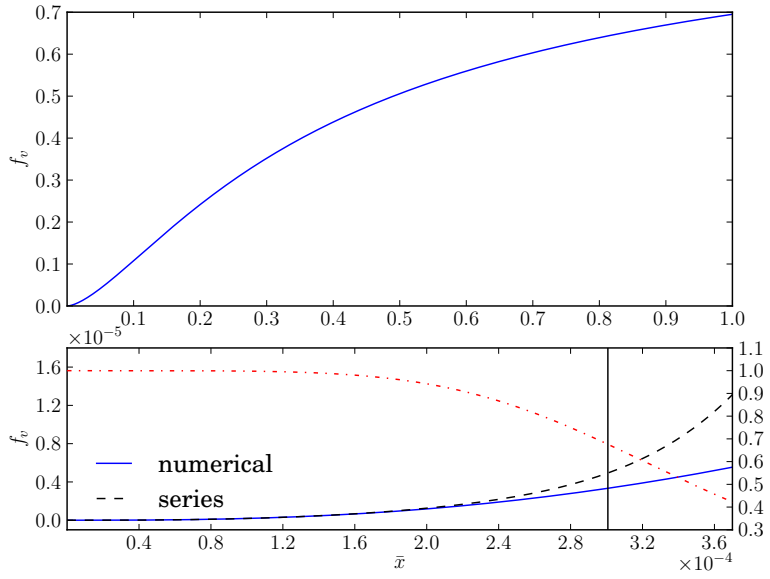

FIGURE 2.2: Void fraction, f_v for the full numerical solution as a function of the bare scale factor $\bar{x} = \bar{a}/\bar{a}_0$ is show in the top panel. In the bottom panel void fractions from the numerical solution and the series solution are compared. The dash-dotted line shows the ratio of the numerical to series solution with its y-axis shown at the right. The vertical line is drawn at the matter and radiation equality.

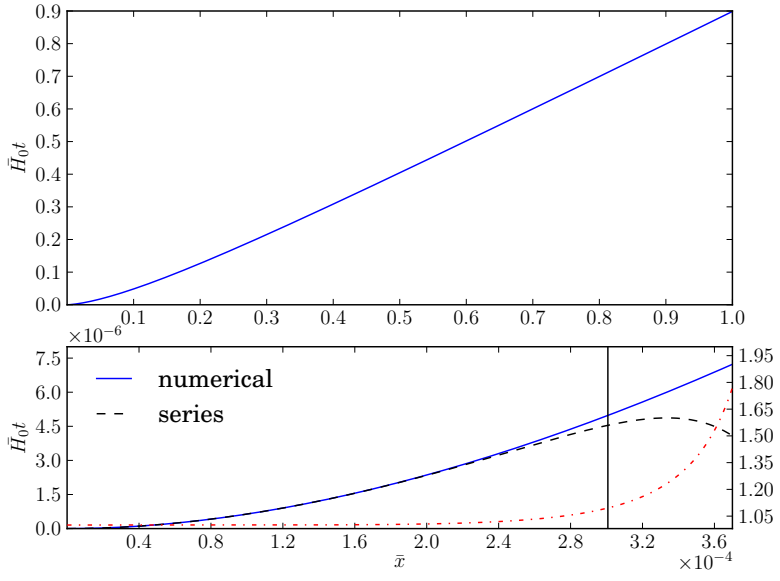

FIGURE 2.3: Bare time, t, for the full numerical solution as a function of the bare scale factor $\bar{x} = \bar{a}/\bar{a}_0$ is show in the top panel. In the bottom bare time from the numerical and the series solutions are compared. The dash-dotted line shows the ratio of the numerical to series solution with its y-axis shown at the right. The vertical line is drawn at the matter and radiation equality.

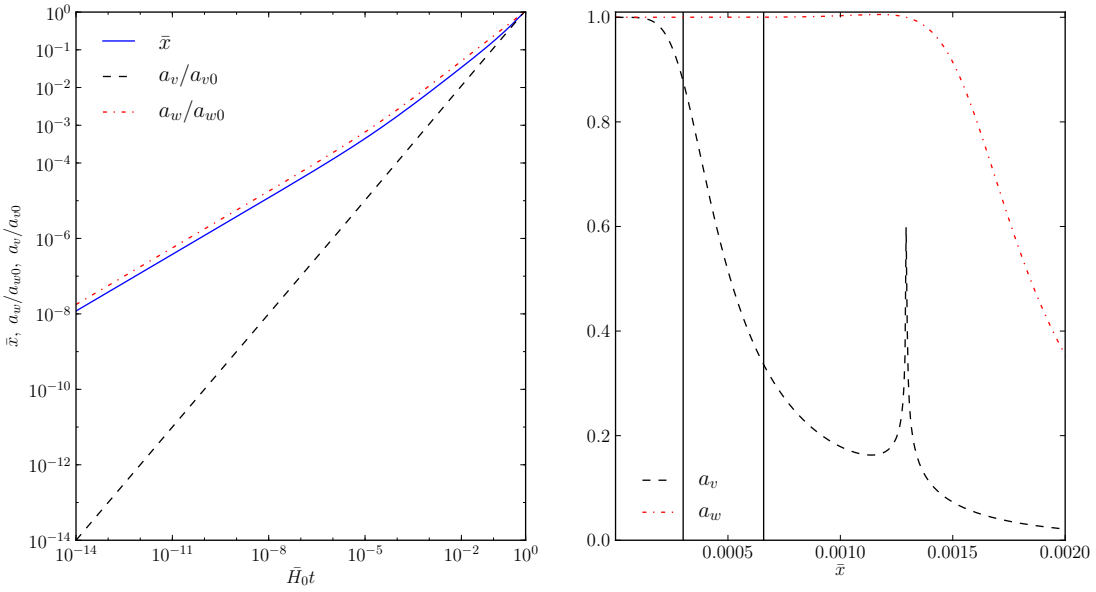

FIGURE 2.4: The bare, wall and void scale factors are shown as a function of the bare time on the left. The ratios of the numerical to series solutions are shown for the wall and void scale factors as a function of the bare scale factor $\bar{x} = \bar{a}/\bar{a}_0$ on the right. The vertical lines from left to right are drawn at the epoch of equality and decoupling respectively.

of this local metric. In Sec. 1.4.2 we discussed how the local metric is extended and adjoined to a global spherically symmetric metric via radial null geodesic matching. This matching also relates the locally inferred dressed cosmological parameters of the wall/galaxy observer to the volume–average parameters of the volume–average observer. In Fig. 2.5 the bare density parameters are shown[3] with the dressed redshift of the wall observers in the bottom x-axis and the bare redshift of the volume–average observer in the top x-axis. The numerical solutions smoothly transition from an FLRW-like evolution during radiation domination to the matter dominated epoch analytical solution found by Wiltshire [2007b]. In the timescape model the late time energy budget is dominated by spatial curvature energy density $\bar{\Omega}_{\rm K}$ and the average evolution is not that of a FLRW model.

The early time series solutions when used with our numerical integration strategy produce solutions of the Buchert equations that originate from a close to FLRW like evolution at early times and transition to an ensemble of spatially flat wall regions and negatively curved void regions at late times.

[3] A similar figure was obtained by Duley [2011], who used an alternative method to numerically integrate the timescape model equations in some particular cases. As he had not found a method for determining initial conditions with series solutions the equivalent figure is only qualitatively rather than quantitatively correct.

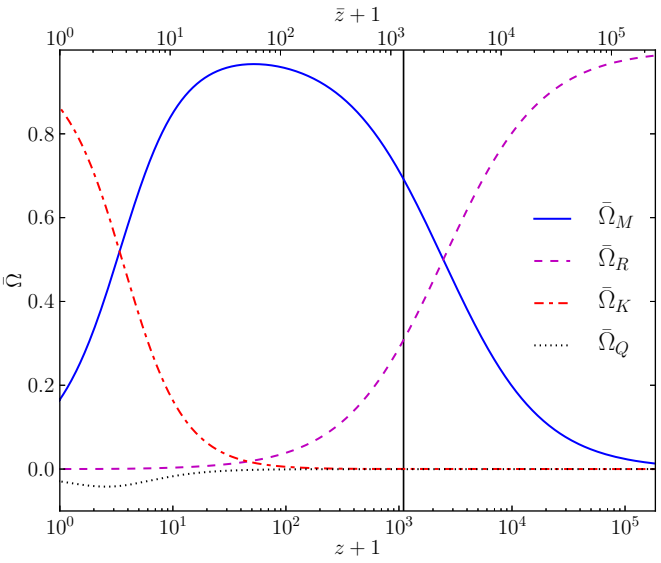

FIGURE 2.5: Bare density parameters Eq. (2.78)–(2.81) for the full numerical solution, as a function of $z+1=\bar{\gamma}\bar{a}_0/\left(\bar{\gamma}_0\bar{a}\right)$, with $\bar{H}_0=50.1\,\mathrm{km\,s^{-1}\,Mpc^{-1}}$, $f_{\mathrm{v}0}=0.695$. The redshift, z, is the dressed parameter measured by wall observers, and $\bar{z}$ is the bare redshift. The vertical bar at $1094.88<z<1100.46$ is the redshift width of the epoch of decoupling for baryon to photon ratio in the range $4.6\leq 10^{10}\bar{\eta}_{B\gamma}\leq 5.6$.

2.4.3 Recombination history in the timescape cosmology

Later on in Chapter 3 the method we employ for the analysis of CMB anisotropies requires that we know the precise values for redshift of decoupling, z_{dec}, and angular diameter distance, $d_{\mathrm{A}}(z_{\mathrm{dec}})$, to the last scattering surface. Here we give details of the recombination history of the universe in the timescape model. We stress that at early times the timescape solution is very close to an FLRW model with matter and radiation so that the universe in both models evolve almost identically. Moreover, the physical processes underling the recombination of He and H are unchanged from those in the standard model. For example, in the timscape model H recombines when the energy in CMB photons falls below its ionization energy, He^{++} becomes neutral in two steps by first gaining a single electron, and so on just as in the standard model of cosmology.

The overall temperature of the universe falls as $1/\bar{x}$. The important distinction we make is that this temperature is $\bar{T}$, the temperature measured by a volume–average observer. A wall observer sees a temperature

$$T=\bar{\gamma}\bar{T}\,. \tag{2.100}$$

The temperatures are indistinguishable before recombination when $\bar{\gamma}\approx 1$ but are significantly different today when $1.2\leq\bar{\gamma}_0\leq 1.32$. We solve for the recombination history in

volume–average temperature, $\bar{T}$, with the bare expansion, $\bar{H}$, and bare density parameters and recalibrate the solutions to get the decoupling and drag epochs measured by a wall observer according to the relations,

$$1 + z = \frac{\bar{\gamma}}{\bar{\gamma}_0}\,(1 + \bar{z})\ , \tag{2.101}$$

$$\Omega_{\rm M} = \bar{\gamma}^3 \bar{\Omega}_{\rm M}\,, \tag{2.102}$$

$$\Omega_{\rm R} = \bar{\gamma}^4 \bar{\Omega}_{\rm R}\,. \tag{2.103}$$

Numerical errors in recombination can bias extraction of cosmological parameters [Wong et al., 2008; Rubino-Martin et al., 2010]. To keep the numerical errors below statistical uncertainties in data from experiments such as Planck the recombination codes [Seager et al., 1999; Ali-Haimoud and Hirata, 2011; Chluba and Thomas, 2011] model a large number of processes to include the many relevant atomic transitions. Our aim here is not to suggest modifications to these codes in the case of an inhomogeneous universe. Rather, we want a recombination code that accurately produces the decoupling, $z_{\rm dec}$, and drag, $z_{\rm drag}$, epochs. For our purposes we found it sufficient to solve for the electron ionization fraction with the Saha equations as long as recombination to and ionization from the ground state of hydrogen is rapid and equilibrium is maintained in the chemical reaction

$$p + e \rightleftharpoons H_{1\rm s}\ .$$

When recombination to the excited states of hydrogen becomes non negligible then we employ the Peebles equations from Peebles [1968] as described below.

We follow Ma and Bertschinger [1995] and model helium and hydrogen recombination by the Saha equations

$$\frac{\bar{n}_{\rm e} X_{n+1}}{X_n} = \frac{2 g_{n+1}}{g_n}\left(\frac{m_{\rm e} k_{\rm B} \bar{T}}{2\pi\hbar^2}\right)^{3/2} \exp\left(-\chi_n/k_{\rm B}\bar{T}\right)\ , \tag{2.104}$$

$$\frac{\bar{n}_{\rm e} X_H}{1 - X_H} = \left(\frac{m_{\rm e} k_{\rm B} \bar{T}}{2\pi\hbar^2}\right)^{3/2} \exp\left(-B_1/k_{\rm B}\bar{T}\right)\ , \tag{2.105}$$

where $n = 0$ or 1, the degeneracy factors for helium are $g_0 = g_1 = 1$, $g_2 = 2$, and

$$X_H = \frac{\bar{n}_{\rm H^+}}{\bar{n}_{\rm H}}\ , \quad X_1 = \frac{\bar{n}_{\rm He^+}}{\bar{n}_{\rm He}}\ , \quad X_2 = \frac{\bar{n}_{\rm He^{++}}}{\bar{n}_{\rm He}}\ , \quad X_0 = 1 - X_1 - X_2\ .$$

Here $\bar{n}_{\rm H}$ and $\bar{n}_{\rm He}$ are the total bare number density of ionized or unionized hydrogen and helium nuclie respectively. It turns out that helium recombination is effectively completed by the epoch when the ratio $X_{\rm e} \equiv \bar{n}_{\rm e}/\bar{n}_{\rm H}$ is reduced to 0.99. The coupled equations (2.104), (2.105) are used up to this point.

From thereon we use the Peebles equations from Peebles [1968] as given in [Ma and Bertschinger, 1995] or the Weinberg equation[4] of Weinberg [2008, pp. 113-129].

$$\frac{dX_{\rm e}}{d\bar{T}} = \frac{-1}{\bar{H}\bar{T}}\left(\frac{\Gamma_{2s}+3P\Gamma_{2p}}{\Gamma_{2s}+3P\Gamma_{2p}+\beta}\right)\left[-X_{\rm e}^2+S^{-1}(1-X_{\rm e})\right]\mathcal{A}\bar{n} \tag{2.106}$$

$$S = (1-Y_{\rm p})\bar{n}_{\rm B}\left(\frac{m_{\rm e}k_{\rm B}\bar{T}}{2\pi\hbar^2}\right)^{-3/2}\exp(B_1/k_{\rm B}\bar{T}) \tag{2.107}$$

where $\mathcal{A}(\bar{\mathcal{T}})$ is the effective recombination rate to the excited $2s$ and $2p$ states; $\Gamma_{2s} = 8.22458\,{\rm s}^{-1}$ and $\Gamma_{2p} = 4.699\times10^8\,{\rm s}^{-1}$ are the decay rates from the $2s$ and $2p$ states to the ground state;

$$\beta = \left(\frac{m_{\rm e}k_{\rm B}\bar{T}}{2\pi\hbar^2}\right)^{3/2}\exp(-B_2/k_{\rm B}\bar{T})\mathcal{A} \tag{2.108}$$

is the ionization rate from the excited states;

$$P = \frac{8\pi\bar{H}}{3\lambda_\alpha^3\Gamma_{2p}\bar{n}_{1s}} \tag{2.109}$$

is the photon survival probability, with $\lambda_\alpha = 1215.682\times10^{-8}\,{\rm cm}$ and

$$B_n = \frac{m_{\rm e}{\rm e}^4}{(2\hbar^2n^2)} = 13.6n^{-2}{\rm eV}$$

is the binding energy of the state with principal quantum number n. The bare number density of hydrogen in its ground state, for a helium fraction $Y_{\rm p}$, can be approximated as $\bar{n}_{1s}\simeq(1-Y_{\rm p})\bar{n}_{\rm B}(1-X_{\rm e})$, where

$$\bar{n}_{\rm B} = \frac{3\bar{H}_0^2\bar{\Omega}_{\rm B0}}{8\pi G m_{\rm p}}\left(\frac{\bar{T}}{\bar{T}_0}\right)^3 . \tag{2.110}$$

Detailed numerical calculations of $\mathcal{A}(\bar{T})$ can be fit by the formula

$$\mathcal{A} = \frac{1.4337\times10^{-10}\bar{T}^{-0.6166}\,{\rm cm}^3{\rm s}^{-1}}{1+5.085\times10^{-3}\bar{T}^{0.5300}} , \tag{2.111}$$

where $\bar{T}$ is given in degrees Kelvin.

The Peebles and Weinberg equations produce an electron fraction $X_{\rm e}$ that agrees with Recfast (see [Seager et al., 1999; Scott and Moss, 2009]) to better than a percent during recombination, when used with an FLRW cosmology. The electron fraction $X_{\rm e}$ differs up to 30% at very low redshift, but this does not affect the calculations during recombination and $z_{\rm dec}$, $z_{\rm drag}$ are accurately calculated.

[4] Before helium has recombined $\bar{n}_{\rm e} = 2\bar{n}_{\rm He^{++}}+\bar{n}_{\rm He^{+}}+\bar{n}_{\rm H^{+}}$ and after helium has recombined $X_{\rm H} = X_{\rm e}$ as all free electrons come from ionized hydrogen.

With a solution of X_e in hand we find the decoupling epoch from the peak of the *visibility function*,

$$g(t) \equiv -c\frac{d\tau_0}{dt}\exp(-c\tau_0)\ . \tag{2.112}$$

This gives the probability that a photon last scattered at time $t(\bar{T})$ when the temperature was $\bar{T}$, where

$$\tau_0 \equiv \int_{t(\bar{T})}^{t_0} \sigma_T \bar{n}_e dt \tag{2.113}$$

is the photon *optical depth* and σ_T the Thomson scattering cross-section. In figure 2.6

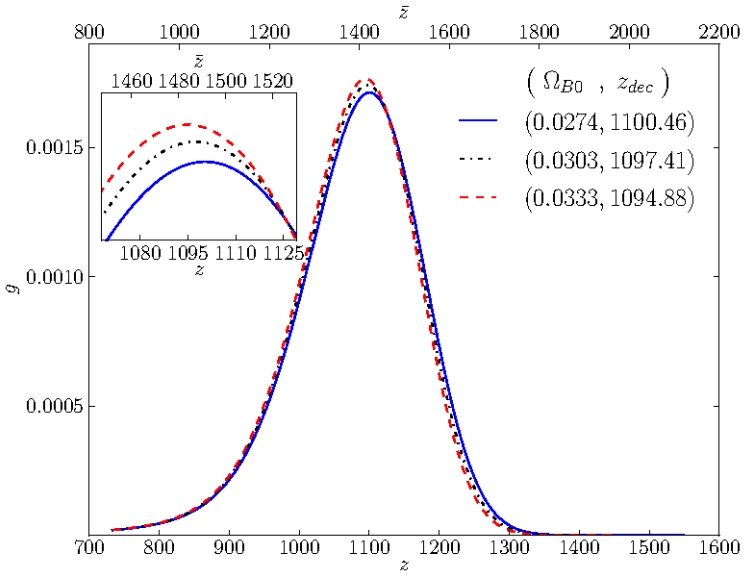

FIGURE 2.6: The photon visibility function (2.112) is shown as a function of the dressed redshift, z, bottom x-axis and bare redshift, $\bar{z}$, top x-axis. For this example, $H_0 = 61.7\,\mathrm{km\,s^{-1}\,Mpc^{-1}}$ (or $\bar{H}_0 = 50.1\,\mathrm{km\,s^{-1}\,Mpc^{-1}}$), $\Omega_{M0} = 0.410$ (or $\bar{\Omega}_{M0} = 0.167$), with three different values of the baryon to photon ratio: $10^{10}\eta_{B\gamma} = \{4.6, 5.1, 5.6\}$ (which correspond to $\bar{\Omega}_{B0} = \{0.0274, 0.0303, 0.0333\}$ respectively).

we show the visibility function with the dressed redshift of wall observer in the bottom x-axis and the bare redshift of the volume–average observer in the top x-axis. On account of Eq. (2.100) the volume–average observer sees decoupling at $\bar{z}_{dec} \neq z_{dec}$. In figure 2.7 and 2.8 we show the full range of possible variations in the dressed redshifts of decoupling and drag as we change the base parameters (h, f_{v0}).

We use the *drag depth* (see [Hu and Sugiyama, 1996])

$$\tau_d(t) \equiv \int_t^{t_0} \frac{\dot{\tau} dt}{\bar{a}R} = \int_t^{t_0} \frac{\sigma_T \bar{n}_e}{\bar{a}R}\ , \tag{2.114}$$

where $R \equiv 0.75\bar{\rho}_B/\bar{\rho}_\gamma = 0.75\left(\bar{\Omega}_{B0}\bar{a}\right) / \left(\bar{\Omega}_\gamma \bar{a}_0\right)$ to find the baryon drag epoch from the condition $c\tau_d = 1$. The drag epoch marks the epoch when baryons are released from the Compton effect; which is at a later period than photon decoupling, $z_{drag} < z_{dec}$, since there are many more photons than baryons. The drag epoch is particularly important

in baryon acoustic oscillation (BAO) studies [Anderson et al., 2013], which use galaxy clustering statistics to constrain the size of the sound horizon

$$r_{\rm s} = \int_0^{t(\bar{z}_{\rm drag})} \frac{c_{\rm s}}{\bar{a}} dt = \frac{c}{\sqrt{3}\bar{a}_0} \int_0^{x(\bar{z}_{\rm drag})} \frac{1}{\bar{x}^2 \bar{H} \sqrt{1 + 0.75 \bar{x} \bar{\Omega}_{\rm B0}/\bar{\Omega}_{\gamma 0}}} dx \tag{2.115}$$

at that time.

We find the dressed redshifts of decoupling and drag are close to the FLRW values. This is not a coincidence because by construction the wall metric is very close to a spatially flat FLRW geometry [Wiltshire, 2009]. In figure 2.9 we display contours of

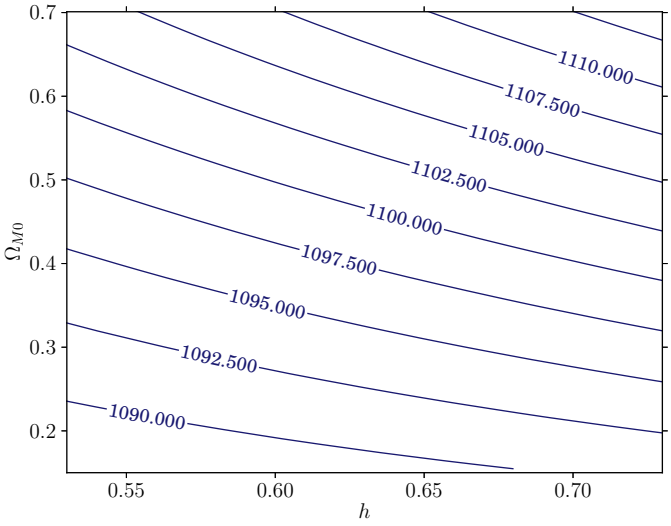

FIGURE 2.7: Contours of decoupling redshift, $z_{\rm dec}$, in the space of dressed parameters $(h,\, \Omega_{\rm M0})$, (where $H_0 = 100\,h\,{\rm km\,s^{-1}\,Mpc^{-1}}$). Contours are shown for the case $\eta_{B\gamma} = 5.1 \times 10^{-10}$.

the $\bar{\Omega}_{\rm M}/\bar{\Omega}_{\rm R}$ ratio at $z_{\rm dec}$. While there is no direct constraint on the degree to which $\bar{\Omega}_{\rm M}/\bar{\Omega}_{\rm R}$ can differ from that of the concordance ΛCDM cosmology, it is certainly the case that matter-radiation equality has to occur well before decoupling in order that the standard physics of recombination applies. In this manner we can rule out parameters $\Omega_{\rm M0} < 0.2$ if $H_0 < 65\,{\rm km\,s^{-1}\,Mpc^{-1}}$.

Here we have demonstrated that the methodologies developed for use in the standard model of cosmology to pinpoint the decoupling and drag epochs extend seamlessly for studying recombination in a Buchert averaged universe with the timescape model interpretation.

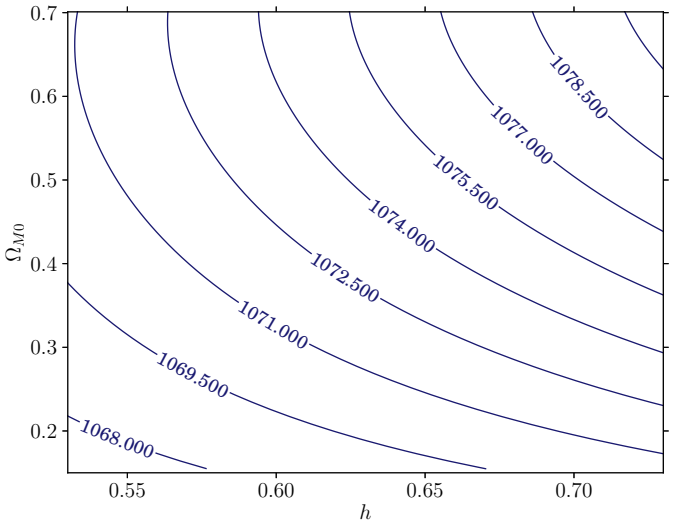

FIGURE 2.8: Drag redshift contours, $z_{\rm dec}$, in the space of dressed parameters (h, $\Omega_{\rm M0}$), (where $H_0 = 100\,h\,{\rm km\,s^{-1}\,Mpc^{-1}}$). Contours are shown for the case $\eta_{B\gamma} = 5.1 \times 10^{-10}$.

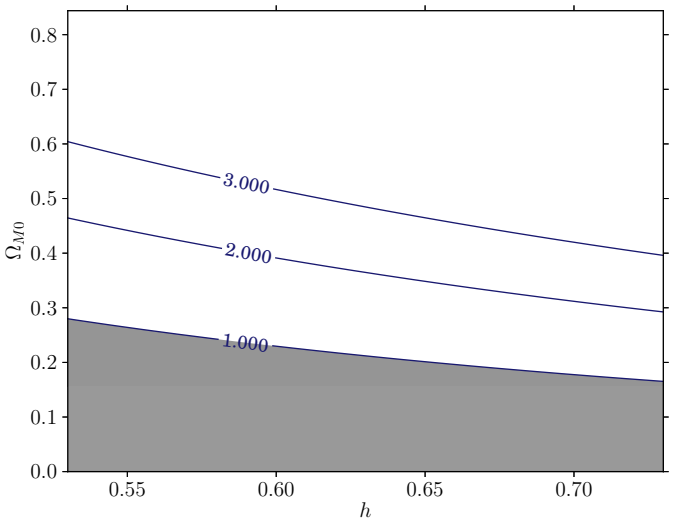

FIGURE 2.9: Contours of $\Omega_{\rm M}/\Omega_{\rm R}$ at $z_{\rm dec}$, in the space of dressed parameters (h, $\Omega_{\rm M0}$), (where $H_0 = 100\,h\,{\rm km\,s^{-1}\,Mpc^{-1}}$). The shaded region with $\Omega_{\rm M}/\Omega_{\rm R} < 1$ is certainly ruled out.

Chapter 3

Cosmic microwave background anisotropies and the timescape model

3.1 Introduction

After a variety of observational tests [Leith et al., 2008; Smale and Wiltshire, 2011; Smale, 2011; Duley et al., 2013] the timescape model remains a viable alternative to the standard model. On large scales its expansion history is so close to that of the standard model that differences in luminosity distances are at the level of current systematic uncertainties in type Ia supernova data [Smale and Wiltshire, 2011]; which model fits better depends on the method by which supernova light curves are reduced. On small scales, a study motivated by the timescape model has led to the discovery that the spherically averaged expansion of the universe below the scale of statistical homogeneity is significantly more uniform in the rest frame of the Local Group of galaxies than in the standard CMB rest frame [Wiltshire et al., 2013], a result which is very difficult to reconcile with the standard model.

To fully compete, observational tests of the timescape scenario need to be developed to a similar extent to the standard cosmology. One particularly important test is the detailed fitting of the acoustic peaks in the CMB anisotropy spectrum. Thus far we have successfully fit the angular diameter distance of the sound horizon at decoupling, which controls the overall angular scale of the acoustic peaks, thereby constraining cosmological parameters [Leith et al., 2008; Duley et al., 2013]. However, a fit of the ratios of the peak heights has not yet been performed. This work remedies that situation as we perform

the first detailed fits of the acoustic peaks in the timescape scenario. The work in this chapter was also presented in the research article Nazer and Wiltshire [2015].

The problem is a very nontrivial one, since the timescape model revisits many of the foundational questions of cosmology from first principles, and much has to be rebuilt from scratch. The timescape scenario is based on a particular physical interpretation of the Buchert averaging formalism [Buchert, 2000], and ideally in considering the early radiation dominated universe we should begin with the version of the formalism that directly includes the effects of pressure in the averaging procedure [Buchert, 2001].

A from–first–principles investigation of the Buchert formalism in the radiation–dominated epoch using the constraining principles of the timescape scenario is a huge challenge, however. Thus we will adopt the same simplification that was made in our recent paper [Duley et al., 2013], in which we assume a standard perturbed FLRW evolution at early epochs which is smoothly matched to a matter plus radiation solution in which the effects of backreaction from the radiation fluid are neglected in determining background average cosmic evolution. Only nonrelativistic matter (both baryonic and nonbaryonic) is assumed to contribute to cosmic backreaction.

Such an approximation is justified by the fact that the Universe was definitely close to being homogeneous and isotropic at early times. This approximation also allows us to make use of standard CMB codes, to the extent that all quantities must be calibrated to late epoch evolution from the timescape model, which in itself requires considerable recoding, as will be described.

The plan of this chapter is as follows: in Sec. 3.2 we briefly review the key features of the standard CMB acoustic peak analysis in the FLRW and LTB models. In Sec. 3.3 we extend this methodology to the timescape cosmology. In Sec. 3.4 our numerical computation strategy is discussed. In Sec. 3.5 we present our key results of fitting the timescape cosmology to the CMB acoustic peaks with the Planck satellite data.

3.2 CMB anisotropy overview

3.2.1 The standard FLRW model

The standard FLRW models are phenomenologically highly successful, and much of this success is built on their application to the problem of the evolution of perturbations in the early universe, and the observable signatures of these perturbations as temperature fluctuations of order $\Delta T/T \sim 10^{-5}$ in the mean CMB temperature, $T = 2.725\,\mathrm{K}$. The tools that have been developed for the analysis of CMB anisotropies, and the theoretical

framework on which they are based, have taken decades of development. Since we assume that the standard approach is a good approximation at early times, we will adopt standard tools where possible. It is there useful to firstly recall the key features of the standard approach, in order to describe which features will remain unchanged and which will be revisited.

In the standard approach CMB anisotropies are determined from density fluctuations in the early universe, which are calculated numerically by tracing the time evolution of the distributions of baryons, nonbaryonic Cold Dark Matter (CDM) and photons. The starting point is Boltzmann's equation

$$\hat{L}[f] = C[f] \tag{3.1}$$

for the time evolution of each particle distribution function, f, where $\hat{L}$ is the relativistic Liouville operator on the particle's phase space and C is a collision term describing particle production and destruction. The total time rate of change can be written along particle geodesics of a FLRW geometry with first order perturbations, such as (3.2) in the case of the Newtonian gauge.

$$\mathrm{d}s^2 = -(1+2\Phi)c^2\mathrm{d}t^2 + a^2(1-2\Psi)\delta_{ij}\mathrm{d}x^i\mathrm{d}x^j \ . \tag{3.2}$$

The Einstein field equations couple the distributions of all the interacting constituents into a system of differential equations generally referred to as the Einstein-Boltzmann equations. The presence of the collision term means that particle numbers are not necessarily conserved in phase space.

The principal epochs that are of relevance can be summarized as follows:

1. *Inflation.* Following an early period of exponentially rapid expansion and particle production, initial quantum fluctuations manifested themselves as perturbations in the densities and bulk velocities of matter fields in the energy momentum tensor. By Einstein's equations these fluctuations give rise to gravitational potentials which perturb the background metric.

2. *Big Bang Nucleosynthesis (BBN).* As the universe expanded and the temperature dropped, the light elements ^{2}H, ^{3}He, ^{4}He, and ^{7}Li were formed by a series of nuclear reactions, with final abundances relative to hydrogen which are largely determined by the baryon–to–photon ratio, $\eta_{B\gamma}$, but also by the effective number of neutrino species N_ν.

3. *Acoustic oscillations.* Before the time of last scattering and during recombination the Thomson scattering of electrons and CMB photons facilitated the transfer

of energy and momentum between these species, and also between CMB photons, protons and other charged light nuclei. The series of peaks and troughs seen in the CMB power spectrum today arise from the acoustic oscillations that propagated through the plasma of electrons, protons and CMB photons in this era. The 13.6 eV binding energy of hydrogen restricts the amplification or diminution of the amplitude of the acoustic waves in the primordial plasma to this same era.

4. *Reionization.* After recombination the direct mechanism of photon–electron scattering which alters CMB photon energies stopped until the universe was once again ionized by the bursts of radiation from the formation of the first stars. The imprint left on the CMB anisotropy spectrum from reionization is comparatively marginal, featuring principally as a reduction in amplitude which does not change the overall salient features if neglected.

5. *Light propagation through intervening structures.* Our observations of the CMB temperature anisotropies depend on the propagation of photons over the entire period from last scattering until today. Photon geodesics are affected both by the background cosmology, and the deviations from the background due to the growth of structure. One key effect is the *late time integrated Sachs–Wolfe (ISW) effect*: when CMB photons traverse a region where the gravitational potential changes over time, the boost in energy when CMB photons fall into a potential well is not cancelled by the reduction in energy when the photons climb out of the potential well. This has a significant effect for large angles in the anisotropy spectrum.

   The power spectrum is also affected by a number of secondary effects caused by cosmic structures, including the Sunyaev-Zel'dovich effect, weak gravitational lensing and changes to photon polarization. In this work, however, we are simply concerned with the primary anisotropies.

Within a specific FLRW model the features seen in the CMB power spectrum can be attributed to the relative magnitudes of the various parameters including: the Hubble constant, H_0, and the density parameters of all nonrelativistic matter, $\Omega_{\rm M0}$; baryons, $\Omega_{\rm B0}$; all radiation species, $\Omega_{\rm R0}$; photons, $\Omega_{\gamma 0}$; scalar curvature, $\Omega_{\rm K0}$; and dark energy $\Omega_{\Lambda 0}$.

A physical understanding of the features of the CMB anisotropies was made possible by the semi–analytic methods first developed by Hu and Sugiyama [1994], and later on replicated and refined by numerous other authors [Weinberg, 2008; Dodelson, 2003; Mukhanov, 2005]. A concise exposition can be found in [Lesgourgues et al., 2013], the key points relevant to our discussion of CMB anisotropies in the timescape cosmology being:

(i) The location of the first peak of the CMB temperature power spectrum in multipole space depends on the angle $\theta = d_s(t_{\rm dec})/d_{\rm A}(t_{\rm dec})$ at which the sound horizon is seen today. The angular diameter distance to the last scattering surface[1]

$$d_{\rm A}(t_{\rm dec}) = \frac{a(t_{\rm dec})\,c}{a_0 H_0 |\Omega_{\rm K0}|^{1/2}}\,{\rm sinn}\left[|\Omega_{\rm K0}|^{1/2}\int_0^{z_{\rm dec}}\frac{H_0\,{\rm d}z}{H}\right]$$

depends on the expansion rate and can change substantially with changes in $\Omega_{\Lambda 0}$, $\Omega_{\rm K0}$, and H_0. The proper scale of the sound horizon $d_s(t) = a(t)\int_0^t c_s {\rm d}t/a$ is changed when $\Omega_{\rm B0}$, $\Omega_{\rm M0}$ and $\Omega_{\rm R0}$ are changed.

(ii) The peaks and troughs in the power spectrum arise from constructive and destructive interference of the sound waves in the baryon–photon fluid. This interference is not exactly in phase or out of phase and the resulting ratios of odd to even peaks depend on $\Omega_{\rm B0}/\Omega_{\gamma 0}$ (or equivalently on $\eta_{B\gamma}$ the baryon–to–photon ratio) that determine the relative phase of the oscillating waves.

(iii) On small angular scales, or equivalently for large multipoles $\ell \sim (k/a)d_{\rm A}$ the CMB photons can diffuse and wash away anisotropies. This is apparent as a decaying of the CMB power spectrum amplitude as the multipole moments increase. In the hydrodynamic limit, with the energy momentum tensor taken to be that of an imperfect fluid, this damping of sound waves for wavelengths smaller than the diffusion length

$$\lambda_d^2 = a_L^2\int_0^{t_L}\frac{1}{6a^2(1+R)\sigma_{\rm T}n_e}\left\{\frac{16}{15}+\frac{R^2}{(1+R)}\right\}c\,{\rm d}t$$

is due to viscosity and heat conduction in the baryon–photon plasma. Here $R = (3/4)\rho_B/\rho_\gamma$, $\sigma_{\rm T}$ is the Thomson cross section and n_e is the number density of free electrons. The power spectrum at a given multipole is damped by a factor

$$\exp\left(-\frac{k^2}{a^2}\lambda_d^2\right) \approx \exp\left(-\frac{\ell^2}{d_{\rm A}^2}\lambda_d^2\right).$$

The parameters $\Omega_{\rm B0}$, $\Omega_{\rm M0}$, $\eta_{B\gamma}$ modify the power spectrum by changing $d_{\rm A}$ and λ_d in the damping factor.

(iv) The influence of reionization is to suppress the power spectrum by a factor $\exp(-\tau_{\rm reion})$, where the optical depth $\tau = \int \sigma_{\rm T} n_e\,{\rm d}t$ is evaluated at the reionization epoch. With the exception of very small multipoles the rescaling is $C_l^{\rm obs} \to \exp(-2\tau_{\rm reion})C_l^{\rm obs}$.

(v) The overall amplitude of the power spectrum is proportional to the amplitude A_s of the primordial perturbations. In this work we use the high-ℓ Planck power

[1]Here ${\rm sinn}(x) \equiv \{\sin(x),\ \Omega_{\rm K0} < 0;\ x,\ \Omega_{\rm K0} = 0;\ \sinh(x),\ \Omega_{\rm K0} > 0\}$.

spectrum data $\ell \geq 50$ and for these multipoles the reionization effect is degenerate with the primordial perturbation amplitude because the product $\exp(-\tau_{\rm reion})A_s$ multiplies the power spectrum.

(vi) The power spectrum is calculated by convolving the temperature multipoles Θ_ℓ with the primordial spectrum and integrating over all Fourier modes

$$C_l = \frac{1}{2\pi} A_s \int \frac{dk}{k} \left[\Theta_\ell(t_0, k)\right]^2 \left(\frac{k}{k_0}\right)^{n_{\rm s}-1} .$$

For small values of ℓ (large angles) the temperature multipoles are only related to the monopole at recombination and the integral can be performed analytically. For spectral index $n_{\rm s} = 1$, $C_l \sim 1/[\ell(\ell+1)]$. This scaling is visible as the Sachs-Wolfe plateau. For $n_{\rm s} < 1$, $C_l \sim 1/[\ell^{n_{\rm s}}(\ell+1)]$ and there is more power at these multipoles compared to the case of $n_{\rm s} = 1$. In general the effect of $n_{\rm s}$ on CMB power spectrum is not a simple shifting of the peaks or increase in amplitude.

3.2.2 Exact inhomogeneous models

In a step up in complexity from the homogeneous isotropic FLRW solutions the CMB has been also been studied in the spherically symmetric but inhomogeneous LTB model [Lemaître, 1933; Tolman, 1934a; Bondi, 1947]. On small scales this solution is an excellent approximation for the voids [Hoyle and Vogeley, 2002, 2004; Pan et al., 2012; Tikhonov and Karachentsev, 2006] that dominate the universe at the present epoch. Applied to gigaparsec scales the solution becomes a toy model that is physically unlikely, and which violates the Copernican principle. Nonetheless, being an exact solution of the Einstein field equations, it is amenable to direct analytic study, and such studies have included the investigation of the CMB for gigaparsec voids [Bolejko and Wyithe, 2009; Biswas et al., 2010; Clarkson and Regis, 2011; Moss et al., 2011; Nadathur and Sarkar, 2011].

The LTB solutions have a dust energy–momentum tensor, and can only apply at epochs in the matter–dominated era. An early time spherically symmetric radiation plus matter background which evolves to an LTB solution is beyond the realm of current investigations. Consequently, the study of CMB anisotropies in LTB cosmologies has to date used models which initially coincide with a FLRW model. The primary temperature anisotropies are evolved using the Boltzmann hierarchy with a FLRW background at early times and the resulting CMB power spectrum is then modified to account for differences in expansion rate, matter densities and angular diameter distances between the FLRW and LTB background solutions [Bolejko and Wyithe, 2009; Biswas et al., 2010; Clarkson and Regis, 2011; Moss et al., 2011; Nadathur and Sarkar, 2011].

Since the timescape model is close to a FLRW model at early times, a similar approach will be adopted in this work. Specifically we will adapt the method outlined in [Vonlanthen et al., 2010], in which it is shown that the CMB power spectra in two different models can be mapped on to each other as follows. Consider two cosmological models with angular diameter distances $d'_{\rm A}$ and $d_{\rm A}$ and a common proper length scale L at the surface of last scattering. This is viewed at an angle $\theta' = L/d'_{\rm A}$ and $\theta = L/d_{\rm A}$ respectively in the two models. Vonlanthen et al. [2010] show that the CMB angular power spectra in these models are related via the integral

$$C_l = \sum_{\tilde{l}} \frac{2\tilde{l}+1}{2} C'_{\tilde{l}} \int_0^\pi \sin\theta \, {\rm d}\theta \, P_{\tilde{l}} \left[\cos(\theta \, d_{\rm A}/d'_{\rm A})\right] P_\ell(\cos\theta). \tag{3.3}$$

Eq. (3.3) is derived using the assumption that apart from the overall amplitude of the two CMB power spectra, the only differences between the two spectra are due to the differences in the distance to the surface of last scattering characterized by $d'_{\rm A}$ and $d_{\rm A}$. Furthermore, for high multipoles ($\ell \geq 50$) Vonlanthen, Räsänen and Durrer show that (3.3) can be approximated as

$$C_l \approx \left(\frac{d'_{\rm A}}{d_{\rm A}}\right)^2 C'_{\frac{d'_{\rm A}}{d_{\rm A}}\ell} \, . \tag{3.4}$$

Let us refer to the cosmology with $d'_{\rm A}$ as a *reference model*. Then the C_l in the second model at any multipole ℓ is found from the scaled $\tilde{l} = \ell \, d'_{\rm A}/d_{\rm A}$ of the reference model. Zibin et al. [2007] first derived (3.4) using a different method and the revised results in [Clifton et al., 2009] also agree with (3.4).

3.3 CMB anisotropy overview for the timescape model

We will use (3.4) to calculate the CMB power spectrum in the timescape model from a reference FLRW power spectrum. In doing so, we must implicitly assume that the key features of the CMB anisotropy spectrum are close to those of a FLRW model apart from the shift factor. In particular, we neglect:

- the effects of backreaction on average cosmic evolution in the radiation dominated epoch [Buchert, 2001];
- differences in the late time ISW effect between the timescape and FLRW models.

Even if the timescape model is close to a FLRW model in the radiation dominated epoch, the detailed treatment of the late time ISW effect may differ. However, this might be

expected to only affect large angle multipoles ($\ell \lesssim 50$), and we will not include these multipoles in fitting the Planck data.

Our method of determining an appropriate FLRW reference model is complicated by the fact that in the timescape scenario one is not dealing with a single set of cosmological parameters common to all observers. In the presence of inhomogeneity there is more than one single class of average observers, and in general there are both bare and dressed cosmological parameters [Buchert and Carfora, 2002, 2003]. We will first briefly review the details of the relationship between bare and dressed parameters in the timescape model, and then describe how the methodology of Sec. 3.2 is modified to find reference FLRW models, whose expansion history from last scattering till the present is closest to that of the timescape scenario.

3.3.1 Cosmological parameters in the timescape scenario

We follow Duley et al. [2013] and Sec. 2.4 in considering a universe containing nonrelativistic matter plus radiation (photons and neutrinos), of respective densities $\rho_{\rm M}$ and $\rho_{\rm R}$, whose evolution is governed by the Buchert equations [Buchert, 2000, 2001]. The radiation pressure $P_{\rm R} = \frac{1}{3}\rho_{\rm R}c^2$ is assumed to commute under the Buchert average[2] [Buchert, 2000],

$$\partial_t \langle P_{\rm R}\rangle - \langle \partial_t P_{\rm R}\rangle = \langle P_{\rm R}\vartheta\rangle - \langle P_{\rm R}\rangle\langle\vartheta\rangle = 0, \tag{3.5}$$

throughout the evolution of the universe, so that it is solely the growth of gradients in the nonrelativistic matter density which drives the growth of inhomogeneity in the universe and backreaction on average cosmic evolution as compared to a FLRW model.

To avoid repetitive referrals to the previous chapters we re-list here the most relevant equations. With the assumption of a homogeneous background radiation the independent Buchert equations may be written as (see Sec. 2.4)

$$\bar{\Omega}_{\rm M} + \bar{\Omega}_{\rm R} + \bar{\Omega}_{\rm K} + \bar{\Omega}_{\mathcal{Q}} = 1, \tag{3.6}$$

$$\ddot{f}_{\rm v} + \frac{\dot{f}_{\rm v}^2(2f_{\rm v}-1)}{2f_{\rm v}(1-f_{\rm v})} + 3\dot{f}_{\rm v}\bar{H} - \frac{3}{2}(1-f_{\rm v})\bar{\Omega}_{\rm K}\bar{H}^2 = 0, \tag{3.7}$$

where

$$\bar{H} \equiv \frac{\dot{\bar{a}}}{\bar{a}} = f_{\rm w}H_{\rm w} + f_{\rm v}H_{\rm v}\,, \tag{3.8}$$

[2] Here ϑ is the expansion scalar and angle brackets denote the spatial volume average of a scalar quantity on the surface of average homogeneity, so that $\langle P_{\rm R}\rangle \equiv \left(\int_{\mathcal{D}} {\rm d}^3x\sqrt{\det {}^3g}\, P_{\rm R}(t,\mathbf{x})\right)/\mathcal{V}(t)$, where $\mathcal{V}(t) \equiv \int_{\mathcal{D}} {\rm d}^3x\sqrt{\det {}^3g}$ is the average spatial volume, ${}^3g_{ij}$ being the 3-metric. The domain $\mathcal{D}$ is taken to be the particle horizon volume in our case.

with $H_{\rm w} \equiv \dot{a}_{\rm w}/a_{\rm w}$ and $H_{\rm v} \equiv \dot{a}_{\rm v}/a_{\rm v}$, is the bare or volume–average Hubble parameter, and

$$\bar{\Omega}_{\rm M} = \frac{8\pi G\bar{\rho}_{M0}\bar{a}_0^3}{3\bar{H}^2\bar{a}^3}\,, \tag{3.9}$$

$$\bar{\Omega}_{\rm R} = \frac{8\pi G\bar{\rho}_{R0}\bar{a}_0^4}{3\bar{H}^2\bar{a}^4}\,, \tag{3.10}$$

$$\bar{\Omega}_{\rm K} = \frac{\alpha^2 f_{\rm v}^{1/3}}{\bar{a}^2\bar{H}^2}\,, \tag{3.11}$$

$$\bar{\Omega}_{\mathcal{Q}} = \frac{-\dot{f}_{\rm v}^{\,2}}{9f_{\rm v}(1-f_{\rm v})\bar{H}^2}\,, \tag{3.12}$$

are the volume–average or "bare" density parameters of nonrelativistic matter, radiation, average spatial curvature and kinematic backreaction.

3.3.2 Calibrating CMB anisotropies

With our ansatz for the statistical ensemble of walls and voids as discussed in Sec 1.4.2 and 2.4, and initial conditions consistent with the amplitude of density perturbations inferred from the CMB, it turns out that at any instant the magnitudes of the bare density parameters in (3.6) do not differ vastly from those of *some* Friedmann model. For example, for typical solutions [Duley et al., 2013] at last scattering the void fraction is tiny, $f_{\rm v} \sim 2\times 10^{-5}$ and $\bar{\Omega}_{\mathcal{Q}} \sim -1\times 10^{-5}$. We caution that the initial tiny void fraction does not mean that large underdense spatial regions exist prior to last scattering. Instead this small void fraction is given a perturbative interpretation; i.e., $f_{\rm v}(t)$ is that fraction of the present horizon volume in which underdense density perturbations are not compensated by overdense density perturbations. In the standard cosmology, perturbations are usually assumed to be compensated, so that the average evolution is unchanged from a given FLRW model. However this is not the case in models with backreaction.

The void fraction grows considerably over time, and backreaction grows in amplitude as the voids overtake the walls by volume, but it then subsequently decreases and its amplitude is bounded by $|\bar{\Omega}_{\mathcal{Q}}| < 0.043$. Over very small time periods there is a "closest Friedmann model" in volume–average time. However, given a backreaction term with a magnitude at the few percent level, and a non-rigidly scaling curvature parameter, the overall time evolution does differ very significantly from any single FLRW model without dark energy over long time scales.

Since $|\bar{\Omega}_{\mathcal{Q}}| \lesssim 10^{-5}$ up to last scattering, it seems reasonable to expect that the physics of the early universe is little changed in determining the acoustic oscillations in the

plasma, or any earlier processes. In determining a reference FLRW model for applying (3.4) there are two important considerations:

- Since the equations (3.6), (3.7) which are closest to the Friedmann equations are statistical equations in volume–average time, the calibration of the relevant parameters in the early universe in relation the observations of observers who measure wall time (such as ourselves) has to be carefully considered.
- To apply any existing CMB anisotropy code a reference FLRW model has to be found, whose expansion history evaluated at the present day relative to last scattering is the closest to the expansion history of a solution to (3.6), (3.7) as determined by a volume–average observer.

Let us first consider each of the epochs listed in Sec. 3.2.1 in relation to the question of calibration of parameters.

1. *Inflation.* The timescape model assumes the phenomenology of inflationary models and their predictions for the spectrum of density perturbations up to last scattering. The fact that the universe does not evolve by the Friedmann equation after last scattering means that the usual tight bounds which are often assumed to apply to the density contrast $\delta\rho/\rho(t)$ on scales at late epochs no longer apply, and this quantity can reach values of 6–8% on arbitrarily large scales by the present epoch [Wiltshire, 2008, 2011, 2015]. However, this does not directly affect measurements of the CMB anisotropy spectrum.

   The inflationary paradigm is used as a phenomenology to get an initial spectrum of scale–invariant cosmological perturbations. Strictly speaking, any mechanism such as those listed in Brandenberger [2011] that produces scale–invariant perturbations and solves the horizon problem could be used. The results from this analysis should not be construed as a test of the inflationary paradigm itself.

2. *Big bang nucleosynthesis.* There are no changes to BBN physics. However, a key parameter in determining BBN rates and subsequent light element abundances is the baryon–to–photon ratio, $\eta_{B\gamma}$. In the timescape scenario, on account of the large gradients in spatial curvature between voids and walls and the different relative clocks to which the frequency of a photon is compared, a volume–average isotropic observer will infer mean CMB temperature, $\bar{T}$, which differs from that of a wall observer according to

$$\bar{T} = \bar{\gamma}^{-1} T \,, \tag{3.13}$$

at any epoch. In particular, at the present epoch volume–average temperature $\bar{T}_0 = \bar{\gamma}_0^{-1} 2.725\,\mathrm{K}$ will be up to about 35% cooler. This recalibration of volume–average parameters changes the constraints resulting from light element abundances. In particular, for observational tests performed to date [Leith et al., 2008; Duley et al., 2013] it was possible to find a best fit with a volume–average baryon–to–photon ratio, $\eta_{B\gamma}$, which avoid a primordial lithium abundance anomaly[3] [Steigman, 2006; Cyburt et al., 2008].

3. *Acoustic oscillations.* There are no changes to the physics governing the acoustic oscillations since the effects of backreaction are neglected in the early universe. However, since $\eta_{B\gamma}$ may be recalibrated, the cosmological parameters relevant to the determination of spectral features—in particular, the ratio of nonbaryonic CDM to baryonic matter, $\Omega_{\mathrm{CDM0}} = (\Omega_{\mathrm{M0}} - \Omega_{\mathrm{B0}})/\Omega_{\mathrm{B0}}$—may differ from FLRW model values. As the ^{4}He abundance is potentially changed, this must also be accounted for in the recombination code.

4. *Reionization.* In the work here we do not assume any differences relative to a perturbative FLRW model calibrated by the timescape parameters. Furthermore, the impact of reionization on the CMB powerspectrum is degenerate with the overall amplitude in the multipole range that we consider. We treat the overall amplitude as a nuisance parameter and therefore we can not constrain the optical depth from ionization.

5. *Light propagation through intervening structures.* The dressed timescape geometry (see Sec. 1.4.2 and [Wiltshire, 2007a, 2009; Duley et al., 2013]) is used to determine the angular diameter distance of the sound horizon, and any other average observational quantities. In addition to changing the average expansion history, it is very possible that quantities such as the amplitude of the late time ISW effect may also differ between the timescape cosmology and the standard ΛCDM cosmology. However, this will be neglected here; only small angle multipoles $\ell > 50$ will be used in fitting the Planck data.

3.3.3 Matching volume–average expansion history to a FLRW model

Since the expansion history in volume–average time is assumed to be close to that of a FLRW cosmology in the early universe, and since it is physical processes up to the

[3] Light element data show an intrinsic tension between abundances of deuterium and lithium-7. For the range $\eta_{B\gamma} = (5.1 \pm 0.5) \times 10^{-10}$ all theoretical abundances fall within 2σ of observational measurements. While the agreement between theoretical and observational abundances of helium-3 and deuterium for $\eta_{B\gamma} = 5.1 \times 10^{-10}$ are not as good as for $\eta_{B\gamma} = 6.1 \times 10^{-10}$, given the measurement uncertainties theses abundances are within the acceptable range and do not introduce further anomalies.

decoupling and baryon drag epochs which are principally responsible for the observed acoustic peaks, we will aim to adapt standard numerical codes as far as is possible. However, even though the relevant physical processes occur in the early universe, standard codes for determining the acoustic peaks are calibrated to cosmological parameters, such as H_0, $\Omega_{\rm M0}$, $\Omega_{\Lambda 0}$ etc which are evaluated at the present epoch. These are related to the physical parameters in the early universe assuming the expansion history of a FLRW model. Most significantly, the perturbation equations used as the basis of the Boltzmann hierarchy use a single global background FLRW geometry, which is written in terms of present epoch cosmological parameters.

Replacing the expansion history of the FLRW model by that of the timescape model would require rewriting almost all codes from scratch, a mammoth task which is not easily realizable considering the decades of effort that have resulted in codes such as CAMB [Lewis et al., 2000] and CLASS [Lesgourgues, 2011; Blas et al., 2011]. We therefore adopt the approach of determining the acoustic peaks from a FLRW model with scale factor $\hat{a}$, whose expansion history most closely matches that of the volume–average statistical geometry. This approach is justified since it is the volume–average geometry whose expansion history describes average cosmic evolution in the sense closest to the FLRW models. Using the numerical timescape solution [Duley et al., 2013] we can estimate the difference in cosmological parameters at the epoch of decoupling.

In all cases we will match solutions by determining a FLRW solution for which

$$\frac{\hat{a}_0}{\hat{a}} = \frac{\bar{a}_0}{\bar{a}} = 1 + \bar{z} \tag{3.14}$$

at all epochs, but with a Hubble parameter which differs in general, $\hat{H} \neq \bar{H}$, meaning that the timescape matter and radiation density parameters (3.9), (3.10) will in general differ from those of the matched FLRW model. However, we will always arrange the matching so that $\hat{H} \simeq \bar{H}$ at early times. At late times we have the freedom to choose some parameters of the matched FLRW model to be equal to those of the timescape model at *one* epoch. Our choice will be to make the present epoch Hubble constant, matter and radiation parameters of the matched model (hatted variables) all equal to the corresponding bare parameters in the timescape model:

$$\hat{H}_0 = \bar{H}_0 \tag{3.15}$$

$$\hat{\Omega}_{\rm M0} = \bar{\Omega}_{\rm M0} \tag{3.16}$$

$$\hat{\Omega}_{\rm R0} = \bar{\Omega}_{\rm R0}. \tag{3.17}$$

This ensures that matter–radiation equality occurs at the same (bare) redshift, $\bar{z}$, in the timescape model as in the FLRW counterpart. Since the baryonic matter density

parameter scales in proportion to the matter density parameter, it also follows that

$$\hat{\Omega}_{\rm B0} = \bar{\Omega}_{\rm B0}. \tag{3.18}$$

Furthermore, since the Hubble constants are matched at the present epoch, we have $\hat{\Omega}_{\rm M0}\hat{h}^2 = \bar{\Omega}_{\rm M0}\bar{h}^2$, $\hat{\Omega}_{\rm B0}\hat{h}^2 = \bar{\Omega}_{\rm B0}\bar{h}^2$ and $\hat{\Omega}_{\rm R0}\hat{h}^2 = \bar{\Omega}_{\rm R0}\bar{h}^2$, which are parameter combinations typical in the standard FLRW model. With these choices the present epoch CMB temperature of the FLRW model also matches the volume–average value $\hat{T}_0 = \bar{T}_0 = \bar{\gamma}_0^{-1}T_0$, which is related to $\hat{\Omega}_{\rm R0}$ in the standard fashion,

$$\hat{\Omega}_{\rm R0} = \frac{32\sigma_{\rm B}\pi G}{3c^3\hat{H}_0^2}\left[1 + \frac{7}{8}\left(\frac{4}{11}\right)^{4/3} N_{\rm eff}\right]\hat{T}_0^4\,, \tag{3.19}$$

where $\sigma_{\rm B}$ is the Stefan–Boltzmann constant and $N_{\rm eff}$ is the effective number of neutrino species.

If we assume that the matching FLRW model is the most general model possible with both curvature and cosmological constant parameters satisfying

$$\hat{\Omega}_{\rm M} + \hat{\Omega}_{\rm R} + \hat{\Omega}_{\rm K} + \hat{\Omega}_{\Lambda} = 1, \tag{3.20}$$

then combining (3.20) with (3.15)–(3.16) at the present epoch we find

$$\hat{\Omega}_{\Lambda 0} = 1 - \hat{\Omega}_{\rm K0} - \bar{\Omega}_{\rm M0} - \bar{\Omega}_{\rm R0}. \tag{3.21}$$

This places one constraint on $\hat{\Omega}_{\rm K0}$ and $\hat{\Omega}_{\Lambda 0}$, leaving one further constraint to be found to completely fix the matched FLRW model.

In general, once matter–radiation equality is fixed to be the same in the two models then $\hat{H} \simeq \bar{H}$ at all early times when the matched FLRW equation (3.20) and the first Buchert equation (3.6) are both dominated by the matter and radiation densities, with $\hat{\Omega}_{\rm M} \simeq \bar{\Omega}_{\rm M}$ and $\hat{\Omega}_{\rm R} \simeq \bar{\Omega}_{\rm R}$. However, there are necessarily small differences in these parameters given the differences of the other density parameters appearing in (3.6) and (3.20). Different choices of the final matching constraint are found to give differences of magnitude $\delta\hat{\Omega} < 10^{-4}$ in the matched density parameters at decoupling. We have investigated the following choices (labelled A for *average* expansion history matching):

3.3.3.1 Model A($\bar{H}_{\rm dec}$): Hubble parameter matched exactly at decoupling

We can choose the Hubble parameters of the two models to be *exactly* equal at any one particular early time redshift. Let us match the Hubble parameters at decoupling. Since

we already have the condition (3.15) this further constraint ensures that the universe has decelerated by the precisely the same amount from decoupling until the present epoch in the matched FLRW model as in the volume–average geometry of the timescape model.

Equating $\hat{H}_{\rm dec} = \bar{H}_{\rm dec}$ and evaluating (3.20) at decoupling we have[4]

$$\bar{h}_{\rm dec}^{-2}\left(\hat{\Omega}_{\Lambda 0} + \hat{\Omega}_{\rm K0}\bar{x}_{\rm dec}^2 + \bar{\Omega}_{\rm M0}\bar{x}_{\rm dec}^3 + \bar{\Omega}_{\rm R0}\bar{x}_{\rm dec}^4\right) = 1\,, \tag{3.22}$$

where $\bar{h}_{\rm dec} \equiv \bar{H}_{\rm dec}/\bar{H}_0$, and $\bar{x}_{\rm dec} = \bar{a}_0/\bar{a}_{\rm dec} = 1 + \bar{z}_{\rm dec} = \bar{\gamma}_0(1+z_{\rm dec})/\bar{\gamma}_{\rm dec}$, and $\hat{\Omega}_{\Lambda 0}$ is given by (3.21). We necessarily have $\hat{\Omega}_{k\,\rm dec} < \bar{\Omega}_{k\,\rm dec}$ since $\bar{\Omega}_{\rm M} + \bar{\Omega}_{\rm R} + \bar{\Omega}_{\rm K} = 1 - \bar{\Omega}_{\mathcal{Q}} > 1$ in the timescape case, whereas the FLRW parameters satisfy (3.20). For a typical example, such as the best fit parameters of Duley et al. [2013], $\bar{\Omega}_{k\,\rm dec} - \hat{\Omega}_{k\,\rm dec} \simeq 1.2 \times 10^{-5}$, about 16% of the (small) value of $\bar{\Omega}_{k\,\rm dec}$.

By (3.22) the present present curvature parameter of the matched model is fixed to be

$$\hat{\Omega}_{\rm K0} = \frac{\bar{h}_{\rm dec}^2 + \bar{\Omega}_{\rm M0}(1-\bar{x}_{\rm dec}^3) + \bar{\Omega}_{\rm R0}(1-\bar{x}_{\rm dec}^4) - 1}{\bar{x}_{\rm dec}^2 - 1}\,. \tag{3.23}$$

3.3.3.2 Model A($\bar{r}_{\mathcal{H}}$): Match of effective bare comoving distance of particle horizon

As discussed in Sec. 6.4 of [Wiltshire, 2007a] the solution, $\bar{r}$, of the averaged Sachs optical equation

$$\ddot{\bar{r}} + \frac{\dot{\bar{a}}}{\bar{a}}\,\dot{\bar{r}} + \Big(\frac{\dot{f}_{\rm v}^{\,2}}{3f_{\rm v}(1-f_{\rm v})} - \frac{\alpha^2 f_{\rm v}^{1/3}}{\bar{a}^2}\Big)\bar{r} = 0\,. \tag{3.24}$$

provides an estimate of the effective comoving scale as would be measured by a volume average observer, and consequently of an effective volume–average angular diameter scale, $\langle d_{\rm A}\rangle = \bar{a}(t)\,\bar{r}(t)\,\delta$ for a fiducial source which subtends an angle δ in its rest frame. In work to date, we have not used this quantity since it is not directly measured at late times. Since it averages over both void and wall regions, as a function of volume–average conformal time, $\bar{\eta}$, it lies in the range $\bar{\eta} \le \bar{r}(\bar{\eta}) \le \sinh(\bar{\eta})$, where the bounds correspond to the FLRW limits: (i) $\bar{r}(\bar{\eta}) = \bar{\eta}$ when $f_{\rm v} \equiv 0$, $\dot{f}_{\rm v} \equiv 0$; (ii) $\bar{r}(\bar{\eta}) = \sinh(\bar{\eta})$, when $f_{\rm v} = {\rm const}$, $\dot{f}_{\rm v} \equiv 0$.

For any given timescape parameters, we integrate (3.24) from $t = 0$ until the present $t = t_0$ to obtain the effective bare comoving distance of the particle horizon, $\bar{r}_{\mathcal{H}}$. FLRW parameter values values $\hat{\Omega}_{\rm K0}$, $\hat{\Omega}_{\Lambda 0}$, are then chosen to simultaneously satisfy (3.21) and

[4] $\bar{h}_{\rm dec}$ should not to be confused with the unrelated dimensionless bare Hubble parameter $\bar{h}$.

the constraint

$$\bar{r}_{\mathcal{H}} = \sinh\left(\int_0^1 \frac{\hat{\Omega}_{\rm K0}^{1/2}\,{\rm d}y}{\sqrt{\hat{\Omega}_{\Lambda 0}y^4 + \hat{\Omega}_{\rm K0}y^2 + \bar{\Omega}_{\rm M0}y + \bar{\Omega}_{\rm R0}}}\right), \tag{3.25}$$

which is the equivalent solution to (3.24) in the FLRW limit with $f_{\rm v} \equiv$ const and $\dot{f}_{\rm v} \equiv 0$.

3.3.3.3 Model A($\bar{\eta}_0$): Match of bare conformal time age of universe

For any given timescape parameters, we integrate $\bar{\eta} = \int c\,{\rm d}t/\bar{a}$ from $t = 0$ until the present $t = t_0$, to obtain the bare conformal age of the universe, $\bar{\eta}_0$. FLRW parameter values $\hat{\Omega}_{\rm K0}$, $\hat{\Omega}_{\Lambda 0}$, are then chosen to simultaneously satisfy (3.21) and the constraint

$$\bar{\eta}_0 = \int_0^1 \frac{\hat{\Omega}_{\rm K0}^{1/2}\,{\rm d}y}{\sqrt{\hat{\Omega}_{\Lambda 0}y^4 + \hat{\Omega}_{\rm K0}y^2 + \bar{\Omega}_{\rm M0}y + \bar{\Omega}_{\rm R0}}}\,. \tag{3.26}$$

3.3.3.4 Model A(t_0): Match of bare age of universe

For any given timescape parameters, we determine the age of the universe in volume–average time, t_0. FLRW parameter values values $\hat{\Omega}_{\rm K0}$, $\hat{\Omega}_{\Lambda 0}$, are then chosen to simultaneously satisfy (3.21) and the constraint

$$\bar{H}_0 t_0 = \int_0^1 \frac{y\,{\rm d}y}{\sqrt{\hat{\Omega}_{\Lambda 0}y^4 + \hat{\Omega}_{\rm K0}y^2 + \bar{\Omega}_{\rm M0}y + \bar{\Omega}_{\rm R0}}}. \tag{3.27}$$

3.3.3.5 Model A($\hat{\Omega}_{\Lambda 0} = 0$): $\hat{\Omega}_{\Lambda 0} = 0$

We set $\hat{\Omega}_{\Lambda 0} = 0$ in the matched FLRW model, so that $\hat{\Omega}_{\rm K0}$ is simply given by (3.21).

3.3.3.6 Comparison of volume–average expansion history matching methods

In Fig. 3.1 we show the fractional difference in the matter plus radiation densities of the matched FLRW models which satisfy (3.15)–(3.18) relative to those of the timescape model, for the example of the best fit parameters from [Duley et al., 2013], viz., $H_0 = 61.7\,{\rm km\,s^{-1}\,Mpc^{-1}}$, $f_{\rm v0} = 0.695$, $\eta_{B\gamma} = 5.1 \times 10^{-10}$. The ratio of combined matter and radiation densities

$$\frac{\hat{\Omega}_{\rm M} + \hat{\Omega}_{\rm R}}{\bar{\Omega}_{\rm M} + \bar{\Omega}_{\rm R}} = \frac{1 - \hat{\Omega}_\Lambda - \hat{\Omega}_{\rm K}}{1 - \bar{\Omega}_{\mathcal{Q}} - \bar{\Omega}_{\rm K}} \tag{3.28}$$

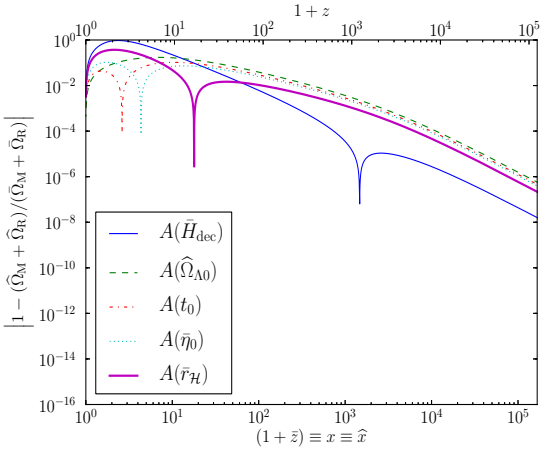

FIGURE 3.1: Fractional difference in the ratio of matter plus radiation densities of the matched FLRW models relative to the volume–average matter plus radiation densities of the timescape model, for the average expansion history matching procedures, using the best fit parameters from [Duley et al., 2013].

is initially very close to unity, and in general its departure from unity is a measure of the extent to which the sum of the dark energy and spatial curvature parameters in the matched FLRW model differ from the backreaction and curvature contributions in the timescape model. Model A($\bar{H}_{\rm dec}$), which has its final matching condition set at decoupling, has the smallest difference in the early universe with

$$\left|1-\left(\hat{\Omega}_{\rm M}+\hat{\Omega}_{\rm R}\right)/\left(\bar{\Omega}_{\rm M}+\bar{\Omega}_{\rm R}\right)\right| \lesssim 10^{-5}$$

before decoupling. For the other average expansion history matching methods, which are based on a matching condition set at late epochs, the corresponding difference is typically two orders of magnitude larger before decoupling, which still means a difference of $\lesssim 10^{-3}$.

The A($\bar{H}_{\rm dec}$) matching method is also seen to produce a closer match at early times (large redshifts) to quantities such as the volume–average Hubble parameter, expansion age and conformal time as compared to the other matching conditions, as is seen in Figs. 3.2, 3.3 and 3.4. This is true for redshifts $\bar{z} \gtrsim 70$ (bare) or $z \gtrsim 50$ (dressed). Since the physics of the early universe is the most crucial for determining the features of the acoustic peaks, we will therefore take model A($\bar{H}_{\rm dec}$) as the canonical matching method for determining the fit of the timescape model to the Planck data.

While a general trend of increased departure from FLRW–like behavior can be seen in all matching types, the largest difference in Fig. 3.1 and 3.2 for the canonical matching type $A(\bar{H}_{\rm dec})$ occurs when the backreaction contribution is at its maximum. In general

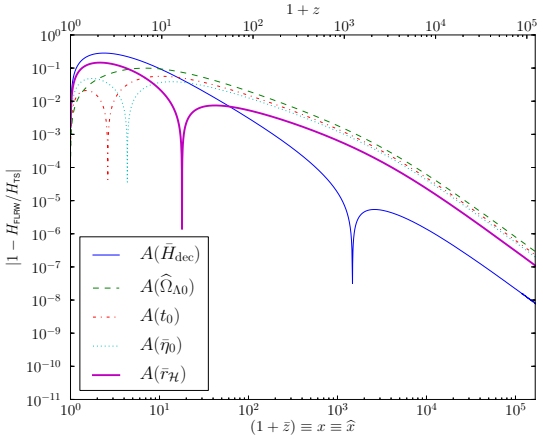

FIGURE 3.2: Fractional difference of the Hubble parameter of the matched FLRW models relative to the volume–average Hubble parameter of the timescape model, for the average expansion history matching procedures, using the best fit parameters from [Duley et al., 2013]. For all procedures $\hat{H}_0 = \bar{H}_0$ at the present epoch.

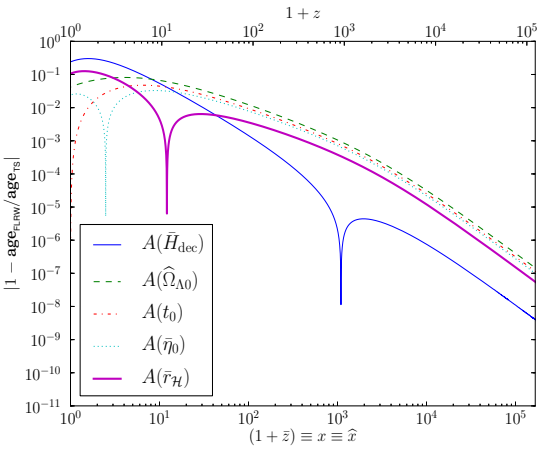

FIGURE 3.3: Fractional difference of the expansion age of the matched FLRW models relative to the volume–average expansion age of the timescape model, for the average expansion history matching procedures, using the best fit parameters from [Duley et al., 2013]. The respective present ages, $\hat{t}_0$, of the matched models are: A($\bar{H}_{\rm dec}$), 21.7 Gyr; A($\bar{r}_{\mathcal{H}}$), 19.2 Gyr; A($\bar{\eta}_0$), 17.9 Gyr; A(t_0), 17.5 Gyr; A($\hat{\Omega}_{\Lambda 0} = 0$), 16.8 Gyr.

Backreaction attains it peak of about $|\bar{\Omega}_{\mathcal{Q}}| \simeq 4.3\%$ in the dressed redshift range $1 \lesssim z \lesssim 5$ (see Fig. 1 in [Wiltshire, 2009] and also Fig. 1 in [Duley et al., 2013]). Since the impact of an increase in backreaction on volume–average time and conformal time is not immediate, but rather cumulative, for the $A(\bar{H}_{\rm dec})$ matched model the fractional difference from unity peaks at a lower redshift as seen in Fig. 3.3 and 3.4, and then drops again once $|\bar{\Omega}_{\mathcal{Q}}|$ decreases.

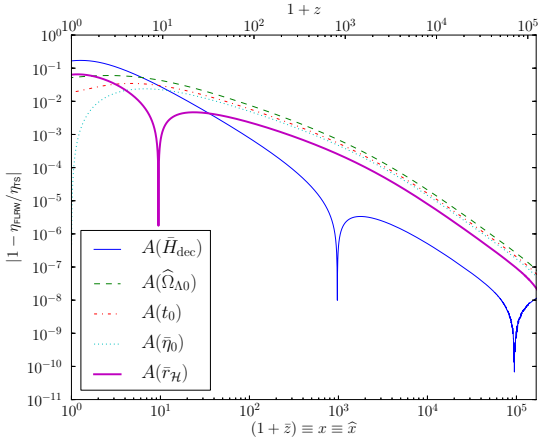

FIGURE 3.4: Fractional difference of the conformal age of the matched FLRW models relative to the volume–average expansion age of the timescape model, for the average expansion history matching procedures, using the best fit parameters from [Duley et al., 2013]. The respective present conformal ages, $\hat{\eta}_0$, of the matched models are: A($\bar{H}_{\rm dec}$), 4.06; A($\bar{r}_{\mathcal{H}}$), 3.70; A($\bar{\eta}_0$), 3.48; A(t_0), 3.41; A($\hat{\Omega}_{\Lambda 0} = 0$), 3.30.

3.3.4 Matching wall expansion history to a FLRW model

The matching methods of Sec. 3.3.3 ensure that the expansion history is as close as possible to that of the volume–average expansion history in one sense or another. It is therefore likely to accurately constrain the two free parameters that essentially describe the timescape expansion history, namely the bare Hubble constant, $\bar{H}_0$, and the void fraction, $f_{\rm v0}$, (or equivalently other pairs of independent parameters such as the dressed Hubble constant, H_0, and dressed matter density parameter, $\Omega_{\rm M0}$).

Although the differences in the density parameters of the timescape model are small as compared to the matched FLRW at early epochs (at the $\delta\hat{\Omega} < 10^{-4}$) differences which are small in terms of determining the background may nonetheless be significant in the treatment of the perturbations of the background, which are a significant part of the standard codes which we adopt in the early universe.

The timescape model incorporates the rationale that the geometry on the finite infinity scale is very close to that of a spatially flat model, becoming close to Einstein–de Sitter at late times. The relevant perturbation theory on finite infinity scales is therefore likely to be closer to that of the spatially flat matter plus radiation solution with no curvature or Λ term.

We will therefore also investigate an alternative matching procedure in which the initial conditions at decoupling are as close as possible to those of the timescape model, but the expansion history is constrained to match that of the wall geometry only rather than the

volume–average geometry. We will also consider a second model in which we perform a similar matching based on the geometry of void centres only. (These models are labeled W for *wall* expansion history matching.)

3.3.4.1 Model W($k = 0$): Match of wall expansion history

We construct a spatially flat matter plus radiation model with initial conditions matched as closely as possible to those of the wall geometry by taking density parameters

$$\widetilde{\Omega}_{\rm M} + \widetilde{\Omega}_{\rm R} = 1, \tag{3.29}$$

with respect to a spatially flat FLRW model with scale factor, $\tilde{a}$, and Hubble parameter, $\widetilde{H}$, which are matched so that the physical densities of the matter, $\tilde{\rho}_{\rm M} = 3\widetilde{H}^2\widetilde{\Omega}_{\rm M}/(8\pi G)$, and radiation, $\tilde{\rho}_{\rm R} = 3\widetilde{H}^2\widetilde{\Omega}_{\rm R}/(8\pi G)$, are equal to those of the timescape model at decoupling. Thus

$$\widetilde{H}_{\rm dec} = \bar{\Omega}_{\rm dec}^{1/2}\, \bar{H}_{\rm dec} \tag{3.30}$$

$$\widetilde{\Omega}_{\rm M\,dec} = \frac{\bar{\Omega}_{\rm M\,dec}}{\bar{\Omega}_{\rm dec}}, \tag{3.31}$$

$$\widetilde{\Omega}_{\rm R\,dec} = \frac{\bar{\Omega}_{\rm R\,dec}}{\bar{\Omega}_{\rm dec}}, \tag{3.32}$$

where

$$\bar{\Omega}_{\rm dec} = \bar{\Omega}_{\rm M\,dec} + \bar{\Omega}_{\rm R\,dec} = 1 - \bar{\Omega}_{\mathcal{Q}\rm dec} - \bar{\Omega}_{\rm K\,dec}\,. \tag{3.33}$$

On account of (3.30) the expansion of the matched model is very close to the timescape model at decoupling, but smaller by an amount $(\bar{H}_{\rm dec} - \widetilde{H}_{\rm dec})/\bar{H}_{\rm dec} < 10^{-4}$.

The expansion of the matched model from matter–radiation equality until decoupling is guaranteed to match that of the timescape model since

$$\frac{\tilde{a}_{\rm eq}}{\tilde{a}_{\rm dec}} = \frac{\widetilde{\Omega}_{\rm R\,dec}}{\widetilde{\Omega}_{\rm M\,dec}} = \frac{\bar{\Omega}_{\rm R\,dec}}{\bar{\Omega}_{\rm M\,dec}}\,. \tag{3.34}$$

The spatially flat FLRW model with matter and radiation has a Hubble parameter given by

$$\widetilde{H} = \frac{\widetilde{H}_{\rm eq}}{\sqrt{2}} \left(\frac{\tilde{a}_{\rm eq}}{\tilde{a}}\right)^2 \sqrt{1 + \frac{\tilde{a}}{\tilde{a}_{\rm eq}}}\,, \tag{3.35}$$

while the solution in terms of conformal time $\widetilde{\eta} = c\int \mathrm{d}\tilde{t}/\tilde{a}$ is given by [Mukhanov, 2005]

$$\frac{\tilde{a}}{\tilde{a}_{\rm eq}} = 2\left(\frac{\widetilde{\eta}}{\widetilde{\eta}_*}\right) + \left(\frac{\widetilde{\eta}}{\widetilde{\eta}_*}\right)^2, \tag{3.36}$$

where $\widetilde{\eta}_*^{-1} = \tilde{a}_{\rm eq}\widetilde{H}_{\rm eq}/(2\sqrt{2}\,c)$. Using (3.30)–(3.35) we find that

$$\widetilde{H} = \bar{H}_{\rm dec}\left(\frac{\tilde{a}_{\rm dec}}{\tilde{a}}\right)^{3/2}\sqrt{\bar{\Omega}_{\rm M\,dec} + \bar{\Omega}_{\rm R\,dec}\frac{\tilde{a}_{\rm dec}}{\tilde{a}}}\,. \tag{3.37}$$

In a similar fashion to the matching methods of Sec. 3.3.3 one final condition is required for the model matching. In this case we take the present epoch matched spatially flat FLRW model to match that of the wall geometry in volume average time [Wiltshire, 2007a,b]

$$\widetilde{H}_0 = H_{\rm w0} = \bar{\gamma}_0^{-1}\bar{H}_0, \tag{3.38}$$

given that the wall geometry is extremely close to an Einstein–de Sitter geometry in volume–average time at late epochs [Wiltshire, 2007b]. As a consistency check, we find numerically the present epoch expansion age of the matched spatially flat FLRW model matches that of the volume–average age of universe in the timescape model.

Combining (3.37), (3.38) we find

$$\sqrt{\bar{\Omega}_{\rm M\,dec}\widetilde{x}_{\rm dec} + \bar{\Omega}_{\rm R\,dec}} = \frac{\bar{H}_0\widetilde{x}_{\rm dec}^2}{\bar{\gamma}_0\bar{H}_{\rm dec}}\,, \tag{3.39}$$

where $\widetilde{x}_{\rm dec} \equiv \tilde{a}_0/\tilde{a}_{\rm dec}$. The expansion of the matched model until the present epoch is now completely fixed.

The notional present epoch CMB temperature of matched FLRW model is also fixed as $\widetilde{T}_0 = \widetilde{x}_{\rm dec}^{-1}\bar{T}_{\rm dec}$ in terms of the physical temperature $\bar{T}_{\rm dec}$ of the primordial plasma at decoupling. In the actual universe we see CMB photon geodesics which traverse both wall and void regions. Since the void regions expand faster, the expansion from decoupling until today is always larger in the actual universe than in the matched model here, which only has wall regions. Consequently the observed CMB temperature is always less than the notional $\widetilde{T}_0$.

For computational convenience we note that given a solution $\widetilde{x}_{\rm dec}$ of (3.39) the present epoch density parameter of the matched model are

$$\widetilde{\Omega}_{\rm M0} = \frac{\bar{\Omega}_{\rm M\,dec}\widetilde{x}_{\rm dec}}{\bar{\Omega}_{\rm M\,dec}\widetilde{x}_{\rm dec} + \bar{\Omega}_{\rm R\,dec}}, \tag{3.40}$$

$$\widetilde{\Omega}_{\rm R0} = \frac{\bar{\Omega}_{\rm R\,dec}}{\bar{\Omega}_{\rm M\,dec}\widetilde{x}_{\rm dec} + \bar{\Omega}_{\rm R\,dec}}, \tag{3.41}$$

$$\tag{3.42}$$

while $\widetilde{\Omega}_{B0}/\widetilde{\Omega}_{\rm M0} = \bar{\Omega}_{\rm B0}/\bar{\Omega}_{\rm M0}$.

3.3.4.2 Model W($k \neq 0$): Match of wall expansion history with initial curvature

Finally, in another variation the matching procedure of Sec. 3.3.4.1 is to replace (3.29)–(3.33) by

$$\widetilde{\Omega}_{\rm M} + \widetilde{\Omega}_{\rm R} + \widetilde{\Omega}_{\rm K} = 0, \tag{3.43}$$

where

$$\widetilde{H}_{\rm dec} = \bar{\Omega}_{\rm dec}^{1/2}\, \bar{H}_{\rm dec} \tag{3.44}$$

$$\widetilde{\Omega}_{\rm M\,dec} = \frac{\bar{\Omega}_{\rm M\,dec}}{\bar{\Omega}_{\rm dec}}, \tag{3.45}$$

$$\widetilde{\Omega}_{\rm R\,dec} = \frac{\bar{\Omega}_{\rm R\,dec}}{\bar{\Omega}_{\rm dec}}, \tag{3.46}$$

$$\widetilde{\Omega}_{\rm K\,dec} = \frac{\bar{\Omega}_{\rm K\,dec}}{\bar{\Omega}_{\rm dec}}, \tag{3.47}$$

with

$$\bar{\Omega}_{\rm dec} = \bar{\Omega}_{\rm M\,dec} + \bar{\Omega}_{\rm R\,dec} + \bar{\Omega}_{\rm K\,dec} = 1 - \bar{\Omega}_{\mathcal{Q}\,\rm dec}\,. \tag{3.48}$$

Once again, the expansion between matter–radiation equality and decoupling, $\tilde{a}_{\rm dec}/\tilde{a}_{\rm eq}$, matches that of the timescape model, but the matched model now has a spatial curvature term.

We are effectively still largely matching the expansion history of the wall geometry, but incorporating an initial negative curvature consistent with the initial conditions, to see whether this leads to any noticeable differences.

One may use the Friedmann equation for the matched FLRW model to determine each of the density parameters $\widetilde{\Omega}_{\rm M0}$, $\widetilde{\Omega}_{\rm R0}$ and $\widetilde{\Omega}_{\rm K0}$ at the present epoch in terms of their values at decoupling, $\widetilde{\Omega}_{\rm M\,dec}$, $\widetilde{\Omega}_{\rm R\,dec}$, $\widetilde{\Omega}_{\rm K\,dec}$, and the redshift factor $\widetilde{x}_{\rm dec} = \tilde{a}_0/\tilde{a}_{\rm dec} \equiv 1 + \widetilde{z}$. If one combines the resulting expression with (3.44)–(3.48) one finds

$$\widetilde{\Omega}_{\rm M0} = \frac{\bar{\Omega}_{\rm M\,dec}\widetilde{x}_{\rm dec}}{\Delta}, \tag{3.49}$$

$$\widetilde{\Omega}_{\rm R0} = \frac{\bar{\Omega}_{\rm R\,dec}}{\Delta}, \tag{3.50}$$

$$\widetilde{\Omega}_{\rm K0} = \frac{\bar{\Omega}_{\rm K\,dec}\widetilde{x}_{\rm dec}^2}{\Delta}, \tag{3.51}$$

where

$$\Delta \equiv \bar{\Omega}_{\rm K\,dec}\widetilde{x}_{\rm dec}^2 + \bar{\Omega}_{\rm M\,dec}\widetilde{x}_{\rm dec} + \bar{\Omega}_{\rm R\,dec}. \tag{3.52}$$

Since there is now a constant negative spatial curvature, which is a feature of neither walls nor voids in the timescape model, there is no appropriate expansion rate to match to at the present epoch. Instead we will take the present epoch expansion age of the matched solution to be the age of the universe in volume–average time, similar to the case of Sec. 3.3.4.1. This leads to the constraint

$$\bar{H}_{\rm dec} t_0 = \int_0^{\widetilde{x}_{\rm dec}} \frac{u\,{\rm d}u}{\sqrt{\bar{\Omega}_{\rm K\,dec} u^2 + \bar{\Omega}_{\rm M\,dec} u + \bar{\Omega}_{\rm R\,dec}}}\,, \tag{3.53}$$

which can be used to solve for $\widetilde{x}_{\rm dec}$ and consequently fully constrain the matched model, with density parameters given by (3.49)–(3.52) and present epoch Hubble parameter

$$\widetilde{H}_0 = \bar{H}_{\rm dec} \sqrt{\bar{\Omega}_{\rm K\,dec} \widetilde{x}_{\rm dec}^{-2} + \bar{\Omega}_{\rm M\,dec} \widetilde{x}_{\rm dec}^{-3} + \bar{\Omega}_{\rm R\,dec} \widetilde{x}_{\rm dec}^{-4}}. \tag{3.54}$$

This concludes the possible matching procedures we have investigated. There is no equivalent procedure based on the void expansion rate only. The voids initially form a tiny fraction of the volume and are not representative of average conditions. At late epochs the voids dominate by volume with an expansion rate close to that of an empty Milne universe. An empty universe model cannot be used as the basis of perturbation theory, however.

3.4 CMB analysis: computational methodology

Insofar as the details of the evolution of the primordial plasma in the universe can be assumed to be given by a standard FLRW model then for multipoles $\ell > 50$ we might expect the matching procedures of Sec. 3.3.3, 3.3.4 to give reasonably accurate quantitative estimates of CMB constraints on timescape model parameters. We therefore use the timescape theoretical CMB temperature power spectrum which we obtain from each matched FLRW model and eq. (3.4) with the Planck CMB data [Ade et al., 2014a] to constrain timescape parameters.

To find timescape parameters that fit the Planck CMB temperature power spectrum data [Ade et al., 2014a] we employ Bayesian analysis to obtain parameter constraints with the affine invariant[5] Markov chain Monte Carlo (MCMC) algorithm [Goodman and

[5] Unlike the traditional Metropolis–Hastings [Metropolis et al., 1953] algorithm the affine invariant MCMC does not require a knowledge of the covariance matrix of the MCMC parameters and has the additional advantage of a high acceptance rate. The algorithm only requires the user to select the initial MCMC values close to the best fit parameters and provide an estimate of the errors in the parameters. The algorithm then explores the full parameter space. In a comparison of the Metropolis–Hastings [Lewis and Bridle, 2002], nested sampling and the affine invariant sampling techniques by Allison and Dunkley [2013], the affine invariant algorithm is shown to perform very well.

Weare, 2010] using its python implementation [Foreman-Mackey et al., 2013]. We fit the parameters of each matched FLRW universe by computing its CMB power spectrum with the CLASS Boltzmann code [Lesgourgues, 2011; Blas et al., 2011]. We modified the code to allow for the different parameter ranges with extended bounds, as required by the matched FLRW models.

All FLRW model matching procedures also require that we solve the timescape equations with matter and radiation to find the exact present epoch timescape parameter values, as described in [Duley et al., 2013]. We must further extend our previous numerical computations [Duley et al., 2013], as the photon–baryon ratio, $\eta_{B\gamma}$, will now also be included as a base parameters for the MCMC analysis. In this section we outline the details of all our numerical computations.

3.4.1 Big bang nucleosynthesis

To date all studies of the timescape model have assumed a range of values for the baryon–to–photon ratio, $\eta_{B\gamma}$, consistent with observed light element abundances that avoid the lithium–7 abundance anomaly [Steigman, 2006; Cyburt et al., 2008]. However, $\eta_{B\gamma}$ was not constrained from CMB data. Here we will constrain $\eta_{B\gamma}$ directly from the Planck data. We take $\eta_{B\gamma}$ as an MCMC parameter and treat $h^2\bar{\Omega}_{\rm B0}$ as a derived parameter, in contrast to ΛCDM model studies which commonly use $h^2\Omega_{\rm B0}$ as a base MCMC parameter.

Since FLRW model calibrations are built into the BBN characterization of many standard CMB codes, we perform our own BBN calculations by adapting the *fastbbn* code[6] of Sarkar and collaborators [Fiorentini et al., 1998; Lisi et al., 1999]. The code takes $\eta_{B\gamma}$ and $N_{\rm eff}$ as free parameters and determines light element abundances, including the helium fraction, $Y_{\rm P}$ [Fiorentini et al., 1998; Lisi et al., 1999]. This value of $Y_{\rm P}$ is then used in the timescape recombination calculation, and is also passed to the Boltzmann code of the matched FLRW model.

For the base timescape model we have fixed $N_{\rm eff} = 3.046$ and used $Y_{\rm P} = Y_{\rm P}(N_{\rm eff} = 3.046, \eta_{B\gamma})$ so that $Y_{\rm P}$ is determined by $\eta_{B\gamma}$ alone. We have also investigated $Y_{\rm p} = Y_{\rm p}(N_{\rm eff}, \eta_{B\gamma})$ with $N_{\rm eff}$ free to parametrize additional relativistic components.

Another alternative is to ignore the BBN determination of $Y_{\rm p}$ from $N_{\rm eff}$ and $\eta_{B\gamma}$ altogether and add $Y_{\rm p}$ to the list of MCMC parameters. This way $Y_{\rm p}$ is allowed to vary freely and the Planck CMB data alone sets its value. This can be done with $N_{\rm eff} = 3.046$

[6] http://www-thphys.physics.ox.ac.uk/users/SubirSarkar/bbn/fastbbn.f

fixed or free to vary. We have not investigated this last possibility, which if carried out can be regarded as a consistency check of BBN theoretical predictions.

3.4.2 Decoupling and recombination

To determine timescape parameters we numerically integrate the timescape equations with matter and radiation, using methods given in Duley et al. [2013] and Sec 2.4. We also determine precise values for the redshift of decoupling—both bare $\bar{z}_{\rm dec}$ and dressed $z_{\rm dec}$—and the dressed angular diameter distance to the last scattering surface at decoupling [Wiltshire, 2007a]

$$d_{\rm A\,dec} = \bar{a}_{\rm dec}\bar{\gamma}_{\rm dec}(1-f_{\rm v\,dec})^{1/3}\int_{t_{\rm dec}}^{t_0}\frac{{\rm d}t}{\bar{\gamma}\,(1-f_{\rm v})^{1/3}\,\bar{a}}, \tag{3.55}$$

which is needed to shift the CMB power spectrum in multipole space and also for matching procedures A($\bar{H}_{\rm dec}$), W($k=0$) and W($k\neq 0$).

In our previous work [Duley et al., 2013] the effects of helium recombination were not included, and we used the Saha equation only for hydrogen at $\bar{T} = 4226\,{\rm K}$ to set the initial condition for the electron ionization fraction in Eq. (2.106) of Sec. 2.4.3. To produce more accurate results, we wrote a simple recombination code that solves for hydrogen and helium ionization fractions, following methods given in [Weinberg, 2008; Ma and Bertschinger, 1995; Peebles, 1968] and outlined in Sec. 2.4.3 in terms of the volume–average temperature $\bar{T}$ in the timescape model. Our recombination code produces results that are consistent with HyRec [Ali-Haimoud and Hirata, 2011] and RECFAST [Seager et al., 1999; Scott and Moss, 2009] when used with an FLRW solution. We code for helium recombination [Ma and Bertschinger, 1995; Peebles, 1968] beginning at bare redshift $\bar{z} = 10000$, with the initial helium fraction determined directly from our own BBN code as the parameters $\eta_{B\gamma}$ and $N_{\rm eff}$ are varied.

Including the effects of helium recombination changes the dressed redshift of decoupling slightly as compared to [Duley et al., 2013], but has a somewhat more substantial effect on the estimate of the baryon drag epoch. This can be seen in Figs. 3.5, 3.6, where we plot contours of $z_{\rm dec}$ and $z_{\rm drag}$ for three values of the baryon–to–photon ratio: $\eta_{B\gamma} = 5.1\times10^{-10}$ as used in Fig. 3 and 4 of ref. [Duley et al., 2013], $\eta_{B\gamma} = 6.04\times10^{-10}$ which is a best fit to the ΛCDM model with the Planck data [Ade et al., 2014b], and $\eta_{B\gamma} = 6.465\times10^{-10}$ which is a best fit for fixed $N_{\rm eff} = 3.046$ using the canonical $A(\bar{H}_{\rm dec})$ matching method.

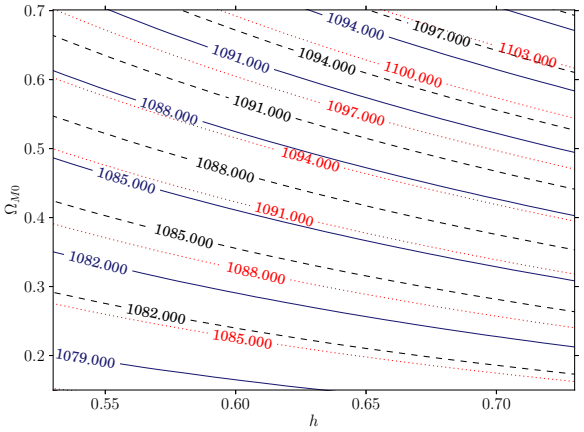

FIGURE 3.5: Contours of dressed redshift of decoupling, $z_{\rm dec}$, in the space of dressed parameters (h, $\Omega_{\rm M0}$), (where $H_0 = 100\,h\,{\rm km\,s^{-1}\,Mpc^{-1}}$). Contours are shown for the cases $10^{10}\eta_{B\gamma} = 5.1$ (dotted line), 6.04 (solid line) and 6.465 (dashed line).

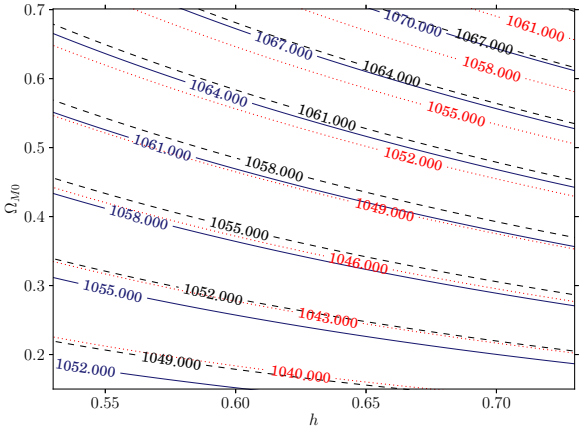

FIGURE 3.6: Contours of the dressed redshift of the baryon drag epoch, $z_{\rm drag}$, in the space of dressed parameters (h, $\Omega_{\rm M0}$), (where $H_0 = 100\,h\,{\rm km\,s^{-1}\,Mpc^{-1}}$). Contours are shown for the cases $10^{10}\eta_{B\gamma} = 5.1$ (dotted line), 6.04 (solid line) and 6.465 (dashed line).

3.4.3 MCMC parameters and priors

In the top part of Table 3.1 we identify the base parameters, i.e., the timescape parameters varied in the MCMC analysis. All other timescape parameters are derived from these. Of the 7 base parameters the 5 parameters $\{f_{\rm v0},\ h,\ T_0 = 2.7255\,{\rm K},\ \eta_{B\gamma},\ N_{\rm eff}\}$ comprise the set that fixes the background timescape model, while the additional two parameters $\{n_{\rm s},\ A_{\rm s}\}$ are needed for the matched perturbed FLRW model. The CMB temperature $T_0 = 2.7255\,{\rm K}$ measured by a wall observer is constrained by observation [Fixsen, 2009], and is not varied.

TABLE 3.1: The timescape parameters varied in MCMC analysis with their assumed priors shown in the top section. The derived parameters relevant to a volume–average observer is in the middle section and the dressed derived parameters measured by a wall/galaxy observer is shown in the third group. A brief description of the parameters is also given.

Parameter	Prior range	Description
$f_{\rm v0}$	$[0.3, 0.9]$	Fraction of horizon volume in voids today
H_0	$[0.3, 0.9]$	Dressed Hubble parameter
$10^{10}\eta_{B\gamma}$ ...	$[4.0, 7.0]$	$10^{10}\times$ Bare baryon–to–photon ratio
$N_{\rm eff}$	$[0., 0.6]$	The effective number of neutrino species
$n_{\rm s}$	$[0.9, 1.1]$	Scalar spectrum power-law index, pivot $k_0 = 0.05\,{\rm Mpc}^{-1}$
$10^9 A_{\rm s}$	$[2.0, 20.]$	Amplitude of the primordial curvature perturbations ($k_0 = 0.05$ Mpc^{-1})
T_0		CMB temperature of 2.725K measured by a wall observer
$\left(\bar\Omega_{\rm M}/\bar\Omega_{\rm R}\right)_{\rm dec}$	$> 1.$	The ratio of matter to radiation energy density at decoupling
$\bar H_0$		Bare Hubble constant
$\bar T_0$		CMB temperature seen by a volume–average observer
t_0		Age of universe (volume–average observer in Gyr)
$\bar\gamma_0$		Present phenomenological lapse function
$Y_{\rm p}$		Helium fraction
$\bar\Omega_{\rm B0}$		Bare baryon density parameter
$\bar\Omega_{\rm CDM0}$		Bare cold dark matter density parameter
$\bar\Omega_{\rm M0}$		Bare total matter density
$\bar\Omega_{\rm K0}$		Bare curvature parameter
$\bar\Omega_{\mathcal{Q}0}$		Bare backreaction parameter
$\bar z_{\rm dec}$		Bare redshift of decoupling
$\bar z_{\rm drag}$		Bare redshift of drag epoch
$\bar D_{\rm s}(\bar z_{\rm dec})$....		proper size of sound horizon at $\bar z = \bar z_{\rm dec}$ (Mpc)
$\bar D_{\rm s}(\bar z_{\rm drag})$...		proper size of sound horizon at $\bar z = \bar z_{\rm drag}$ (Mpc)
$\tau_{\rm w0}$		Age of universe (galaxy/ wall observer in Gyr)
$\Omega_{\rm B0}$		Dressed baryon density parameter
$\Omega_{\rm CDM0}$		Dressed cold dark matter density parameter
$\Omega_{\rm M0}$		Dressed total matter density parameter
$z_{\rm dec}$		Dressed redshift of decoupling
$z_{\rm drag}$		Dressed redshift of drag epoch
$100\theta_{\rm dec}$		$100\times$ angular scale of sound horizon at $z = \bar z_{\rm dec}$
$100\theta_{\rm drag}$		$100\times$ angular scale of sound horizon at $z = \bar z_{\rm drag}$
$d_{\rm A}$		Dressed angular diameter distance to sound horizon at decoupling (Mpc)
$d_{\rm A,drag}$		Dressed angular diameter distance to sound horizon at drag epoch (Mpc)

We use $N_{\rm eff} = 3.046$ for the base timescape model, as our main aim is to explore the parameter space in the timescape cosmology while remaining consistent with known particle physics. We also study the case in which $N_{\rm eff}$ is a free MCMC parameter without elaborating what the extra radiation component represents. (We do not aim to constrain neutrino masses, for example.)

For other base parameters we choose a wide prior range to explore the full parameter space. Flat priors are chosen, with the exception that the ratio of matter to radiation

energy density at decoupling is constrained to be larger than unity, $\bar{\Omega}_{\mathrm{M\,dec}}/\bar{\Omega}_{\mathrm{R\,dec}} > 1$, as a strict prior. The range of priors for $f_{\mathrm{v}0}$, h are chosen to be larger than their bounds found in previous studies [Smale and Wiltshire, 2011; Smale, 2011].

We assume that the primordial scalar perturbations are adiabatic with a spectrum

$$\mathcal{P}_{\mathcal{R}} = A_{\mathrm{s}} \left(\frac{k}{k_0} \right)^{n_{\mathrm{s}}-1} , \tag{3.56}$$

where we have chosen the pivot scale $k_0 = 0.05\,\mathrm{Mpc}^{-1}$. We have not investigated alternative initial conditions such as isocurvature scalar perturbations, tensor perturbations and set the running of the spectral index $\mathrm{d}n_{\mathrm{s}}/\mathrm{d}\ln k = 0$.

We treat the amplitude of the power spectrum A_{s} as a nuisance parameter that we cannot constrain. Nevertheless we use a wide prior range for A_{s} to get the normalized power spectrum required by the Planck `CamSpec` likelihood code. We configure the CLASS code to get the lensed temperature power spectrum with reionization turned on for the timescape matched FLRW model. We assume the reionization optical depth τ_{rion} to be completely degenerate with A_{s}.

3.4.4 Choice of matched FLRW models

Many of the matching methods of Sec. 3.3.3 require a shift (3.4) of very large ℓ multipoles of equivalent FLRW models with large spatial curvatures of order $0.2 \lesssim \Omega_{\mathrm{K}} \lesssim 0.8$. In these cases the amount of time required to solve the Boltzmann code becomes prohibitively large in combination with the MCMC analysis. We checked that individual runs of the $A(\bar{r}_{\mathcal{H}})$, $A(\bar{\eta}_0)$, $A(t_0)$, $A(\hat{\Omega}_{\Lambda 0} = 0)$ matched models gave similar χ^2 values to the canonical $A(\bar{H}_{\mathrm{dec}})$ matched model, but were unable to determine best fit parameter values with the computing resources available. Our MCMC analysis is therefore restricted to matched models $A(\bar{H}_{\mathrm{dec}})$, $W(k = 0)$ and $W(k \neq 0)$.

The wall geometry matching methods $W(k = 0)$ and $W(k \neq 0)$ cannot give as good a fit as the canonical $A(\bar{H}_{\mathrm{dec}})$ method to the volume–average expansion history. However, they may provide better matching for those aspects of the power spectra which are independent of the distance to the surface of last scattering. Consequently, differences between the two methodologies also provide a measure of the systematic uncertainties inherent in our matched FLRW model approach.

3.4.5 Foreground modeling

Foregrounds can bias estimation of cosmological parameters, a problem which is not unique to our study but also besets all analyses of CMB datasets in the context of FLRW models as well. The `CamSpec` likelihood in the $50 \leq \ell \leq 2500$ multipole range takes 14 additional parameters that are used for relative calibration and unresolved foreground modeling. The Planck team[7] find that foreground modeling does not change the parameter constraints in their baseline six-parameter ΛCDM model $\{\Omega_{\rm b}h^2,\ \Omega_{\rm c}h^2,\ 100\theta_{\rm MC},\ \tau,\ n_{\rm s},\ \ln(10^{10}A_{\rm s})\}$. However, they find that extensions to their baseline model are sensitive to foreground modeling with the independent likelihood code `Plik` converging to slightly different values of $Y_{\rm P}$, $N_{\rm eff}$, $n_{\rm s}$. They report up to a 1σ shift in parameter values from the two likelihood codes in some cases, but manage to obtain better agreement with the inclusion of high–ℓ data which constrain the foregrounds to a higher precision.

We have investigated the possibility that foreground modeling may critically impact the timescape parameter constraints. As a test we fixed the foreground nuisance parameters to the best fit baseline ΛCDM model values from Planck [Ade et al., 2014b], with the hypothesis that the baseline ΛCDM model unambiguously identifies the foreground sources and their impact on the temperature power spectrum. Fixing the foreground parameters in this way we found the best fit parameters for the timescape cosmology to be $f_{\rm v0} = 0.607^{+0.051}_{-0.057}$, $H_0 = 59.72^{+2.76}_{-2.89}\,{\rm km\,s^{-1}\,Mpc^{-1}}$, $10^{10}\eta_{B\gamma} = 6.24^{+0.3}_{-0.29}$, $n_{\rm s} = 0.971^{+0.028}_{-0.030}$ (using the canonical $A(\bar{H}_{\rm dec})$ matched model). Thus the chains converged to roughly the same region in parameter space, the best fit parameters being within the 1σ constraints from Table 3.2, but with a larger value of $-\ln\mathcal{L} = \chi^2/2$ as compared with the case in which foreground model nuisance parameters are free to vary. These results are therefore consistent with the hypothesis that foregrounds do not have a critical impact on parameter estimation.

The precise value of the goodness of fit, $-\ln\mathcal{L} = \chi^2/2$, obtained with fixed foreground nuisance parameters is not of acute importance since we only use the Planck data, and do not combine it with other data sets. If we were to combine the Planck data with other data sets that constrain the CMB anisotropy spectrum, the issues around foreground modeling would need to be revisited.

While we can not entirely rule out the impact of foreground modeling on timescape parameters we proceed with the assumption that our results are not critically impacted by them. We treat the 14 foreground parameters of the baseline model as nuisance parameters and adopt the same prior range for these parameters as for the baseline ΛCDM model in the analysis by the Planck team [Ade et al., 2014b].

[7] See Sec. 4.2 and Appendix C in [Ade et al., 2014b].

TABLE 3.2: The best fit and mean, with $1\,\sigma$ uncertainties for nearly symmetric distributions or error bounds obtained from 68% limits so that 32% of the samples are outside this range for skewed distributions. The timescape parameter values are shown for cases in which the timescape model parameters are matched to FLRW model parameters so that the two models have the same expansion history with density parameter differences $< 10^{-4}$ up until recombination. We show only those matching methods for which the matched FLRW curvature parameter is small enough to permit a full MCMC analysis using available computer resources. The A($\bar{H}_{\rm dec}$) average expansion history mathing method provides the canonical constraint on timescape parameters. The wall expansion history matching methods, W($k=0$) and W($k\neq 0$), are computed for illustrative purposes.

Matching type	A($\bar{H}_{\rm dec}$)		W($k=0$)		W($k\neq 0$)	
Parameter	Best fit	mean/error bounds/σ	Best fit	mean/error bounds/σ	Best fit	mean/error bounds/σ
$f_{\rm v0}$	0.628	$0.627^{+0.014}_{-0.012}$	0.545	$0.550^{+0.017}_{-0.015}$	0.559	$0.557^{+0.017}_{-0.015}$
H_0	60.984	$60.997^{+0.791}_{-0.733}$	56.148	$56.364^{+0.700}_{-0.694}$	56.774	$56.710^{+0.707}_{-0.714}$
$10^{10}\eta_{B\gamma}$	6.465	$6.489^{+0.101}_{-0.102}$	6.043	$6.048^{+0.086}_{-0.087}$	6.080	$6.080^{+0.091}_{-0.089}$
$n_{\rm s}$	0.995	0.992 ± 0.009	0.956	0.957 ± 0.009	0.963	0.960 ± 0.009
$\bar{H}_0$	51.640	$51.658^{+0.251}_{-0.257}$	49.846	$49.882^{+0.223}_{-0.218}$	50.016	$49.996^{+0.227}_{-0.225}$
$\bar{T}_0$	2.074	2.074 ± 0.010	2.142	2.137 ± 0.013	2.130	2.131 ± 0.013
t_0	16.587	16.579 ± 0.042	16.640	16.664 ± 0.055	16.675	$16.671^{+0.058}_{-0.053}$
$\bar{\gamma}_0$	1.314	1.314 ± 0.007	1.273	1.275 ± 0.008	1.280	1.279 ± 0.008
$Y_{\rm p}$	0.248	0.248 ± 0.00015	0.247	0.247 ± 0.00014	0.247	0.247 ± 0.00014
$\bar{\Omega}_{\rm B0}$	0.039	0.039 ± 0.001	0.043	0.043 ± 0.001	0.042	0.043 ± 0.001
$\bar{\Omega}_{\rm CDM0}$	0.176	$0.176^{+0.008}_{-0.010}$	0.238	$0.234^{+0.012}_{-0.013}$	0.227	$0.228^{+0.012}_{-0.013}$
$\bar{\Omega}_{\rm M0}$	0.215	$0.216^{+0.009}_{-0.011}$	0.281	$0.277^{+0.012}_{-0.014}$	0.269	$0.271^{+0.012}_{-0.014}$
$\bar{\Omega}_{\rm K0}$	0.819	$0.818^{+0.010}_{-0.008}$	0.757	$0.762^{+0.013}_{-0.012}$	0.768	$0.767^{+0.013}_{-0.011}$
$\bar{\Omega}_{\mathcal{Q}0}$	-0.034	-0.034 ± 0.001	-0.038	-0.038 ± 0.001	-0.038	-0.038 ± 0.001
$\bar{z}_{\rm dec}$	1429.729	$1429.425^{+7.171}_{-6.165}$	1387.674	$1390.524^{+8.570}_{-7.723}$	1394.902	$1394.064^{+8.473}_{-7.723}$
$\bar{z}_{\rm drag}$	1396.292	$1396.341^{+8.081}_{-6.996}$	1348.949	$1351.776^{+9.231}_{-8.309}$	1356.537	$1355.719^{+8.522}_{-8.515}$
$\bar{D}_{\rm s}(\bar{z}_{dec})$	0.135	0.135 ± 0.001	0.132	0.132 ± 0.001	0.133	0.133 ± 0.001
$\bar{D}_{\rm s}(\bar{z}_{drag})$	0.140	0.140 ± 0.001	0.139	0.139 ± 0.001	0.139	0.139 ± 0.001
$\tau_{\rm w0}$	13.811	$13.806^{+0.067}_{-0.065}$	14.267	$14.261^{+0.058}_{-0.052}$	14.229	$14.233^{+0.059}_{-0.054}$
$\Omega_{\rm B0}$	0.089	0.089 ± 0.001	0.089	0.089 ± 0.001	0.089	0.089 ± 0.001
$\Omega_{\rm CDM0}$	0.400	$0.400^{+0.014}_{-0.016}$	0.490	0.484 ± 0.017	0.475	0.477 ± 0.017
$\Omega_{\rm M0}$	0.489	$0.489^{+0.014}_{-0.016}$	0.579	0.573 ± 0.017	0.564	0.566 ± 0.017
$z_{\rm dec}$	1087.568	$1087.503^{+0.480}_{-0.520}$	1090.141	$1090.039^{+0.494}_{-0.495}$	1089.800	$1089.822^{+0.498}_{-0.507}$
$z_{\rm drag}$	1062.128	$1062.323^{+0.723}_{-0.732}$	1059.713	$1059.655^{+0.638}_{-0.646}$	1059.820	$1059.836^{+0.666}_{-0.667}$
$100\theta_{\rm dec}$	1.048	1.047 ± 0.001	1.041	1.041 ± 0.001	1.041	1.041 ± 0.001
$100\theta_{\rm drag}$	1.064	1.064 ± 0.001	1.061	1.061 ± 0.001	1.061	1.061 ± 0.001
$d_{\rm A}$	12.888	12.883 ± 0.063	12.699	$12.729^{+0.067}_{-0.066}$	12.753	$12.750^{+0.067}_{-0.066}$
$d_{\rm A,drag}$	13.191	13.183 ± 0.062	13.058	$13.088^{+0.066}_{-0.065}$	13.108	$13.104^{+0.067}_{-0.066}$

3.5 Results and analysis

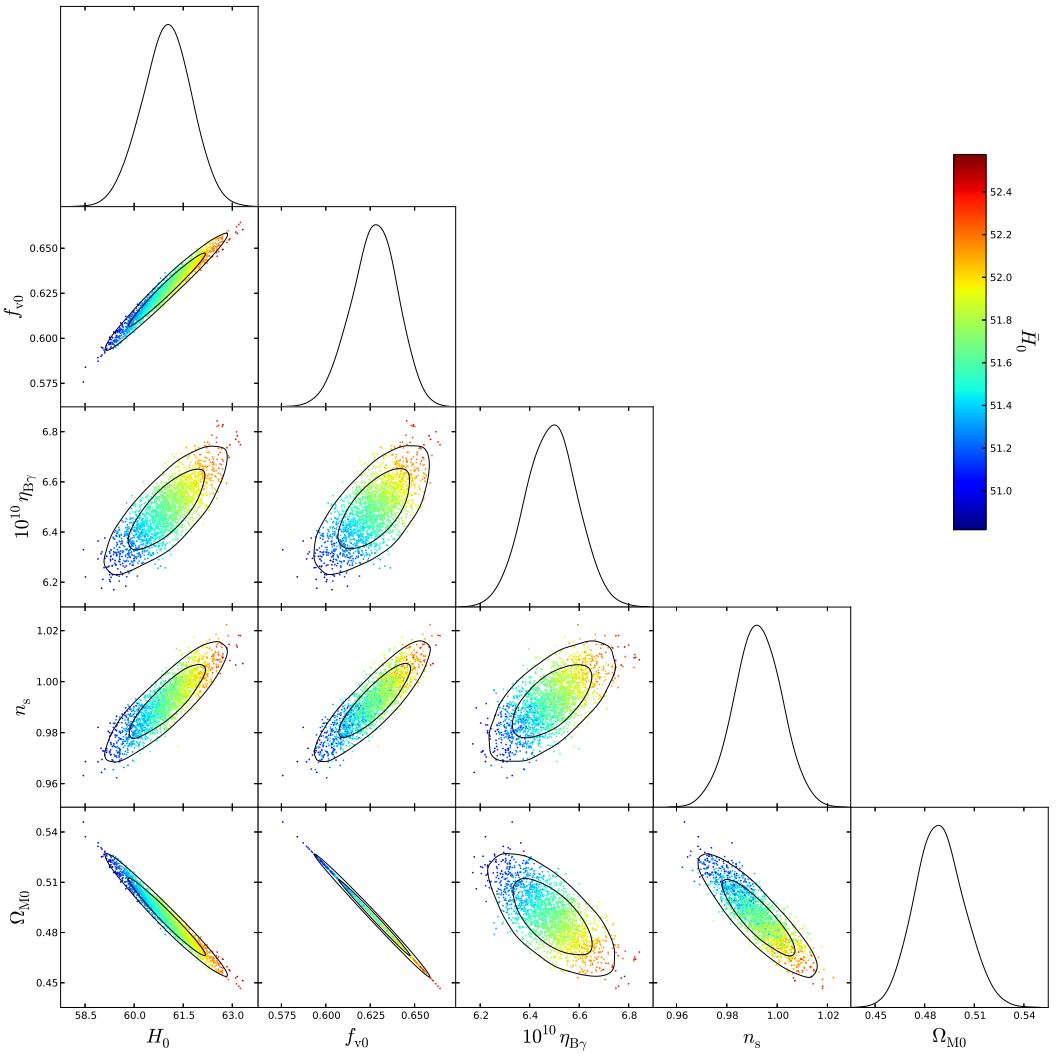

FIGURE 3.7: Constraints on the base MCMC parameters for the timescape parameters listed in table 3.1, and the total dressed matter density, $\Omega_{\rm M0}$ for timescape parameters with matched model A($\bar{H}_{\rm dec}$). We have also shown a scatter plot of the parameters color coded with the value of the bare Hubble constant, $\bar{H}_0$, relevant to a volume–average observer.

Here we present the parameter constraints obtained from the Planck temperature power spectrum data in the range $50 \leq \ell \leq 2500$. Our analysis includes the parameters that model the foreground in this multipole range.

In table 3.2 we record the best fit, and mean marginalized constraints on timescape parameters obtained for each of the matching procedures A($\bar{H}_{\rm dec}$), W($k = 0$) and W($k \neq 0$) with $N_{\rm eff} = 3.046$ fixed. The chains analyses and all statistical information were obtained with the `getdist` software in the CosmoMc package [Lewis and Bridle, 2002]. We ran eight chains for the canonical $A(\bar{H}_{\rm dec})$ matching method and five chains each

for the rest. We have checked to ensure that the base MCMC parameters satisfy the Gelman–Rubin[8] diagnostic $R-1<0.01$ and the chains have converged. Not all of the derived parameters satisfy this criteria but even then all parameters satisfy $R-1<0.02$ and are in fact closer to 0.01 than to 0.02. In what follows we treat the $\mathrm{A}(\bar{H}_{\rm dec})$ model as the canonical matching procedure and its results will be used for timescape parameter constraints. The other matching procedures are used for the purpose of understanding the effects of matching assumptions on parameter constraints and possible systematic uncertainties.

In Fig. 3.7 the marginalized probability distribution and 2D posterior constraints for the base timescape parameters and the dressed total matter density are shown for the canonical matching. The constraints on all parameters can be understood in terms of the angular scale of the sound horizon $\theta_{\rm dec}=\bar{D}_{\rm s}(\bar{z}_{\rm dec})/d_{\rm A}$ and the ratios of the acoustic peaks.

Before proceeding any further let us first make the relationship between $\Omega_{\rm M0}$ and $f_{\rm v0}$ conspicuous. At late epochs the full timescape solution with radiation is very well approximated by the tracker limit of the matter only solution [Wiltshire, 2007b], leading to the following relations between the present void fraction and dressed matter density

$$\Omega_{\rm M0}\approx\frac{1}{2}\,(1-f_{\rm v0})\,(2+f_{\rm v0})\;,\qquad \left.\frac{{\rm d}\Omega_M}{{\rm d}f_{\rm v}}\right|_0\approx-\left(\frac{1}{2}+f_{\rm v0}\right),\tag{3.57}$$

which explains the negative correlation between $\Omega_{\rm M0}$ and $f_{\rm v0}$. The Planck data tightly constrains the position of the first peak $\theta_{\rm dec}$ and therefore any changes in H_0, $\Omega_{\rm M0}$, $f_{\rm v0}$ which are indirectly reflected as an increase in $d_{\rm A}$ are simultaneously met with an increase in $\bar{D}_{\rm s}$ and vice versa. A larger angular diameter distance, $d_{\rm A}$, to the last scattering surface can be obtained by increasing either H_0 or $f_{\rm v0}$ but there is a concurrent increase in $\bar{D}_{\rm s}$ which also changes the ratios of the acoustic peak heights.

Matching the ratios of the peak heights requires a delicate balance between the proportions of baryonic and nonbaryonic matter. The extent to which $f_{\rm v0}$ can change while keeping $\theta_{\rm dec}$ constant is limited because the ratio $\Omega_{\rm M0}/\Omega_{\rm B0}$ (or equivalently $f_{\rm v0}/\eta_{B\gamma}$) fixes the ratios of the first, second and third acoustic peak heights, which are also tightly constrained by the Planck data.

In the FLRW models one of the two parameters, $\Omega_{\rm K0}$ and $\Omega_{\Lambda0}$ (as constrained from the Friedman equation) can be adjusted to determine the overall angular scale of the peaks without directly influencing the ratios of the acoustic peak heights. By contrast, in the

[8] The Gelman–Rubin diagnostic is used to test that all chains converge to the same posterior distribution [Gelman and Rubin, 1992]. The $R-1$ statistic in the diagnostic compares the variance of the chains means to the mean value of the variances within each chain. Generally $R-1<0.2$ is optimal but even then low values indicate but do not guarantee convergence.

timescape model the void fraction constrains both the matter density parameter—either dressed (3.57) or bare $\bar{\Omega}_{\rm M0} \approx 4(1 - f_{\rm v0})/(2 + f_{\rm v0})^2$)—and the volume average curvature density parameter, $\bar{\Omega}_{\rm K0} \approx 9 f_{\rm v0}/\left(2 + f_{\rm v0}\right)^2$. Thus timescape parameters are very tightly constrained; a change to $f_{\rm v0}$ can significantly affect both the angular scale and, insofar as it changes the ratio $\Omega_{\rm B0}/\Omega_{\rm M0}$, also the ratios of the peak heights.

The results of MCMC analysis on the canonical A($\bar{H}_{\rm dec}$) model yield the values $H_0 = 61.0^{+0.79}_{-0.73}\,{\rm km\,s^{-1}\,Mpc^{-1}}$ and $f_{\rm v0} = 0.627^{+0.014}_{-0.012}$. The value of the dressed Hubble constant agrees with our previous estimate, $61.7 \pm 3.0\,{\rm km\,s^{-1}\,Mpc^{-1}}$ [Duley et al., 2013] at the 1σ level. However, the void fraction is almost 2σ less than the previous estimate [Duley et al., 2013], $f_{\rm v0} = 0.695^{+0.041}_{-0.051}$. Of course, we should caution that the uncertainties given in Table 3.2 do not included any estimate of the systematic uncertainties that must surely arise from the matched FLRW procedure. Since the wall geometry based matching procedures W($k = 0$) and W($k \neq 0$) do not reliably estimate volume average quantities, the significantly smaller values of H_0, $f_{\rm v0}$ obtained for these procedures probably overestimate the systematic uncertainties. However, as an upper bound they indicate that the systematic uncertainties could be as high as 8%, as compared to the 1–2% statistical uncertainties.

Even if the systematic uncertainties are not so large, however, here is an obvious reason for the apparent tension between the two estimates of $f_{\rm v0}$. In all previous work [Wiltshire, 2007a; Leith et al., 2008; Duley et al., 2013] we have not directly constrained the baryon–to–photon ratio. In fact, our best previous estimate [Duley et al., 2013] is based on assuming a baryon–to–photon ratio $10^{10}\eta_{B\gamma} = 5.1 \pm 0.5$ for which one can avoid a primordial lithium abundance anomaly [Steigman, 2006; Cyburt et al., 2008]. By contrast here we have used the acoustic peaks height ratio to directly constrain $\eta_{B\gamma}$ for the first time, with the result $10^{10}\eta_{B\gamma} = 6.47 \pm 0.10$. If we had admitted such large values of the baryon–to–photon ratio in our previous estimate then there would not be a discrepancy.

We find that while the timescape model remains consistent a detailed analysis of the acoustic peaks—modulo systematic uncertainties introduced by the model matching procedure—the baryon–to–photon ratio is driven to a value that is even a little higher than ΛCDM model estimates [Ade et al., 2014b; Hinshaw et al., 2013]. Thus based on the analysis here we cannot make the claim that the timescape model solves the primordial lithium abundance anomaly.

One might be concerned that the value of the baryon–to–photon ratio is $4\,\sigma$ larger than the ΛCDM value $10^{10}\eta_{B\gamma} = 6.04 \pm 0.09$. However, the wall geometry based matching procedures give values $10^{10}\eta_{B\gamma} = 6.05 \pm 0.09$ and $10^{10}\eta_{B\gamma} = 6.08 \pm 0.09$, which precisely

match the ΛCDM result. Considering the systematic uncertainties therefore, we have agreement with ΛCDM.

The spectral index is also constrained for the first time. The canonical $A(\bar{H}_{\rm dec})$ matching method leads to a nearly scale invariant primordial spectrum with $n_{\rm s} = 0.992 \pm 0.009$, $n_{\rm s} = 0.960 \pm 0.009$ whereas the wall–geometry matching methods yield $n_{\rm s} = 0.957 \pm 0.009$ and $n_{\rm s} = 0.960 \pm 0.009$, confirming deviations from scale invariance at more than 3 σ level in agreement with the ΛCDM results [Ade et al., 2014b; Hinshaw et al., 2013]. Once again, these 3–4% differences are driven by the systematic uncertainties from that arise from the imperfect nature of the matched model procedures.

Since $10^{10}\eta_{B\gamma}$ and $n_{\rm s}$ constrain spectral features other than the overall angular scale, the difference between the average–geometry and wall–geometry matching procedures give a reasonable estimate of the systematic uncertainties. In fact, the wall–geometry matching procedures produce a somewhat reduced value of $-\ln\mathcal{L} = \chi^2/2$ as compared to the volume–average methods, with $-\ln\mathcal{L} = 3925.16$, 3897.90 and 3896.47 for the $A(\bar{H}_{\rm dec})$, $W(k=0)$, and $W(k\neq 0)$ methods respectively. The likelihoods for the $W(k=0)$ and $W(k\neq 0)$ matching methods are in fact precisely the same as one obtains for best fit ΛCDM model in the multipole range $50 \leq \ell \leq 2500$, where the Planck team obtain[9] $-\ln\mathcal{L} = 3895.5$ using `MINUIT` or $-\ln\mathcal{L} = 3896.9$ using `CosmoMC`.

It therefore appears that the FLRW perturbation theory for the wall–geometry matching methods produces a better fit to the features of the acoustic peaks which relate solely to its shape. It is possible that the values of $10^{10}\eta_{B\gamma}$ and $n_{\rm s}$ obtained by wall geometry matching therefore give a more accurate estimate of the values that we would obtain if we could both use the most relevant perturbation equations, and simultaneously use the timescape solution in all of the codes, rather than having to rely on matched models using CLASS [Lesgourgues, 2011; Blas et al., 2011].

In Fig. 3.8 the power spectra for the best fit values are shown for the three matching procedures for which the MCMC analysis was possible. To show the level of concurrence of the other volume–average expansion history matching procedures from Sec. 3.3.3, we determined their power spectra using the best fit parameters for $A(\bar{H}_{\rm dec})$ matching found by the MCMC analysis. In Fig. 3.9 we plot the ratios of these power spectra relative to a fiducial ΛCDM spectrum obtained from the best fit parameters using the Planck data only [Ade et al., 2014b]. We also plot the same ratio for the three best fit models of Table 3.2.

We see in Fig. 3.9 that the difference in individual C_ℓ values from the ΛCDM model is of up to order 1% for the wall expansion history matching methods over all multipoles.

[9] http://pla.esac.esa.int/pla/index.html

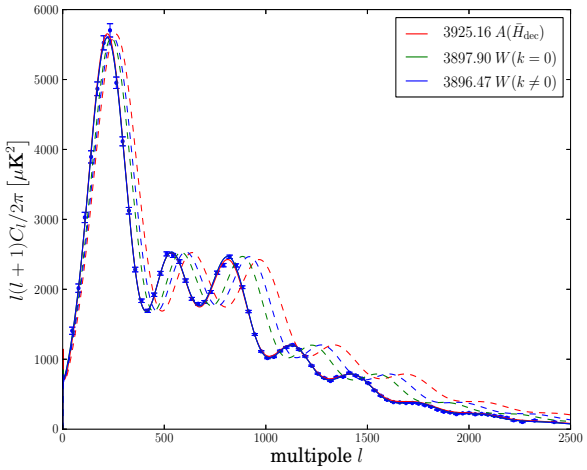

FIGURE 3.8: Power spectra for the best fit parameters of for the three matching methods $A(\bar{H}_{\rm dec})$ (red); $W(k=0)$ (green); $W(k\neq 0)$ (blue), with $-\ln\mathcal{L}$ values shown. In each case the dashed lines show the spectrum before the application of the shift (3.4), and the solid lines after.

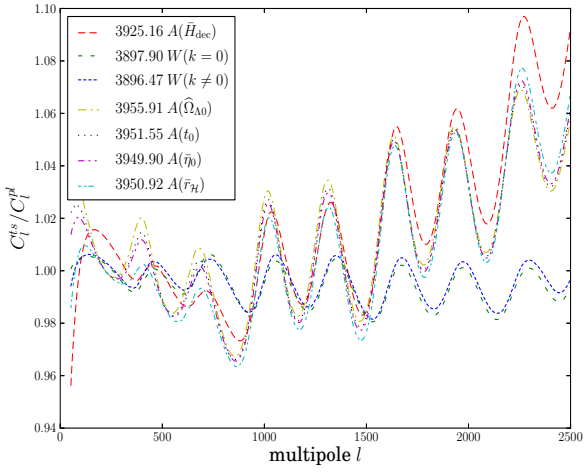

FIGURE 3.9: Ratio of timescape power spectra to that of the ΛCDM model with the best fit Planck parameters, which is used as a reference model. For the $A(\bar{H}_{\rm dec})$, $W(k=0)$, $W(k\neq 0)$ methods the best fit values from Table 3.2 have been used. For the $A(\bar{r}_{\mathcal{H}})$, $A(\bar{\eta}_0)$, $A(t_0)$, and $A(\hat{\Omega}_{\Lambda 0})=0$ we have used the best fit parameters from the $A(\bar{H}_{\rm dec})$ model. The values of $-\ln\mathcal{L}=\chi^2/2$ shown do not therefore represent the best fit values in these cases.

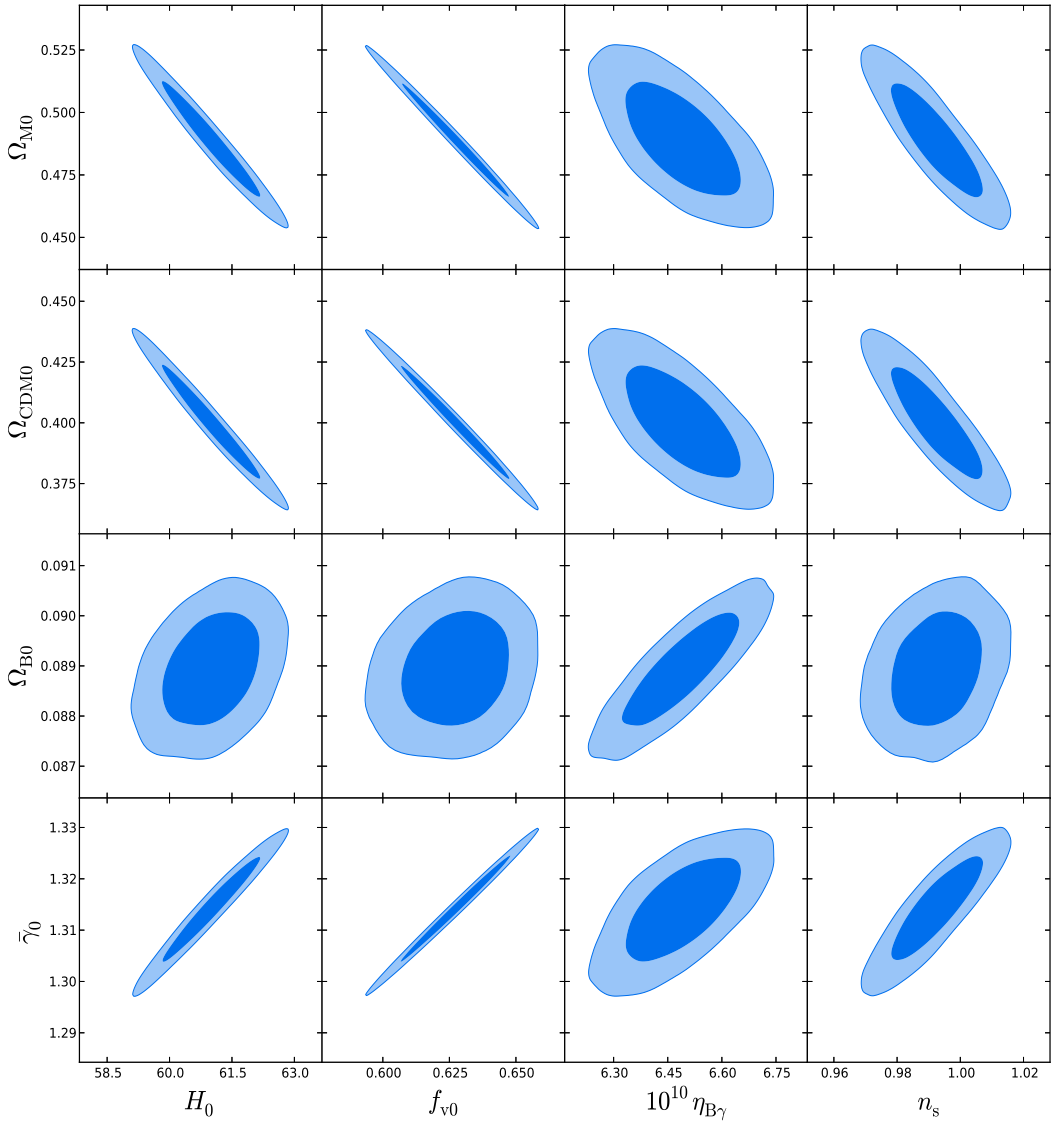

FIGURE 3.10: Variations in the various dressed parameters are shown with respect to the base MCMC parameters for the timescape model. The parameter constraints—showing 68% and 95% statistical uncertainties—are determined for the case of the A($\bar{H}_{\rm dec}$) matching method.

For the volume–average matching methods the differences are individually up to 2%–3% for $50 \lesssim \ell \lesssim 1600$, and slowly rise to a maximum $\sim$ 8–9% for $2300 \lesssim \ell \lesssim 2500$. While the small angle differences may seem large, it must be remembered that individual foreground parameters will also be somewhat different so that the overall $(-\ln \mathcal{L})$ value for the best fit $A(\bar{H}_{\rm dec})$ matched model is only 0.7% larger than for the best fit ΛCDM model [Ade et al., 2014b].

We note that in Fig. 3.9 the increased power in the canonical $A(\bar{H}_{\rm dec})$ matching method as compared to the fiducial ΛCDM power spectrum at very large multipoles will be partly due to the difference in spectral index $n_{\rm s} = 0.992 \pm 0.009$ compared to $n_{\rm s} =$

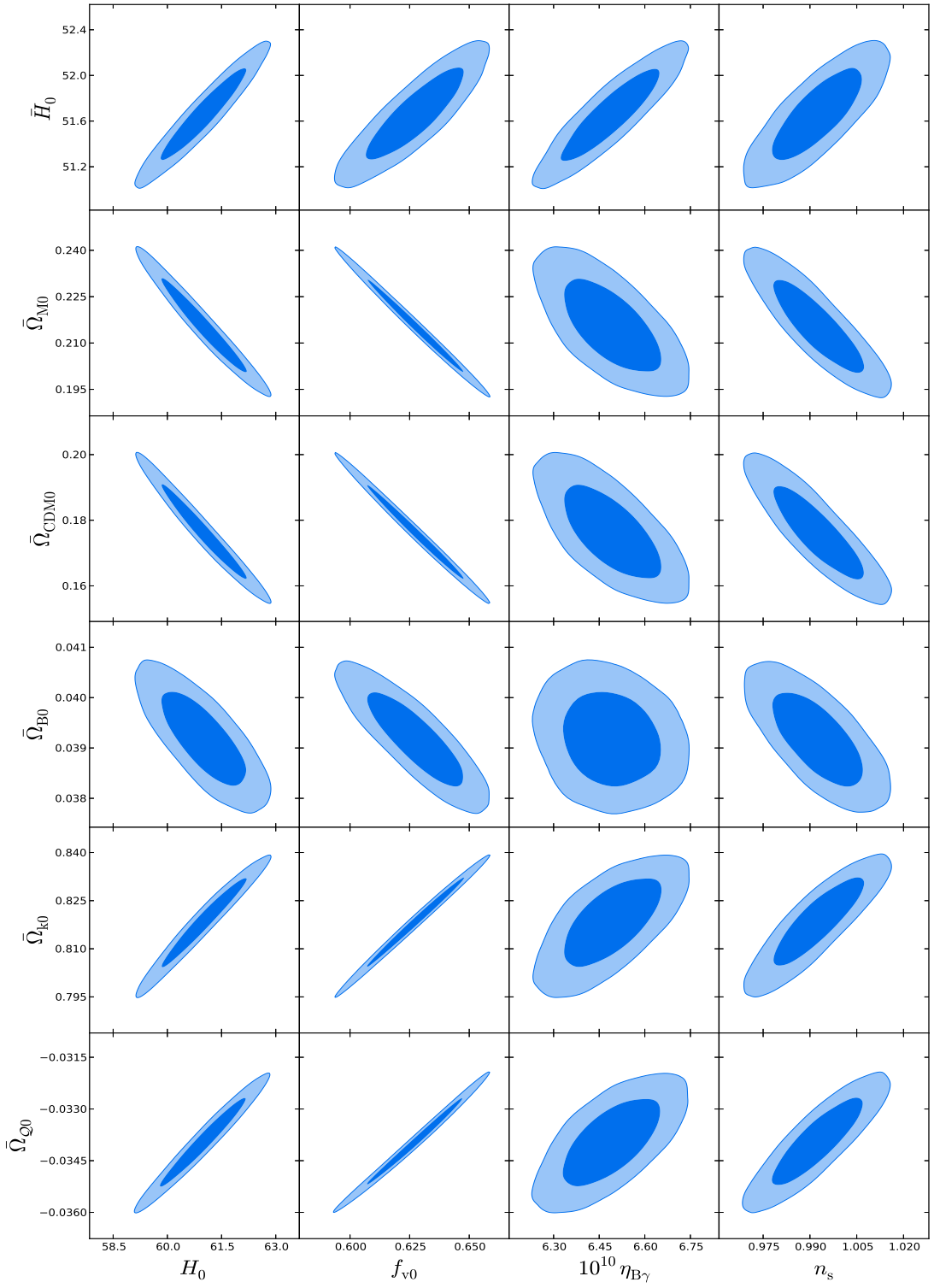

FIGURE 3.11: Variations in the various bare parameters are shown with respect to the base MCMC parameters for the timescape model. The parameter constraints—showing 68% and 95% statistical uncertainties—are determined for the case of the A($\bar{H}_{\rm dec}$) matching method.

0.9616 ± 0.0094. Increasing $n_{\rm s}$ increases the power at the third peak and higher multipoles (small angles) compared to the first two peaks [Mukhanov, 2005].

In figure 3.10 and 3.11 the posterior constraints on the dressed and bare parameters are shown against the base MCMC parameters. These figures illustrate a number of interesting points which relate the observations we have already made concerning $\eta_{B\gamma}$ and $n_{\rm s}$. In Fig. 3.11 the bare baryon density $\bar{\Omega}_{\rm B0}$ appears to be uncorrelated to $\eta_{B\gamma}$. Thus since $\eta_{B\gamma} \propto \bar{\Omega}_{\rm B0}\bar{H}_0^2$, any increase in $\eta_{B\gamma}$ must be met with an increase in $\bar{H}_0$. By contrast, the dressed baryon density parameter, $\Omega_{\rm B0}$ is positively correlated with $\eta_{B\gamma}$, as shown in Fig. 3.10. The phenomenological lapse function, $\bar{\gamma}$, and its time derivative, $\mathrm{d}\bar{\gamma}/\mathrm{d}t$, which relate the dressed and bare parameters according to $\Omega_{\rm B0} = \bar{\Omega}_{\rm B0}/\bar{\gamma}_0^3$ and $H_0 = (\bar{\gamma}\bar{H} - \mathrm{d}\bar{\gamma}/\mathrm{d}t)\big|_0$, are involved here in subtle ways which are difficult to disentangle. This also explains why the volume–average geometry and wall–geometry matching methods lead to different results for $\eta_{B\gamma}$. Essentially, one cannot separate parameters concerning the average expansion history from those that relate to spectral features such as the ratios of acoustic peak heights.

The variation in the spectral index, $n_{\rm s}$, between the different matching methods can be similarly understood. Figs. 3.10 and 3.11 reveal a degeneracy between $n_{\rm s}$ and the dressed and bare parameters $\Omega_{\rm M0}$, $\bar{\Omega}_{\rm M0}$, $\Omega_{\rm B0}$, $\bar{H}_0$. One cannot disassociate the early universe physics which is influenced by $n_{\rm s}$ from the late time evolution on account of parameter degeneracies. The lesson here is that, as yet, the constraints on the timescape parameters are limited by systematic uncertainties from the matching method which are larger than the statistical uncertainties. Furthermore, the exclusion of $\ell < 50$ data is also a handicap for us since the Sachs–Wolfe plateau on the largest scales is sensitive to $n_{\rm s}$, where the largest wavelengths remain frozen outside the horizon before recombination and are unaffected by causal physics.

In figure 3.12 the correlations between the derived bare and dressed parameters are shown. The narrow 68% and 95% confidence contours between various parameters largely reinforce what we already know about their degeneracies from the timescape matter–only tracker solution [Wiltshire, 2007b, 2009]. In the limit of vanishing radiation energy density the width of the contours would shrink to zero. The 2-dimensional posteriors involving baryon density are not as tightly constrained because the tracker solution fixes the total matter density but not its split into baryonic and non-baryonic components. Interpreting H_0 as the Hubble constant determined by wall observers, and $\bar{H}_0$ as the Hubble constant of the volume–average statistical geometry, the contours in the H_0–$\bar{H}_0$ plane in Fig. 3.12 show that bounds on the bare parameter provide reasonably tight bounds on the dressed parameter and vice versa.

Finally in figure 3.13 the marginalized likelihoods for all the timescape parameters of the canonical matching listed in table 3.1 are shown for completeness.

We have also investigated the case when $N_{\rm eff}$ is left free to vary. The results in this case are not significantly different from the $N_{\rm eff} = 3.046$ case. Table 3.3 has the timescape constraints with $N_{\rm eff}$ free to vary. One reason for investigation of the extended timescape model with a free $N_{\rm eff}$ was to check if the lithium anomaly problem could be somewhat alleviated at the cost of $N_{\rm eff}$ that deviates[10] from 3.046. Deviations are possible if there are extra radiation components or a neutrino/anti-neutrino asymmetry just to list some scenarios. This could be possible if BBN determination of $Y_{\rm p} = Y_{\rm p}(N_{\rm eff}, \eta_{B\gamma})$ forced $\eta_{B\gamma}$ towards lower values $\eta_{B\gamma} \approx 5.1$ which in timescape resolves the lithium problem [Steigman, 2006; Cyburt et al., 2008]. On the contrary we found preference for $N_{\rm eff} > 3.046$ and because $N_{\rm eff}$ is positively correlated with $\eta_{B\gamma}$ this lead to a slightly even larger $\eta_{B\gamma}$. This is accompanied with a preference for increased $f_{\rm v0}$ because $\eta_{B\gamma}$ is positively correlated with $f_{\rm v0}$ but negatively with $\Omega_{\rm M0}$ (see Fig. 3.10).

[10] See App. B

TABLE 3.3: The best fit and mean, with $1\,\sigma$ uncertainties for nearly symmetric distributions or error bounds obtained from 68% limits so that 32% of the samples are outside this range for skewed distributions. The timescape parameter values are shown for cases in which the timescape model parameters are matched to FLRW model parameters so that the two models have the same expansion history with density parameter differences $< 10^{-4}$ up until recombination. We show only those matching methods for which the matched FLRW curvature parameter is small enough to permit a full MCMC analysis using available computer resources. The A($\bar{H}_{\rm dec}$) average expansion history mathing method provides the canonical constraint on timescape parameters. The wall expansion history matching methods, W($k=0$) and W($k\neq 0$), are computed for illustrative purposes. The differences here from Table 3.2 are because of $N_{\rm eff}$ which is free to vary here.

Matching type	A($\bar{H}_{\rm dec}$)		W($k=0$)		W($k\neq 0$)	
Parameter	Best fit	mean/error bounds/σ	Best fit	mean/error bounds/σ	Best fit	mean/error bounds/σ
$f_{\rm v0}$	0.637	0.630 ± 0.014	0.551	$0.549^{+0.021}_{-0.018}$	0.560	$0.562^{+0.019}_{-0.018}$
H_0	62.263	$61.451^{+1.047}_{-1.034}$	56.533	$56.398^{+2.162}_{-2.110}$	57.157	$57.419^{+2.395}_{-1.831}$
$N_{\rm eff}$	3.243	$3.110^{+0.098}_{-0.110}$	3.062	$3.060^{+0.387}_{-0.371}$	3.129	$3.168^{+0.404}_{-0.348}$
$10^{10}\eta_{\rm B\gamma}$	6.533	$6.518^{+0.108}_{-0.109}$	6.066	6.047 ± 0.109	6.124	$6.112^{+0.111}_{-0.108}$
$n_{\rm s}$	1.001	$0.996^{+0.011}_{-0.012}$	0.959	$0.956^{+0.020}_{-0.018}$	0.962	$0.965^{+0.020}_{-0.016}$
$\bar{H}_0$	52.425	$51.942^{+0.513}_{-0.512}$	50.001	$49.918^{+1.487}_{-1.426}$	50.317	$50.466^{+1.598}_{-1.253}$
$\bar{T}_0$	2.066	2.072 ± 0.011	2.136	$2.138^{+0.015}_{-0.018}$	2.129	$2.127^{+0.014}_{-0.017}$
t_0	16.398	$16.510^{+0.117}_{-0.116}$	16.633	$16.657^{+0.369}_{-0.425}$	16.584	$16.560^{+0.339}_{-0.430}$
$\bar{\gamma}_0$	1.319	1.316 ± 0.007	1.276	$1.275^{+0.011}_{-0.009}$	1.280	1.282 ± 0.009
$Y_{\rm p}$	0.2507	$0.2489^{+0.00142}_{-0.00152}$	0.248	$0.247^{+0.006}_{-0.005}$	0.249	$0.249^{+0.006}_{-0.004}$
$\bar{\Omega}_{\rm B0}$	0.038	0.039 ± 0.001	0.043	$0.043^{+0.002}_{-0.003}$	0.042	$0.042^{+0.002}_{-0.003}$
$\bar{\Omega}_{\rm CDM0}$	0.170	$0.175^{+0.009}_{-0.010}$	0.233	$0.234^{+0.012}_{-0.016}$	0.226	$0.225^{+0.012}_{-0.014}$
$\bar{\Omega}_{\rm M0}$	0.208	0.213 ± 0.010	0.275	$0.277^{+0.014}_{-0.018}$	0.268	$0.266^{+0.014}_{-0.017}$
$\bar{\Omega}_{\rm k0}$	0.825	$0.820^{+0.010}_{-0.009}$	0.763	$0.761^{+0.017}_{-0.013}$	0.769	$0.771^{+0.016}_{-0.013}$
$\bar{\Omega}_{\mathcal{Q}0}$	-0.033	-0.034 ± 0.001	-0.038	-0.038 ± 0.001	-0.038	-0.038 ± 0.001
$\bar{z}_{\rm dec}$	1434.924	$1431.143^{+7.060}_{-6.898}$	1391.235	$1390.203^{+11.336}_{-9.740}$	1395.612	$1396.985^{+10.853}_{-9.437}$
$\bar{z}_{\rm drag}$	1402.388	$1398.465^{+8.044}_{-7.965}$	1352.757	$1351.460^{+12.537}_{-10.983}$	1357.923	$1359.065^{+12.386}_{-10.305}$
$\bar{D}_s(\bar{z}_{\rm dec})$	0.134	0.134 ± 0.001	0.132	0.132 ± 0.003	0.132	0.132 ± 0.003
$\bar{D}_s(\bar{z}_{\rm drag})$	0.139	0.140 ± 0.001	0.139	0.139 ± 0.003	0.138	$0.138^{+0.003}_{-0.004}$
$\tau_{\rm w0}$	13.606	13.732 ± 0.144	14.228	$14.260^{+0.369}_{-0.449}$	14.145	$14.114^{+0.327}_{-0.448}$
$\Omega_{\rm B0}$	0.087	0.088 ± 0.001	0.089	$0.089^{+0.003}_{-0.005}$	0.088	$0.088^{+0.003}_{-0.004}$
$\Omega_{\rm CDM0}$	0.391	0.397 ± 0.015	0.483	$0.485^{+0.016}_{-0.019}$	0.474	$0.472^{+0.017}_{-0.018}$
$\Omega_{\rm M0}$	0.478	$0.486^{+0.015}_{-0.016}$	0.572	$0.574^{+0.019}_{-0.022}$	0.563	$0.560^{+0.019}_{-0.020}$
$z_{\rm dec}$	1087.557	$1087.479^{+0.484}_{-0.499}$	1090.001	$1090.064^{+0.530}_{-0.535}$	1089.781	$1089.869^{+0.563}_{-0.551}$
$z_{\rm drag}$	1062.892	$1062.638^{+0.831}_{-0.839}$	1059.849	$1059.672^{+1.401}_{-1.412}$	1060.345	$1060.272^{+1.520}_{-1.263}$
$100\theta_{\rm dec}$	1.047	1.047 ± 0.001	1.041	1.041 ± 0.001	1.041	1.041 ± 0.001
$100\theta_{\rm drag}$	1.063	1.064 ± 0.001	1.061	1.061 ± 0.002	1.060	$1.060^{+0.001}_{-0.002}$
$d_{\rm A}$	12.774	12.840 ± 0.101	12.706	$12.724^{+0.279}_{-0.283}$	12.686	$12.673^{+0.249}_{-0.310}$
$d_{\rm A,drag}$	13.065	$13.136^{+0.097}_{-0.096}$	13.062	$13.083^{+0.296}_{-0.304}$	13.033	$13.022^{+0.264}_{-0.331}$

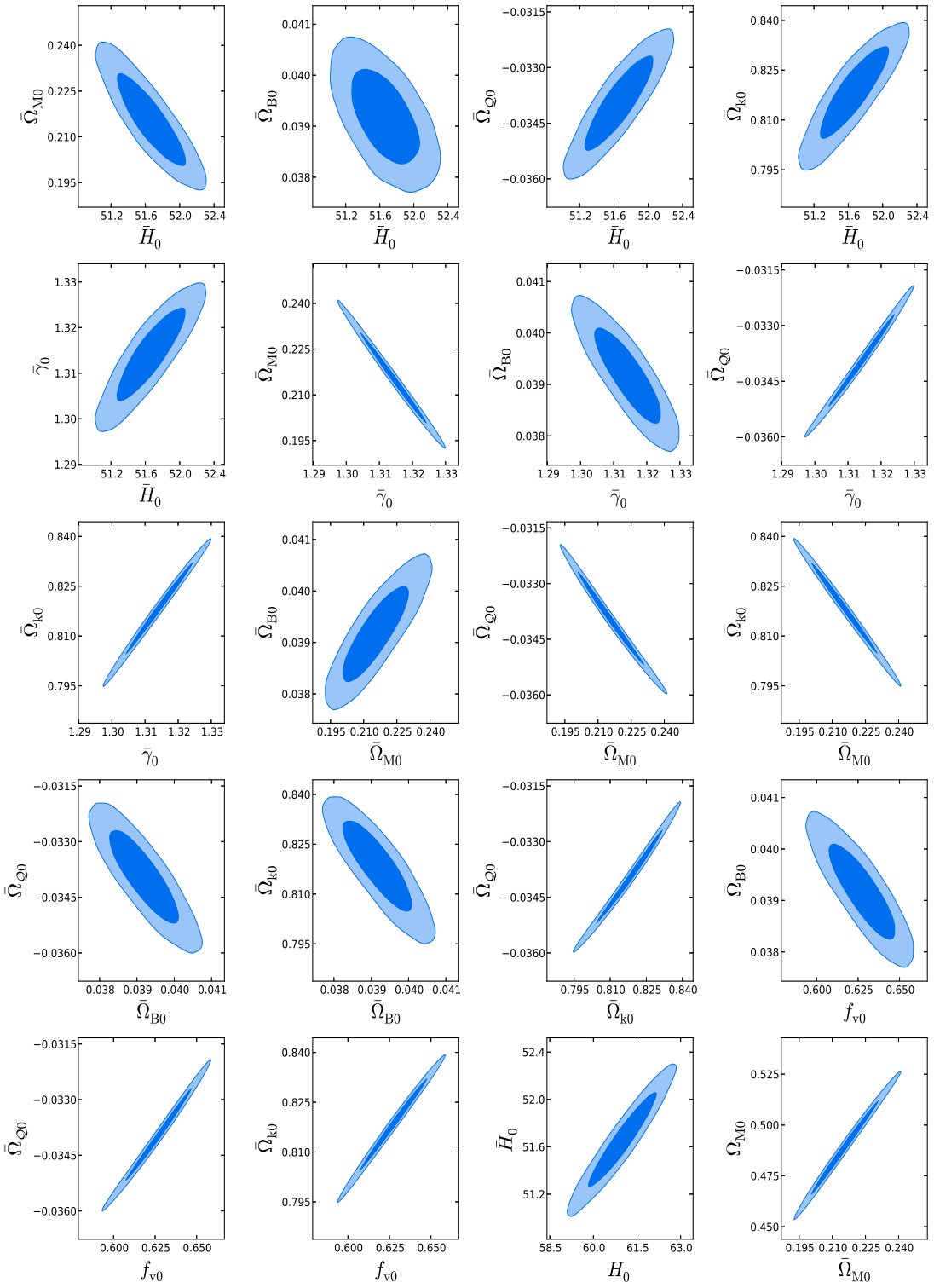

FIGURE 3.12: Correlations between selected bare and dressed timescape parameters are shown. The parameter constraints—showing 68% and 95% statistical uncertainties—are determined for the case of the A($\bar{H}_{\rm dec}$) matching method.

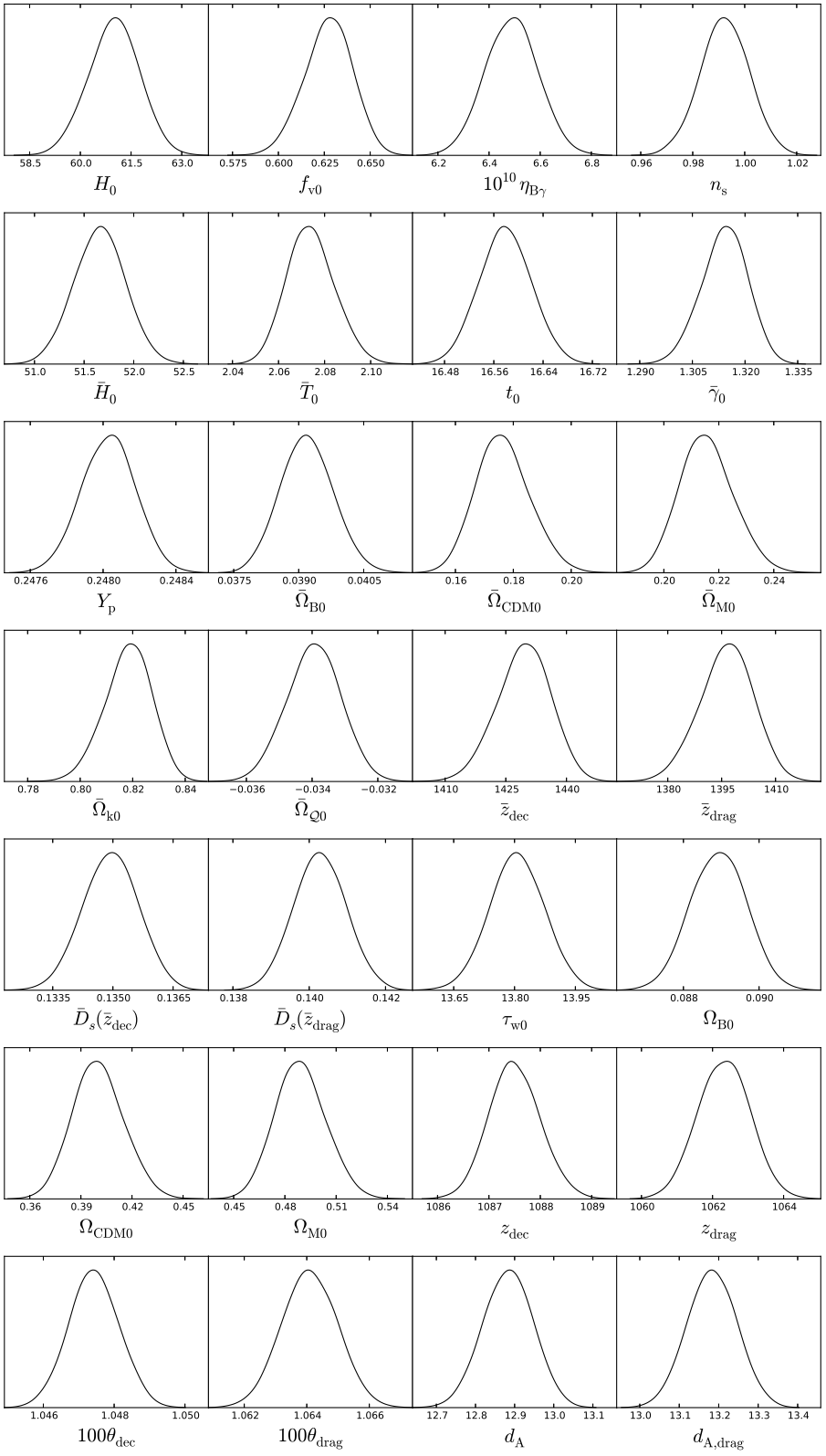

FIGURE 3.13: Marginalized posteriors for the base MCMC parameters, the bare parameters and the dressed parameters in the timescape cosmology. The parameter constraints are determined for the case of the A($\bar{H}_{\rm dec}$) matching method.

Chapter 4

Discussion and Conclusions

4.1 Summary of the main results

In Chapter 2 Sec. 2.4 we have derived solutions to the timescape-Buchert equations (2.61)–(2.65) with matter and radiation fluid. Our work extends the matter only solutions from Wiltshire [2007b] to include both matter and radiation. The new solutions smoothly interpolate between a very early epoch universe, in which the relevant physics was that of the standard hot big bang with an almost homogeneous FLRW background, and a late time universe in which the average evolution is not that of a FLRW model even though a statistical notion of homogeneity persists when one averages on $\gtrsim 100\,h^{-1}\,$Mpc scales.

To summarize, in the timescape model the horizon volume grows with the volume–average scale factor $\bar{a}$. It is $\bar{a}$ in terms of which the averaged Hubble expansion $\bar{H} = \dot{\bar{a}}/\bar{a}$ is defined, and $\bar{a} \to 0$ in the limit $t \to 0$ defines the big bang singularity. The timescape equation for $\bar{a}$ is complemented with the equation for the fraction of horizon volume in voids $f_{\rm v}$. The void fraction $f_{\rm v}$ sets the spatial curvature (see Eq.(2.80)) and its derivative w.r.t. volume–average time t, i.e., $\mathrm{d}f_{\rm v}/\mathrm{d}t$ enters the equation for backreaction from inhomogeneities (see Eq. (2.81)).

A crucial step in numerically solving the timescape equations is to find the appropriate initial conditions that ultimately evolve to the present universe. For this we found early time series solutions for the volume–average scale factor $\bar{a}$, given by Eq. (2.86), and void fraction $f_{\rm v}$, given by Eq. (2.87). The series for $f_{\rm v}$ also sets the initial condition for $\mathrm{d}f_{\rm v}/\mathrm{d}t$ and through this the initial spatial curvature is also fixed. This way the value of a nonzero but almost negligible initial spatial curvature is determined that ultimately dominates the energy density at late times. The form of the series solution for $\bar{a}$, when

compared to the series expansion for the FLRW scale factor in the Friedmann equations with matter and radiation, supports our argument that at early times the timescape model solutions evolve almost like a spatially flat FLRW model.

In Sec. 2.4.3 we used the timescape solutions with matter and radiation to study the helium and hydrogen recombination history in the timescape scenario. We followed standard procedures in which perturbations to the background metric do not enter the calculations for helium and hydrogen. Only the expansion rate from the background metric competes against the scattering rate between photons and electrons, eventually breaking the equilibrium in chemical reactions for the recombination and ionization of hydrogen. In our study the background expansion competing against the photon-electron scattering rates is that from an averaged expansion, specifically the volume–average expansion rate $\bar{H}$ relevant to the volume–average observer. Since the recombination history is independent of perturbations to the background geometry we believe that our simple adaptation of hydrogen recombination from the standard model as outline in Sec. 2.4.3 accurately represents the average electron ionization fraction until well after the decoupling and drag epochs. At late times the Eq. (2.106) does not accurately model the electron ionization fraction because on the one hand Eq. (2.106) neglects the difference between baryons and radiation temperature [Seager et al., 1999; Ali-Haimoud and Hirata, 2011; Chluba and Thomas, 2011], and on the other hand reionization is also absent in Eq. (2.106).

As shown in Sec. 2.4.3, we first find the volume–average decoupling redshift, $\bar{z}_{\rm dec}$, and drag redshift, $\bar{z}_{\rm drag}$, epochs and then infer the corresponding dressed redshifts, $z_{\rm dec}$ and $z_{\rm drag}$, that are seen by a wall/galaxy observer with the relation given in (2.101), namely

$$1 + z = \frac{\bar{\gamma}}{\bar{\gamma}_0} \, (1 + \bar{z}) \; .$$

The clock rate difference between volume–average and wall/galaxy observers at the decoupling and drag epochs is negligible i.e., $\gamma(z_{\rm dec}) = \gamma(\bar{z}_{\rm dec}) \approx 1$ and $\gamma(z_{\rm drag}) = \gamma(\bar{z}_{\rm drag}) \approx 1$. But at present typically (see Table 3.2) $\gamma_0 \approx 1.3$ and thus on account of (4.1) the decoupling and the drag epochs as seen by volume–average or wall/galaxy observers are at different redshifts. This was of course known from the beginning, see for example Wiltshire [2007a]. However, in previous timescape studies such as those by Wiltshire [2007a]; Leith et al. [2008] a value $z_{\rm dec} = 1100$ was assumed and the drag epoch, $z_{\rm drag}$, was not used at all. The exact scale of the sound horizon which is referred to by Wiltshire [2007a]; Leith et al. [2008] is sensitive to the baryonic content in the universe, and the precise redshift of decoupling $\bar{z}_{\rm dec}$ changes as $\bar{\Omega}_{\rm B0}$ is changed. Thus our work is an improvement on these previous studies of the timescape cosmology as

we are able to determine the precise redshift of decoupling and the associated scale of sound horizon for a given set of timescape parameters.

Furthermore, based on the reasoning that matter–radiation equality should precede the decoupling epoch, i.e.,

$$\left(\frac{\bar{\Omega}_{\rm M}}{\bar{\Omega}_{\rm R}}\right)_{\rm dec} > 1\,,$$

we where able to put constraint on the present dressed matter content and rule out portion of the parameter space in the h–$\bar{\Omega}_{\rm M0}$ plane. See Fig. 2.9. The new results allow us to rule out portions of the parameter space, such as $\Omega_{\rm M0} < 0.2$ if $H_0 < 65\ {\rm km\,s^{-1}\,Mpc^{-1}}$, which were still admissible in previous studies [Leith et al., 2008; Smale and Wiltshire, 2011].

In Chapter 3 we have used the timescape matter and radiation solution and recombination history to study the CMB anisotropies in the timescape scenario. In Chapter 3 we have for the first time investigated the parameter bounds that can be put on the timescape cosmology through a full analysis of the acoustic peaks in the power spectrum of CMB temperature anisotropies, using Planck satellite data [Ade et al., 2014b].

Since the expansion history of the timescape model differs only slightly from that of a FLRW model at early epochs, we performed our analysis by directly computing relevant processes (such as nucleosynthesis and recombination) for the timescape model in the early universe, and then matched the expansion history of the timescape model to that of the closest equivalent FLRW model in volume–average coordinates. Therefore, rather then carrying out the CMB analysis for the timescape model from first principles we have relied on the very close proximity between the timescape model and some FLRW model during the early stages of the evolution of the universe. This was based on the reasoning that the acoustic peaks in the CMB are laid down in the same era when some FLRW model can approximately match the expansion history of the timescape model. Thus those features of the CMB temperature powerspectrum which are from an era when the timescape expansion history is significantly different from the FLRW expansion history, such as the late-time ISW, could not be accounted for in our study.

However, finding a FLRW cosmology that has an expansion history as close as possible to the timescape model is a challenge in itself. For this reason, we have investigated a number of matching procedures, but used the $A(\bar{H}_{\rm dec})$ matching in Sec. 3.3.3.1 to provide statistical bounds on parameters related to the average expansion history.

We conclude that there are parameters for which the timescape model is a good fit to the Planck data, and it remains competitive with the ΛCDM model. However, we can no longer claim a resolution of the primordial lithium abundance problem, as seemed

possible with fits based solely on the angular diameter distance of the sound horizon at decoupling and the baryon drag epoch [Duley et al., 2013]. This result is an outcome of directly constraining the baryonic content in the timescape model with the acoustic peaks in the CMB.

It is clear, however, that this conclusion is driven by the ratio of the heights of the acoustic peaks which depend strongly on the ratio of baryons to nonbaryonic dark matter in the primordial plasma. Furthermore, these results depend heavily on perturbation theory in the early universe for which a standard ΛCDM model has been assumed, with possibly different constituent ratios.

Although backreaction is negligible in determining the background solution, in our numerical examples $\bar{\Omega}_{\mathcal{Q}\,\mathrm{dec}} \sim \times 10^{-5}$ is of the same order as the density perturbations, $\delta\rho/\rho$, in baryons at decoupling. Thus although the backreaction terms are inconsequential in determining the background at early times they very probably should *not* be neglected in considering the evolution of perturbations in determining the acoustic peaks. By analogy, in the standard treatment both density and velocity perturbations are small and do not significantly affect the background but being of similar order they must be considered as a coupled system.

The very fact that they systematic uncertainties which arise from different FLRW matching procedures are typically 3–4 times larger than the MCMC statistical uncertainties directly shows that initial small differences are significant in the CMB anisotropy analysis. These up tp 8–11% differences at the present epoch arise from differences of $\lesssim 10^{-5}$ in density parameters at last scattering. Consequently even though backreaction terms only modify average evolution at this level early on, their impact on the seeding of structure formation is very likely to be much more important than on the initial early evolution of the average background.

Ideally therefore we should consider the backreaction formalism with pressure [Buchert, 2001] for a matter plus radiation plasma which begins in close to homogeneous and isotropic state. Since the average evolution is not *exactly* a Friedmann model, such an analysis is subtly different from a perturbative approach which assumes that average evolution is exactly a solution of Einstein's equations. The problem of backreaction in the primordial plasma has not been studied in any more detail than Buchert's initial formal study [Buchert, 2001]. There is much discussion of backreaction in models which are close to FLRW backgrounds, but debate has centred on the question of whether backreaction can cause significant deviations of the average evolution from FLRW evolution in the case of dust cosmologies [Clarkson et al., 2011]. The question here differs both by the virtue of the matter content, and by the fact that we are interested in changes to the

growth of perturbations rather than the average evolution itself. As far as physical cosmology is concerned, this is completely uncharted territory.

To summarize our results, if we take the canonical $A(\bar{H}_{\rm dec})$ matching method to estimate the parameters which describe the average expansion history, but use the difference in the wall geometry matching method results of Table 3.2 to estimate systematic uncertainties then for the volume–average base parameters, we have $H_0 = 61.0\,{\rm km\,s^{-1}\,Mpc^{-1}}$ ($\pm 1.3\%$ stat) ($\pm 8\%$ sys), and a present void volume fraction $f_{\rm v0} = 0.627$ ($\pm 2.33\%$ stat) ($\pm 11\%$ sys). Since the wall–geometry matching methods are better adapted to those aspects of the timescape model that do not relate directly to volume–average evolution, we reverse the procedure to provide our best estimates on $\eta_{B\gamma}$ and $n_{\rm s}$. In particular, we use the $W(k \neq 0)$ method—which has the best likelihood overall—to estimate the parameters, and the $A(\bar{H}_{\rm dec})$ method for the range of systematic uncertainties. In the case of the systematic uncertainties, the lower bound is what was actually obtained using the $W(k = 0)$ and $W(k \neq 0)$ matching procedures in Table 3.2. However, since other matching procedures could be also envisioned, we use the bound obtained as a best estimate percentage systematic uncertainty. This gives $10^{10}\eta_{B\gamma} = 6.08$ ($\pm 1.5\%$ stat) ($\pm 8.5\%$ sys) and $n_{\rm s} = 0.96$ ($\pm 0.9\%$ stat) ($\pm 4.3\%$ sys). These best fit values are close to their ΛCDM counterparts [Ade et al., 2014b], but the systematic uncertainties more fully reflect the limitations of our procedure.

Importantly we note that for the canonical matching procedure the best fit $f_{\rm v0} = 0.628$ and mean $f_{\rm v0} = 0.628^{+0.014}_{-0.012}$ both imply, on account of Eq. (1.28), that the galaxy/wall observer infers an accelerating universe. However, the best fit and mean constraints on $f_{\rm v0}$ from the complementary matching methods in Table 3.2 give a decelerating dressed expansion for the galaxy/wall observer. This is because the dressed deceleration parameter, q_0 in Eq. (4.1) changes sign when $f_{\rm v0} \simeq 0.5867$. If we demand that the galaxy/wall observer must infer an accelerating universe—which better matches other data sets such as type Ia supernovae [Leith et al., 2008; Smale and Wiltshire, 2011]—then the results from the complementary matching procedures, which we primarily used to get a handle on systematic uncertainties, can be disregarded, as best estimates of the average expansion history. We also note that the constraints on the timescape model parameters from the CMB with the canonical matching method, with a FLRW expansion history closest to that of the timescape model, have an apparently accelerating dressed expansion rate.

To bring the timescape scenario into the realm of "precision cosmology", it is of course necessary to eliminate the large systematic uncertainties that arise from the imprecise nature of the matched FLRW model procedures. This would require a huge computational effort. However, our results highlight the fact that important details of the

acoustic peaks are strongly constrained by the ratio of baryonic to nonbaryonic matter in the primordial plasma, which can in principle differ in the timescape scenario. To treat this question rigorously we must address the effect of backreaction in the primordial plasma, and the manner in which the growth of structure is changed when the average evolution is very close to, but not exactly, a perturbative FLRW model. While it is not possible to give an exact a priori value for backreaction in the primordial plasma, one can comment on its significance. The terms from pressure inhomogeneities themselves are likely to be smaller than $\bar{\Omega}_{\mathcal{Q}\,\mathrm{dec}} \sim 10^{-5}$ in energy density, as the Buchert equations (2.51)–(2.59) themselves change, and the lapse becomes dynamical. We would expect to end up with parameter values within the range of systematic uncertainties we have estimated, but cannot pin down their values a priori. These effects have not been studied, but are crucially important.

4.2 Final remarks

Our analysis of the timescape model with the CMB data here and also presented in Nazer and Wiltshire [2015], together with previous tests against the supernovae data [Leith et al., 2008; Smale and Wiltshire, 2011] and gamma-ray burst distances [Smale, 2011] show that timescape cosmology can fit these data and the model remains viable. These works provided a self consistency check that the model can fit diverse data sets with the same model parameters. This is extremely important because data from different observational experiments probe different aspects of the model.

The work carried out in Chapter 3 is the first time the timescape cosmology has been put to the test against the CMB data. The constraints on the timescape cosmology as a result of the CMB analysis have changed what we previously thought were the best fit timescape parameters but remain statistically consistent with prior parameter constraints. This change has resulted from constraining the ratio of baryonic to nonbaryonic matter in timescape model with the CMB temperature power spectrum. The baryonic content in the timescape model had not been probed in prior studies.

With our work we have taken an important step forward in developing the timescape cosmology. The picture of the universe now according to the timescape cosmology is that an observer located in a wall region—we ourselves as galaxy bound observers live on the edge of a wall—sees a 13.8 billion years old universe with 9% ordinary matter and 40% cold dark matter with the remainder of the energy budget almost entirely attributed to spatial curvature. The galaxy/wall observers infers an accelerating universe in which voids make up just over 60% of the present horizon volume, i.e., $f_{\mathrm{v}0} = 0.627$. The volume–average observer does not infer acceleration.

Wiltshire's attempt in the timescape model to incorporate concepts such as gravitational energy—a notoriously difficult topic in its own right—in a working model for the universe is ambitious. From a practical point of view such strict adherence to relativistic principles in cosmology makes the task of developing the model that much more difficult. By comparison the standard cosmology approach might be considered ad hoc. For example, N-body Newtonian dynamics simulations are used to infer results about structure formation in the relativistic FLRW cosmology.

Determination of the BAO scale in galaxy clustering statistics provides another potentially important test of the timescape model. The BAO scale has now been detected at several redshifts in galaxy clustering statistics [Blake et al., 2011; Anderson et al., 2013] and the Lyman–α forest [Delubac et al., 2015]. In fact, the timescape and ΛCDM predictions are so close, that the differences lie within current uncertainties for the statistics used. If the radial and angular BAO scales are reliably separated, to perform a full Alcock–Paczyński test [Alcock and Paczyński, 1979] then this could potentially better discriminate between the models [Wiltshire, 2009, 2015]. One further complicating factor is that redshift–space distortions need to be modelled in reducing the data, and this is often done using standard FLRW model assumptions. The BAO measure will be important in future cosmological tests, but more work needs to be done in the timescape cosmology, so that we can be sure that any assumptions entering the data reduction do not depend crucially on the cosmological model.

The success of the timescape model thus far makes it a candidate for further research. Future challenges on the theoretical front are to develop the timescape cosmology further into a fully fledged model akin to the standard model of cosmology, and also to develop data analysis tools specific to the model. The timescape model fits the data against which it has been tested so far but further tests need to be carried out with all the observational data available to us. As of yet the timescape cosmology has not been developed to provide theoretical predictions for galaxy clustering statistics, bulk flows and weak lensing.

Based on previous works and the work in this thesis, we conclude that it is quite possible that the inferred acceleration of the universe in the context of standard FLRW cosmologies is not something physical but an artefact due to the assumptions that average expansion is strictly that of a homogeneous FLRW model. Therefore, inhomogeneous cosmological studies, whether based on exact inhomogeneous solutions of the Einstein's equations, or spatial averaging procedures in general and the timescape model in particular should be given serious consideration[1] as we continue our efforts to understand

[1]Of course the aforementioned methods are not the only ways of studying and probing the inhomogeneous nature of the universe. I am also involved in a study in which the inhomogeneity in the universe is investigated by looking at the nonlinear variations in the Hubble expansion below the scale

and explain the universe that is revealed to us by the numerous data.

of statistical homogeneity. The Python code for this project which includes code that solves the evolution and geodesic equations for the Lemaître-Tolman-Bondi model has been made publicly available at https://github.com/Ahsan-.

Appendix A

Numerical integration: timescape cosmology with matter and radiation

For the purposes of numerical integration it is convenient to write the derivatives with respect to $x \equiv \bar{a}/\bar{a}_0$, yielding the system of three couple ODEs

$$\frac{dt'}{dx} = \frac{x\sqrt{1+x^2F^2}}{f_{\rm v}^{1/3}x^2 + \alpha_{\rm M0}x + \alpha_{\rm R0}}\,, \tag{A.1}$$

$$\frac{df_{\rm v}}{dx} = 3F\sqrt{f_{\rm v}\,(1-f_{\rm v})}\,, \tag{A.2}$$

$$\frac{dF}{dx} = \frac{\left(1+x^2F^2\right)\left[f_{\rm v}^{-1/6}\sqrt{1-f_{\rm v}} + F\left(\alpha_{\rm M0}+2\alpha_{\rm R0}x^{-1}\right)\right]}{2\left(f_{\rm v}^{1/3}x^2+\alpha_{\rm M0}x+\alpha_{\rm R0}\right)} - F\left(\frac{3}{x}+2xF^2\right)\,, \tag{A.3}$$

in the dimensionless variables $t' \equiv \bar{\alpha}\bar{H}_0 t$, $f_{\rm v}$ and $F \equiv \partial_x f_{\rm v}/\left[f_{\rm v}\,(1-f_{\rm v})\right]$, where $\alpha_{\rm M0} \equiv \bar{\alpha}^{-2}\bar{\Omega}_{\rm M0}$, and $\alpha_{\rm R0} \equiv \bar{\alpha}^{-2}\bar{\Omega}_{\rm R0}$. The wall time parameter, $\tau_{\rm w} = \int \bar{\gamma}^{-1}dt$, may be determined also by integrating the equation

$$\bar{\alpha}\bar{H}_0\frac{d\tau_{\rm w}}{dx} = \frac{1-f_{\rm v}\left(1+x^2F^2\right)}{1-f_{\rm v}+xF\sqrt{f_{\rm v}\,(1-f_{\rm v})}}\frac{dt'}{dx}\,. \tag{A.4}$$

Given an initial estimate of $f_{\rm v0}$, the tracker solution [Wiltshire, 2007b, 2009] is used to estimate $\bar{\Omega}_{\rm M0} \simeq 4\,(1-f_{\rm v0})\,/\,(2+f_{\rm v0})^2$, $\bar{\Omega}_{\rm K0} \simeq 9f_{\rm v0}/\,(2+f_{\rm v0})^2$, $\bar{\alpha}^2 \simeq 9f_{\rm v0}^{2/3}/\,(2+f_{\rm v0})^2$ and $\alpha_{\rm M0} = 4\,(1-f_{\rm v0})\,/\left(9f_{\rm v0}^{2/3}\right)$. Since $\bar{\Omega}_{\rm R0} = \kappa g_* T_0^4/\left(\bar{H}_0^2/\bar{\gamma}_0^4\right)$, where $\kappa = 4\pi^3 G k_{\rm B}^4/\left(45\hbar^3c^5\right)$, $g_* = 3.36$ and $T_0 = 2.725\,{\rm K}$, then given a value of $\bar{H}_0$ and the tracker solution estimates for $\bar{\Omega}_{\rm M0}$ and $\bar{\Omega}_{\rm K0}$ we solve Eq. (A.5) to estimate $\bar{\gamma}_0$, $\bar{\Omega}_{\rm R0}$ and

$\alpha_{\rm R0}$.

$$\bar{\gamma}_0 = \frac{\sqrt{1-f_{\rm v0}}\left(\sqrt{1-f_{\rm v0}}+\sqrt{f_{\rm v0}\left(1-f_{\rm v0}\right)\left(\bar{\Omega}_{\rm M0}+\bar{\Omega}_{\rm R0}+\bar{\Omega}_{\rm K0}-1\right)}\right)}{1-f_{\rm v0}\left(\bar{\Omega}_{\rm M0}+\bar{\Omega}_{\rm R0}+\bar{\Omega}_{\rm K0}\right)} \tag{A.5}$$

Initial values of the variables are now determined at an early initial time using the series solutions (A.6) and (A.7) with x as the independent variable.

$$\begin{aligned}\bar{H}_0\bar{\alpha}t = {}& \frac{x^2}{2\alpha_{\rm R0}^{1/2}} - \frac{\alpha_{\rm M0}x^3}{6\alpha_{\rm R0}^{3/2}} + \frac{3\alpha_{\rm M0}^2x^4}{32\alpha_{\rm R0}^{5/2}} - \left(\frac{2\sqrt{5}}{125\alpha_{\rm R0}^2}+\frac{\alpha_{\rm M0}^3}{16\alpha_{\rm R0}^{7/2}}\right)x^5 \\ & + \left(\frac{7\sqrt{5}\alpha_{\rm M0}}{300\alpha_{\rm R0}^3}+\frac{35\alpha_{\rm M0}^4}{768\alpha_{\rm R0}^{9/2}}\right)x^6 - \left(\frac{402\sqrt{5}\alpha_{\rm M0}^2}{14875\alpha_{\rm R0}^4}+\frac{9\alpha_{\rm M0}^5}{256\alpha_{\rm R0}^{11/2}}\right)x^6+\cdots \end{aligned} \tag{A.6}$$

$$\begin{aligned} f_{\rm v} = {}& \frac{\sqrt{5}x^3}{25\alpha_{\rm R0}^{3/2}} - \frac{9\sqrt{5}\alpha_{\rm M0}x^4}{250\alpha_{\rm R0}^{5/2}} + \frac{639\sqrt{5}\alpha_{\rm M0}^2x^5}{21250\alpha_{\rm R0}^{7/2}} - \left(\frac{6}{325\alpha_{\rm R0}^3}+\frac{5553\sqrt{5}\alpha_{\rm M0}^3}{221000\alpha_{\rm R0}^{9/2}}\right)x^6 \\ & + \left(\frac{11106\alpha_{\rm M0}}{300625\alpha_{\rm R0}^4}+\frac{295461027\sqrt{5}\alpha_{\rm M0}^4}{13900900000\alpha_{\rm R0}^{11/2}}\right)x^7+\cdots \end{aligned} \tag{A.7}$$

We then integrate the ODEs (A.1)–(A.4) until the present epoch is reached at $x_0 = 1$, giving the exact numerical values $t_0' = \bar{\alpha}\bar{H}_0 t$, $f_{\rm v0}$, F_0 and $\bar{\alpha}\bar{H}_0\tau_{\rm w0}$. We also have $\bar{\gamma}_0 = \left(1-f_{\rm v0}+F_0\sqrt{f_{\rm v0}\left(1-f_{\rm v0}\right)}\right)/\left(1-f_{\rm v0}\left(1+F_0^2\right)\right)$.

Only two parameters, $\alpha_{\rm M0}$ and $\alpha_{\rm R0}$, appear in the ODEs (A.1)–(A.4). Solutions with fixed $\alpha_{\rm M0}$, $\alpha_{\rm R0}$, therefore represent a class of solutions which are physically equivalent under a rescaling of the parameters $\bar{\alpha}$, $\bar{\Omega}_{\rm M0}$ and $\bar{\Omega}_{\rm R0}$, while keeping the ratio $\bar{\Omega}_{\rm M0}/\bar{\Omega}_{\rm R0}$ fixed. A general solution does not have $\bar{H} = \bar{H}_0$ at $x_0 = 1$; to impose this condition we identify the right hand side of (A.1) at $x_0 = 1$ with $\bar{\alpha}$, from which precise values of $\bar{\Omega}_{\rm M0} = \bar{\alpha}^2\alpha_{\rm M0}$, $\bar{\Omega}_{\rm R0} = \bar{\alpha}^2\alpha_{\rm R0}$ and $\bar{H}_0 t_0$ may be determined.

Appendix B

Neutrinos

Neutrinos make up nearly half of the total radiation energy density, $(\rho_\nu/(\rho_\nu + \rho_\gamma) \approx 0.407)$, if the effective number of neutrinos, $N_{\rm eff} = 3$, exceed the photon energy density $(\rho_\nu/\rho_\gamma \geq 1.02)$ for $N_{\rm eff} \geq 4.5$ and have a sizeable impact on the expansion rate during radiation domination. Independent from cosmological constraints on $N_{\rm eff}$ the compilation in Beringer et al. [2012, pp. 629-630] from particle physics experiments give the number of light neutrinos as 2.984 ± 0.008 for experiments that track Z boson production from e^+e^- annihilation and as 2.92 ± 0.05 for experiments that study the $e^+e^- \to \nu\bar{\nu}\gamma$ process. Here we explain our choice of $N_{\rm eff} = 3.046$ for the base timescape cosmology. The total radiation energy density is the sum of photon and neutrino energy densities

$$\begin{aligned}\bar{\rho}_r &= \bar{\rho}_\gamma + \bar{\rho}_\nu \\ &= g_\gamma \int_0^\infty \frac{4\pi}{(2\pi\hbar)^3} p_\gamma^3 dp_\gamma \frac{1}{\exp(p_\gamma/k_B\bar{T}_\gamma) - 1} + g_\nu \int_0^\infty \frac{4\pi}{(2\pi\hbar)^3} p_\nu^3 dp_\nu \frac{1}{\exp(p_\nu/k_B\bar{T}_\nu) + 1} \\ &= \frac{g_\gamma \pi^2 k_B^4}{30\hbar^3}\bar{T}_\gamma^4 + \frac{7}{8}\frac{g_\nu \pi^2 k_B^4}{30\hbar^3}\bar{T}_\nu^4 \, . \end{aligned} \tag{B.1}$$

At sufficiently high temperatures neutrinos, photons and electrons/positrons form a plasma and $\bar{T}_\nu = \bar{T}_\gamma$ because of reactions such as $e^+ + e^- \rightleftharpoons \nu + \bar{\nu}$ and $e^+ + e^- \leftrightarrow \gamma + \gamma$ that helped maintain thermal equilibrium. After neutrinos decouple their temperature drop as $\bar{T}_\nu \propto 1/\bar{a}$ (maintaining the Fermi-Dirac distribution) whereas photons in the remaining photon, electon/positron plasma has a slightly higher temperature $\bar{T}_\gamma > \bar{T}_\nu$. The relation $\bar{T}_\gamma/\bar{T}_\nu = (11/4)^{1/3}$ is obtained by putting together the facts that entropy is conserved in a comoving volume $s(\bar{T})\bar{a}^3 =$ constant, $(s(\bar{T}) \equiv \left(\rho(\bar{T}) + p(\bar{T})\right)/\bar{T}$, for the combined system of photons and electrons/positrons), $\bar{a} \propto 1/\bar{T}_\nu$ and $\bar{T}_\nu \to \bar{T}_\gamma$ in the

limit that electrons are relativistic. Eq. (B.1) can then be written as

$$\bar{\rho}_r = \frac{g_\gamma \pi^2 k_B^4}{30\hbar^3}\bar{T}_\gamma^4 \left[1 + \frac{7}{8}\left(\frac{4}{11}\right)^{4/3}\frac{g_\nu}{g_\gamma}\right]$$
$$\bar{\rho}_r = \bar{\rho}_\gamma \left[1 + \frac{7}{8}\left(\frac{4}{11}\right)^{4/3} N_{\rm eff}\right] , \tag{B.2}$$

in which $N_{\rm eff} = 3$ means six degrees of freedom for neutrinos (3 species of neutrinos and their antiparticles), $g_\nu = 6$ is assumed.

The parametrization of Eq. (B.2) with $N_{\rm eff}$ is designed to encapsulate more physics than simply a rearrangement of the symbols. The relation $\bar{T}_\gamma/\bar{T}_\nu = (11/4)^{1/3}$ is obtained by assuming instantaneous decoupling of neutrinos, whereas the reaction $e^+ + e^- \rightarrow \nu + \bar{\nu}$ maintains some interaction between neutrinos and the plasma after the instantaneous decoupling epoch and continues to change the neutrino temperature [Mangano et al., 2002]. Neutrinos acquire a slightly higher temperature than in the instantaneous decoupling approximation. When $e^\pm$ annihilate some of their entropy is transferred to neutrinos through this interaction, contrary to the case when all the entropy is transferred to photons. In Mangano et al. [2002] $N_{\rm eff} = 3.0395$ is advocated to account for the non instantaneous decoupling as well as QED corrections to the photon, electron/positron plasma equation of state. In subsequent work Mangano et al. [2005] find $N_{\rm eff} = 3.046$ to account for neutrino flavour oscillations in addition to the aforementioned points.

The Planck collaboration use $N_{\rm eff} = 3.046$ in their base ΛCDM model which we also use in the base timescape cosmology. Values of $N_{\rm eff} > 3.046$ are used, for example, to incorporate extra radiation components such as sterile neutrinos [Lesgourgues and Pastor, 2014; Ichikawa et al., 2008]. In such cases $\bar{\rho}_r = \bar{\rho}_\gamma + \bar{\rho}_\nu$ is replaced by $\bar{\rho}_r = \bar{\rho}_\gamma + \bar{\rho}_\nu + \bar{\rho}_x$ where $\bar{\rho}_x$ is the energy density of the extra radiation component. Our aim here is to explore the parameter space in timescape cosmology whilst remaining consistent with known physics which is why we use $N_{\rm eff} = 3.046$ for the base timescape model. We also explore the case in which $N_{\rm eff}$ is a free MCMC parameter without elaborating what the extra radiation component represents. We do not aim to constrain neutrino masses, for example. In this case we find that a larger value for $N_{\rm eff}$ results in a higher $\eta_{B\gamma}$.

Appendix C

List of used software packages

We acknowledge the use of software packages by various groups of authors made available for public use to the wider scientific community. In some cases the software packages where not used in the final presentation of this thesis but were used during the course of research undertaken. The licenses or terms of use of these packages (in alphabetical order) are as follows:

- *CLASS* is a code written in C to solve the Einstein-Boltzmann equations used in the study of CMB anisotropies. You can use CLASS freely, provided that in your publications, you cite at least the paper [Blas et al., 2011].
- *CosmoMC* is a Fortran and python code for performing and analysing cosmological parameter extractions via Bayesian MCMC methods. (i) Any publication using results of the code must be submitted to arXiv at the same time as, or before, submitting to a journal. arXiv must be updated with a version equivalent to that accepted by the journal on journal acceptance. (ii) If you identify any bugs you report them as soon as confirmed.
- *emcee* is an Affine Invariant MCMC sampler based on the algorithm of Goodman and Weare [2010]. emcee is a free software made available under the MIT License. The authors recommend that Foreman-Mackey et al. [2013] be cited.
- *fastbbn* is a Fortran code for computing primordial light element abundances. The use of this code is free provided Fiorentini et al. [1998]; Lisi et al. [1999] are cited.
- *Monte Python* is a Monte Carlo code for cosmological parameter extraction. Monte Python is released under the MIT license. Its use requires that Audren et al. [2012] is cited.

- *RECFAST* is a code for the recombination history of the Universe. To honour its terms of use we have cited [Seager et al., 1999].

- *Open source software packages* We have used open source packages for scientific computing SciPy, NumPy for numerical computations and matplotlib plotting library for producing the figures in this thesis.

Bibliography

Ade, P. A. R. et al. (2014a). Planck 2013 results. XV. CMB power spectra and likelihood. *Astron. Astrophys.*, 571:A15. arXiv:1303.5075.

Ade, P. A. R. et al. (2014b). Planck 2013 results. XVI. Cosmological parameters. *Astron. Astrophys.*, 571:A16. arXiv:1303.5076.

Ade, P. A. R. et al. (2014c). Planck 2013 results. XXIII. Isotropy and statistics of the CMB. *Astron. Astrophys.*, 571:A23. arXiv:1303.5083.

Alcock, C. and Paczyński, B. (1979). An evolution free test for non-zero cosmological constant. *Nature.*, 281:358.

Ali-Haimoud, Y. and Hirata, C. M. (2011). HyRec: A fast and highly accurate primordial hydrogen and helium recombination code. *Phys. Rev. D.*, 83:043513. arXiv:1011.3758.

Allison, R. and Dunkley, J. (2013). Comparison of sampling techniques for bayesian parameter estimation. arXiv:1308.2675.

Alpher, R. A., Bethe, H., and Gamow, G. (1948). The Origin of Chemical Elements. *Phys. Rev.*, 73:803. aps:10.1103.

Amanullah, A. et al. (2010). Spectra and Light Curves of Six Type Ia Supernovae at $0.511 < z < 1.12$ and the Union2 Compilation. *Astrophys. J.*, 716:712–738. arXiv:1004.1711.

Amendola, L. et al. (2013). Cosmology and fundamental physics with the Euclid satellite. *Living Rev. Rel.*, 16(6). arXiv:1206.1255.

Anderson, L. et al. (2013). The clustering of galaxies in the SDSS-III Baryon Oscillation Spectroscopic Survey: Baryon Acoustic Oscillations in the Data Release 10 and 11 galaxy samples. arXiv:1312.4877.

Arnowitt, R., Deser, S., and Misner, C. W. (1962). *Gravitation: An introduction to current research*, pages 227–265. Wiley, New York. The Dynamics of General Relativity. arXiv:0405109.

Audren, B., Lesgourgues, J., Benabed, K., and Prunet, S. (2012). Conservative Constraints on Early Cosmology: an illustration of the Monte Python cosmological parameter inference code. arXiv:1210.7183.

Bardeen, J. M. (1980). Gauge-invariant cosmological perturbations. *Phys. Rev. D.*, 22:1882.

Baumgarte, T. W. and Shapiro, S. L. (2010). *Numerical Relativity: Solving Einstein's Equations on the Computer*. Cambridge, UK: Cambridge Univ. Press.

Beringer, J. et al. (2012). Review of particle physics. *Phys. Rev. D.*, 86:010001.

Bertschinger, E. (1998). Simulations of structure formation in the universe. *Annu. Rev. Astron. Astrophys.*, 36:599–654.

Beutler, F. et al. (2001). The 6dF Galaxy Survey: Baryon Acoustic Oscillations and the Local Hubble Constant. *Mon. Not. R. Astr. Soc.*, 416:3017–3032. arXiv:1106.3366.

Binetruy, P., Deffayet, C., Ellwanger, U., and Langlois, D. (2000). Brane cosmological evolution in a bulk with cosmological constant. *Phys. Lett. B.*, 477:285–291. arXiv:9910219.

Biswas, T., Notari, A., and Valkenburg, W. (2010). Testing the Void against Cosmological data: fitting CMB, BAO, SN and H_0. *J. Cosmol. Astropart. Phys.*, 11(2010):030. arXiv:1007.3065.

Blake, C. et al. (2011). The WiggleZ Dark Energy Survey: measuring the cosmic expansion history. . *Mon. Not. R. Astr. Soc.*, 418:1752.

Blas, D., Lesgourgues, J., and Tram, T. (2011). The Cosmic Linear Anisotropy Solving System (CLASS) II: Approximation schemes. *J. Cosmol. Astropart. Phys.*, 07:034. arXiv:1104.2933.

Bolejko, K. and Célérier, M.-N. (2010). Szekeres Swiss-Cheese model and supernova observations. *Phys. Rev. D.*, 82:103510. arXiv:1005.2584.

Bolejko, K. and Wyithe, J. S. B. (2009). Testing the Copernican principle via cosmological observations. *J. Cosmol. Astropart. Phys.*, 02:020. arXiv:0807.2891.

Bondi, H. (1947). Spherically symmetrical models in general relativity. *Mon. Not. R. Astr. Soc.*, 107:410. adsabs:1947MNRAS.107..410B.

Bondi, H. (1952). *Cosmology*. Cambridge, UK: Cambridge Univ. Press. pg 168.

Bondi, H. (1960). *Cosmology*. Cambridge, UK: Cambridge Univ. Press, 2nd ed. edition.

Bondi, H. and Gold, T. (1948). The Steady-State Theory of the Expanding Universe. *Mon. Not. R. Astr. Soc.*, 108:252. adsabs:108..252B.

Brandenberger, R. H. (2011). Alternatives to the inflationary paradigm of structure formation. *Int. J. Mod. Phys. Conf. Ser.*, 01:67–79. arXiv:0902.4731.

Brax, P., van de Bruck, C., and Davis, A.-C. (2004). Brane World Cosmology. *Rept. Prog. Phys.*, 67:2183–2232. arXiv:0404011.

Buchert, T. (2000). On Average Properties of Inhomogeneous Fluids in General Relativity: Dust Cosmologies. *Gen. Rel. Grav.*, 32:105–125. arXiv:9906015.

Buchert, T. (2001). On Average Properties of Inhomogeneous Fluids in General Relativity: Perfect Fluid Cosmologies. *Gen. Rel. Grav.*, 33:1381–1405. arXiv:0102049.

Buchert, T. and Carfora, M. (2002). Regional averaging and scaling in relativistic cosmology. *Class. Quant. Grav.*, 19:6109–6145. arXiv:0210037.

Buchert, T. and Carfora, M. (2003). Cosmological parameters are dressed. *Phys. Rev. Lett.*, 90:031101. arXiv:0210045.

Buchert, T. and Ehlers, J. (1997). Averaging inhomogeneous Newtonian cosmologies. *Astron. Astrophys.*, 320:1–7. arXiv:9510056.

Caldwell, R. R., Kamionkowski, M., and Weinberg, N. N. (2003). Phantom energy and cosmic doomsday. *Phys. Rev. Lett.*, 91:071301. arXiv:0302506.

Carroll, S. M. (1998). Quintessence and the Rest of the World: Suppressing Long-Range Interactions. *Phys. Rev. Lett.*, 81:3067–3070. arXiv:9806099.

Célérier, M.-N. (2000). Do we really see a cosmological constant in the supernovae data? *Astron. Astrophys.*, 353:63–71. arXiv:9907206.

Célérier, M.-N., Bolejko, K., and Krasiński, A. (2010). A (giant) void is not mandatory to explain away dark energy with a Lemaitre-Tolman model. *Astron. Astrophys.*, 518:A21. arXiv:0906.0905.

Chluba, J. and Thomas, R. M. (2011). Towards a complete treatment of the cosmological recombination problem. *Mon. Not. R. Astr. Soc.*, 412:748–764. arXiv:1010.3631.

Clarkson, C., Ananda, K., and Larena, J. (2009). The influence of structure formation on the cosmic expansion. *Phys. Rev. D.*, 80:083525. arXiv:0907.3377.

Clarkson, C., Bassett, B., and Lu, T. H. C. (2008). A general test of the Copernican Principle. *Phys. Rev. Lett*, 101:011301. arXiv:0712.3457.

Clarkson, C., Ellis, G. F. R., Larena, J., and Umeh, O. (2011). Does the growth of structure affect our dynamical models of the universe? The averaging, back-reaction and fitting problems in cosmology. *Rept. Prog. Phys.*, 74:112901. arXiv:1109.2314.

Clarkson, C. and Regis, M. (2011). The Cosmic Microwave Background in an Inhomogeneous Universe - why void models of dark energy are only weakly constrained by the CMB. *J. Cosmol. Astropart. Phys.*, 02:013. arXiv:1007.3443.

Clifton, T. et al. (2012). Modified Gravity and Cosmology. *Physics Reports*, 513:1–189. arXiv:1106.2476.

Clifton, T., Ferreira, P. G., and Zuntz, J. (2009). What the small angle CMB really tells us about the curvature of the Universe. *J. Cosmol. Astropart. Phys.*, 07:029. arXiv:0902.1313.

Cole, S. et al. (2005). The 2dF Galaxy Redshift Survey: Power-spectrum analysis of the final dataset and cosmological implications . *Mon. Not. R. Astr. Soc.*, 362:505–534. arXiv:0501174.

Coley, A. A., Pelavas, N., and Zalaletdinov, R. M. (2005). Cosmological Solutions in Macroscopic Gravity. *Phys. Rev. Lett.*, 95:151102. arXiv:0504115.

Copeland, J. E., Sami, M., and Tsujikawa, S. (2006). Dynamics of dark energy. *Int. J. Mod. Phys. D.*, 15:1753–1936. arXiv:0603057.

Copi, C. J. et al. (2010). Large-angle anomalies in the CMB. *Adv. Astron.*, 2010:847541. arXiv:1004.5602.

Cyburt, R. H., Fields, B. D., and Olive, K. A. (2008). An update on the big bang nucleosynthesis prediction for ^{7}Li: The problem worsens. *J. Cosmol. Astropart. Phys.*, 0811:1475–7516. arXiv:0808.2818.

Dabrowski, M. P. and Hendry, M. A. (1998). The Hubble Diagram of Type Ia Supernovae in Non-Uniform Pressure Universes. *Astrophys. J.*, 498:67–76. arXiv:9704123.

Delubac, T. et al. (2015). Baryon Acoustic Oscillations in the Lyα forest of BOSS DR11 quasars. *Astron. Astrophys.*, 574:A59. arXiv:1404.1801.

Dicke, R. H., Peebles, P. J. E., Roll, P. G., and Wilkinson, D. T. (1965). Cosmic Black-Body Radiation. *Astrophys. J.*, 142:414–419. adsabs:148306.

Dodelson, S. (2003). *Modern Cosmology*. Academic Press.

Duley, J. A. G. (2011). Average cosmic evolution in a lumpy universe. Master's thesis, University of Canterbury. http://hdl.handle.net/10092/6345.

Duley, J. A. G., Nazer, M. A., and Wiltshire, D. L. (2013). Timescape cosmology with radiation fluid. *Class. Quantum Grav.*, 30:175006. arXiv:1306.3208.

Eddington, A. S. (1933). *The Expanding Universe: Astronomy's 'Great Debate', 1900-1931*. Cambridge Univ. Press. Digital Ed. 2002.

Einstein, A. (1917). Kosmologische Betrachtungen zur allgemeinen Relativitätstheorie (Cosmological Considerations in the General Theory of Relativity). *Sitz. Preuss. Akad. d. Wiss. Phys.-Math.*, pages 142–152.

Einstein, A. and de Sitter, W. (1932). On the Relation between the Expansion and the Mean Density of the Universe . *Proc. Nat. Acad. Sci. USA*, 18:213–214. ncbi:PMC1076193.

Eisenstein, D. J. et al. (2005). Detection of the Baryon Acoustic Peak in the Large-Scale Correlation Function of SDSS Luminous Red Galaxies. *Astrophys. J.*, 633:560–574. arXiv:0501171.

Eisenstein, D. J. and Hu, W. (1998). Baryonic Features in the Matter Transfer Function. *Astrophys. J.*, 469:605. arXiv:9709112.

Ellis, G. F. R. (1984). Relativistic cosmology: Its Nature, Aims and Problems. *Gen. Rel. Grav.*, 9:215–288. adabs:1984grg..conf..215E.

Ellis, G. F. R. and Stoeger, W. (1987). The 'fitting problem' in cosmology. *Class. Quant. Grav.*, 4(6):1697.

Enqvist, K. and Mattsson, T. (2007). The effect of inhomogeneous expansion on the supernova observations. *J. Cosmol. Astropart. Phys.*, 02:019. arXiv:0609120.

Estathiou, G., Sutherland, W. J., and Maddox, S. J. (1990). The cosmological constant and cold dark matter. *Nature.*, 348:705–707. nature:348705a0.

Fiorentini, G., Lisi, E., Sarkar, S., and Villante, F. L. (1998). Quantifying uncertainties in primordial nucleosynthesis without monte carlo simulations. *Phys. Rev. D.*, 58:063506. arXiv:9803177.

Fixsen, D. J. (2009). The temperature of the Cosmic Microwave Background. *Astrophys. J.*, 709:916–920. arXiv:0911.1955.

Foreman-Mackey, D. et al. (2013). emcee: The MCMC Hammer. *Publ. Astron. Soc. Pac.*, 125(306):arXiv:1202.3665.

Friedmann, A. (1922). Über die Krümmung des Raumes. *Zeitschrift für Physik.*, 10:377–386. English translation: On the curvature of space. *Gen. Rel. Grav.*, 31:1991–2000, 1999.

Friedmann, A. (1924). Über die Möglichkeit einer Welt mit konstanter negativer Krümmung des Raumes. *Zeitschrift für Physik.*, 21:326–332. English translation: On the Possibility of a World with Constant Negative Curvature of Space. *Gen. Rel. Grav.*, 31:2001–2008, 1999.

Fukugita, M. et al. (1990). Test for the cosmological constant with the number count of faint galaxies. *Astrophys. J.*, 361:L1–L4. adsabs:185813.

Gabrielli, A., Labini, F. S., Joyce, M., and Pietronero, L. (2005). *Statistical Physics for Cosmic Structures*. Springer.

Gasperini, M., Marozzi, G., and Veneziano, G. (2010). A covariant and gauge invariance formulation of the cosmological "backreaction". *J. Cosmol. Astropart. Phys.*, 2010:1475–7516. arXiv:0912.3244.

Gehrels, N. et al. (2004). The Swift Gamma-Ray Burst Mission. *Astrophys. J.*, 611:1005–1020. arXiv:0405233.

Gelman, A. and Rubin, D. (1992). Inference from Iterative Simulation Using Multiple Sequences. *Statist. Sci.*, 7(4):457–472. projEuclid:1177011136.

Goodman, J. and Weare, J. (2010). Ensemble samplers with affine invariance. *Comm. Acta Phys.Polon. Math.Comput. Science.*, 5(65). http://msp.org:EnsembleSampler.

Green, R. S. and Wald, M. R. (2011). A new framework for analyzing the effects of small scale inhomogeneities in cosmology. *Phys. Rev. D.*, 83:084020. arXiv:1011.4920.

Green, R. S. and Wald, M. R. (2014). How well is our universe described by an FLRW model? *Class. Quant. Grav.*, 31:234003. arXiv:1407.8084.

Hinshaw, G. et al. (2003). First-Year Wilkinson Microwave Anisotropy Probe (WMAP) Observations: Angular Power Spectrum. *Astrophys. J. Suppl.*, 148:135. arXiv:0302217.

Hinshaw, G. et al. (2013). Nine-Year Wilkinson Microwave Anisotropy Probe (WMAP) Observations: Cosmological Parameter Results. *Astrophys. J. Suppl.*, 208:2. arXiv:1212.5226.

Hoell, J. and Priester, W. (1991). Void structure in the early universe - Implications for a Lambda greater than 0 cosmology. *Astron. Astrophys.*, 251:L23–L26. adsabs:1991A&A...251L..23H.

Hoyle, F. (1948). A New Model for the Expanding Universe. *Mon. Not. R. Astr. Soc.*, 108:372. adsabs:108..372H.

Hoyle, F. and Vogeley, M. S. (2002). Voids in the Point Source Catalogue Survey and the Updated Zwicky Catalog. *Astrophys. J.*, 566:641. arXiv:0109357.

Hoyle, F. and Vogeley, M. S. (2004). Voids in the 2dF Galaxy Redshift Survey. *Astrophys. J.*, 607:751. arXiv:0312533.

Hu, W. and Sugiyama, N. (1994). Anisotropies in the cosmic microwave background: An analytic approach. *Astrophys. J.*, 444:489–506. arXiv:9407093.

Hu, W. and Sugiyama, N. (1996). Small scale cosmological perturbations: An analytic approach. *Astrophys. J.*, 471:542–570. arXiv:9510117.

Hubble, E. (1929). A relation between distance and radial velocity among extragalactic nebulae. *Proc Natl Acad Sci U S A*, 15(3):168–173. pnas:1070.

Ichikawa, K., Sekiguchi, T., and Takahashi, T. (2008). Probing the Effective Number of Neutrino Species with Cosmic Microwave Background. *Phys. Rev. D.*, 78:083526. arXiv:0803.0889.

Ishibashi, A. and Wald, R. M. (2005). Can the acceleration of our universe be explained by the effects of inhomogeneities? *Class. Quantum Grav.*, 23:235–250. arXiv:0509108.

Kardashev, N. (1967). Lemaître's Universe and Observations. *Astrophys. J.*, 150:L135. adsabs:180110.

Katz, J., Lynden-Bell, D., and Bicak, J. (2006). Gravitational energy in stationary spacetimes. *Class. Quant. Grav.*, 23:7111–7128. arXiv:0610052.

Kochanek, C. S. (1995). Gravitational Lensing Limits on Cold Dark Matter and Its Variants. *Astrophys. J.*, 453:545. arXiv:9411082.

Lampeitl, H. et al. (2010). The Effect of Host Galaxies on Type Ia Supernovae in the SDSS-II Supernova Survey. *Astrophys. J.*, 722:566–576. arXiv:1005.4687.

Larena, J. (2009). Spatially averaged cosmology in an arbitrary coordinate system. *Phys. Rev. D.*, 79:084006. arxiv:0902.3159.

Larena, J., Alimi, J.-M., and Kunz, M., C. P.-S. (2009). Testing backreaction effects with observations. *Phys. Rev. D.*, 79:083011. arXiv:0808.1161.

Leith, B. M., Ng, S. C. C., and Wiltshire, D. L. (2008). Gravitational energy as dark energy: Concordance of cosmological tests. *Astrophys. J.*, 672:L91. arXiv:0709.2535.

Lemaître, G. (1927). Un Univers homogène de masse constante et de rayon croissant rendant compte de la vitesse radiale des nébuleuses extra-galactiques. *Ann. Soc. Sci. Bruxelles*, 47:39–59. English translation: Expansion of the universe, A homogeneous universe of constant mass and increasing radius accounting for the radial velocity of extra-galactic nebulae. *Mon. Not. R. Astr. Soc.*, 91:483–490, 1931.

Lemaître, G. (1933). l'univers en expansion. *Ann. Soc. Sci. Bruxelles*, 51(53). English translation: The expanding universe. *Gen. Rel. Grav.*, 29:641–680, 1997.

Lesgourgues, J. (2011). The Cosmic Linear Anisotropy Solving System (CLASS) I:Overview. arXiv:1104.2932.

Lesgourgues, J. et al. (2013). *Neutrino Cosmology*. Cambridge University Press.

Lesgourgues, J. and Pastor, S. (2014). Neutrino cosmology and planck. *New J. Phys.*, 16:065002. arXiv:1404.1740.

Lewis, A. and Bridle, S. (2002). Cosmological parameters from CMB and other data: a Monte-Carlo approach. *Phys. Rev. D.*, 66:103511. arXiv:0205436.

Lewis, A., Challinor, A., and Lasenby, A. (2000). Efficient Computation of CMB anisotropies in closed FRW models. *Astrophys. J.*, 538:473–476. arXiv:9911177.

Lisi, E., Sarkar, S., and Villante, F. L. (1999). Big bang nucleosynthesis limit on N_ν. *Phys. Rev. D.*, 59:123520. arXiv:9901404.

Luminet, J.-P. (2013). Editorial note to: Georges Lemaître, A homogeneous universe of constant mass and increasing radius accounting for the radial velocity of extra-galactic nebulae. *Gen. Rel. Grav.*, 45:1635–1646. arXiv:1305.6470.

Ma, C. P. and Bertschinger, E. (1995). Cosmological Perturbation Theory in the Synchronous and Conformal Newtonian Gauges. *Astrophys. J.*, 455:7–25. arXiv:9506072.

Mangano, G. et al. (2005). Relic neutrino decoupling including flavour oscillations. *Nucl. Phys. B.*, 729:221–234. arXiv:0506164.

Mangano, G., Miele, G., Pastor, S., and Peloso, M. (2002). A precision calculation of the effective number of cosmological neutrinos. *Phys. Lett. B.*, 534:8–16. arXiv:0111408.

Mather, J. C. et al. (1994). Measurement of the Cosmic Microwave Background spectrum by the COBE FIRAS instrument. *Astrophys. J.*, 420:439–444. adsabs:173574.

Metropolis, N., Rosenbluth, A. W., Rosenbluth, M. N., Teller, A. H., and Teller, E. (1953). *The Journal of Chemical Physics*, 21:1087.

Moss, A., Zibin, J. P., and Scott, D. (2011). Precison cosmology defeats void models for acceleration. *Phys. Rev. D.*, 83:103515. arXiv:1007.3725.

Mukhanov, V. (2005). *Physical Foundations Of Cosmology*. Cambridge University Press.

Nadathur, S., Hotchkiss, S., and Sarkar, S. (2012). The integrated Sachs-Wolfe imprint of cosmic superstructures: a problem for ΛCDM. *J. Cosmol. Astropart. Phys.*, 06:042. arXiv:1109.4126.

Nadathur, S. and Sarkar, S. (2011). Reconciling the local void with the CMB. *Phys. Rev. D.*, 83:063506. arXiv:1012.3460.

Nazer, M. A. and Wiltshire, D. L. (2015). Cosmic microwave background anisotropies in the timescape cosmology. *Phys. Rev. D.*, 91. in press. arXiv:1410.3470.

Pan, D. C., Vogeley, M. S., Hoyle, F., Choi, Y. Y., and Park, C. (2012). Cosmic voids in sloan digital sky survey data release 7. *Mon. Not. R. Astr. Soc.*, 421:926.

Paranjape, A. and Singh, T. P. (2007). Spatial averaging limit of covariant macroscopic gravity: Scalar corrections to the cosmological equations. *Phys. Rev. D.*, 76:044006. arXiv:0703106.

Peebles, P. J. E. (1968). Recombination of primeval plasma. *Astrophys. J.*, 153:1.

Peebles, P. J. E. (2012). Seeing Cosmology Grow. *Annu. Rev. Astron. Astrophys.*, 50:1–28.

Perlmutter, S. et al. (1997). Measurements of the Cosmological Parameters Ω and Λ from the First Seven Supernovae at $z \geq 0.35$. *Astrophys. J.*, 483:565–581. arXiv:9608192.

Perlmutter, S. et al. (1999). Measurements of Ω and Λ from 42 High-Redshift Supernovae. *Astrophys. J.*, 517:565–586. arXiv:9812133.

Petrosian, V., Salpeter, E., and Szekeres, P. (1967). Quasi-Stellar Objects in Universes with Non-Zero Cosmological Constant. *Astrophys. J.*, 147:1222–1226. adabs:149122.

Räsänen, S. (2006). Accelerated expansion from structure formation. *J. Cosmol. Astropart. Phys.*, page 1475. arXiv:0607626.

Räsänen, S. (2010). Applicability of the linearly perturbed FRW metric and Newtonian cosmology. *Phys. Rev. D.*, 81:103512. arXiv:1002.4779.

Rassat, A., Starck, J.-L., Paykari, P., Sureau, F., and Bobin, J. (2014). Planck CMB Anomalies: Astrophysical and Cosmological Secondary Effects and the Curse of Masking. *J. Cosmol. Astropart. Phys.*, 2014:006. arXiv:1405.1844.

Rata, B. and Peebles, P. J. E. (1988). Cosmological consequences of a rolling homogeneous scalar field. *Phys. Rev. D.*, 37:3406.

Riess, A. G. et al. (1998). Observational Evidence from Supernovae for an Accelerating Universe and a Cosmological Constant. *Astrophys. J.*, 116:1009–1038. arXiv:9805201.

Riess, A. G. et al. (2007). New Hubble Space Telescope Discoveries of Type Ia Supernovae at $z \geq 1$: Narrowing Constraints on the Early Behavior of Dark Energy. *Astrophys. J.*, 659:98–121. arXiv:0611572.

Robertson, H. P. (1935). Kinematics and World-Structure II. *Astrophys. J.*, 83:187. adabs:10.1086/143716.

Robertson, H. P. (1936). Kinematics and World-Strucrue III. . *Astrophys. J.*, 83:257. adabs:10.1086/143726.

Roukema, B. F., Buchert, T., Ostrowski, J. J., and France, M. J. (2014). Can an inhomogeneous metric be detected with the baryonic acoustic oscillation peak? arXiv:1410.1687.

Roukema, B. F., Ostrowski, J. J., and Buchert, T. (2013). Virialisation-induced curvature as a physical explanation for dark energy. *J. Cosmol. Astropart. Phys.*, 10:043. arXiv:1303.4444.

Rubino-Martin, J. A., Chluba, J., Fendt, W. A., and Wandelt, B. D. (2010). Estimating the impact of recombination uncertainties on the cosmological parameter constraints from cosmic microwave background experiments. *Mon. Not. R. Astr. Soc.*, 403:439–452. arXiv:0910.4383.

Sapone, D., Majerotto, E., and Nesseris, S. (2014). Curvature vs Distances: testing the FLRW cosmology. *Phys. Rev. D.*, 90:023012. arXiv:1402.2236.

Scott, D. and Moss, A. (2009). Matter temperature after cosmological recombination. *Mon. Not. R. Astr. Soc.* arXiv:0902.3438.

Scrimgeour, M. et al. (2012). The WiggleZ Dark Energy Survey: the transition to large-scale cosmic homogeneity. *Mon. Not. R. Astr. Soc.*, 116:425. arXiv:1205.6812.

Seager, S., Sasselov, D. D., and Scott, D. (1999). A new calculation of the recombination epoch. *Astrophys. J.*, 523:L1–L5. arXiv:9909275.

Shklovskii, I. S. (1967). On the Nature of "standard" Absorption Spectrum of the Quasi-Stellar Objects. *Astrophys. J.*, 150:L1. adsabs:180079.

Skrutskie, F. M. et al. (2006). The Two Micron All Sky Survey (2MASS). *Astronomical J.*, 131:1163–1183. adsabs:1163S.

Smale, P. R. (2011). Gamma-ray burst distances and the timescape cosmology. *Mon. Not. R. Astr. Soc.*, 418:2779–2784. arXiv:1107.5596.

Smale, P. R. and Wiltshire, D. L. (2011). Supernova tests of the timescape cosmology. *Mon. Not. R. Astr. Soc.*, 413:367–385. arXiv:1009.5855.

Smoot, G. F. et al. (1992). Structure in the COBE differential microwave radiometer first-year maps. *Astrophys. J. Lett.*, 396:L1–L5. adsabs:186504.

Sotiriou, T. P. and Faraoni, V. (2010). f(R) theories of gravity. *Rev. Mod. Phys.*, 82:451–497. arXiv:0805.1726.

Steigman, G. (2006). Primordial nucleosynthesis: successes and challenges. *Int. J. Mod. Phys. E.*, 15:1–36. arXiv:astro-ph/0511534.

Szabados, L. B. (2004). Quasi-Local Energy-Momentum and Angular Momentum in GR: A Review Article. *Living Rev. Rel.*, 7(4).

Szekeres, P. (1975a). A class of inhomogeneous cosmological models. *Commun. Math. Phys.*, 41:55–64. projEuclid:1103860587.

Szekeres, P. (1975b). Quasispherical gravitational collapse. *Phys. Rev. D.*, 12:2941.

Tikhonov, A. V. and Karachentsev, I. D. (2006). Minivoids in the local volume. *Astrophys. J.*, 653:969–976. arXiv:astro-ph/0609109.

Tolman, R. C. (1929). On the possible line elements for the universe. *Proc. Nat. Acad. Sci.*, 15(4):297–304. ncbi:PMC522452.

Tolman, R. C. (1934a). Effect of inhomogeneity on cosmological models. *Proc. Nat. Acad. Sci.*, 20:169–176. adsabs:1934PNAS...20..169T.

Tolman, R. C. (1934b). Relativity, Thermodynamics and Cosmology. *J. Roy. Astron. Soc. Can.*, 28:324. Review of Publications.

Tomita, K. (2000). Distances and lensing in cosmological void models. *Astrophys. J.*, 529:38. arXiv:9906027.

Umeh, O., Larena, J., and Clarkson, C. (2011). The Hubble rate in averaged cosmology. *J. Cosmol. Astropart. Phys.*, 1103:029. arXiv:1011.3959.

van den Hoogen, R. J. (2009). A Complete Cosmological Solution to the Averaged Einstein Field Equations as found in Macroscopic Gravity. *J. Math. Phys.*, 50(082503). arXiv:0909.0070.

Vonlanthen, M., Räsänen, S., and Durrer, R. (2010). Model-independent cosmological constraints from the CMB. *J. Cosmol. Astropart. Phys.*, 08:023. arXiv:1003.0810.

Walker, A. G. (1936). On Milne's theory of world structure. *Proc. Lond. Math. Soc.*, 42:90.

Weinberg, S. (2008). *Cosmology*. New York: Oxford University Press.

Wiltshire, D. L. (1987). Global properties of Kaluza-Klein cosmologies. *Phys. Rev. D.*, 36:1634–1648.

Wiltshire, D. L. (2007a). Cosmic clocks, cosmic variance and cosmic averages. *New J. Phys.*, 9(377). arXiv:0702082.

Wiltshire, D. L. (2007b). Exact solution to the averaging problem in cosmology. *Phys. Rev. Lett.*, 99:251101. arXiv:0709.0732.

Wiltshire, D. L. (2008). Cosmological equivalence principle and the weak-field limit. *Phys. Rev. D.*, 78:084032. arXiv:0809.1183.

Wiltshire, D. L. (2009). Average observational quantities in the timescape cosmology. *Phys. Rev. D.*, 80:123512. arXiv:0909.0749.

Wiltshire, D. L. (2011). What is dust? – physical foundations of the averaging problem in cosmology. *Class. Quantum Grav.*, 28:164006. arXiv:1106.1693.

Wiltshire, D. L. (2015). Cosmic structure, averaging and dark energy. In Perez Bergliaffa, S. E. and Novello, M., editors, *Proceedings of the XVth Brazilian School of Cosmology and Gravitation*. Cambridge Scientific Publishers. arXiv:1311.3787.

Wiltshire, D. L., Smale, P. R., Mattsson, T., and Watkins, R. (2013). Hubble flow variance and the cosmic rest frame. *Phys. Rev. D.*, 88:083529. arXiv:1201.5371.

Wong, W. Y., Moss, A., and Scott, D. (2008). How well do we understand cosmological recombination? *Mon. Not. R. Astr. Soc.*, 386:1023–1028. arXiv:0711.1357.

Wood-Vasey, W. M. et al. (2007). Observational Constraints on the Nature of Dark Energy: First Cosmological Results from the ESSENCE Supernova Survey. *Astrophys. J.*, 666:694–715. arXiv:0701041.

Zalaletdinov, R. M. (1992a). Averaging out the Einstein equations and macroscopic space-time geometry . *Gen. Rel. Grav.*, 24:1015–1031.

Zalaletdinov, R. M. (1992b). Towards a theory of macroscopic gravity. *Gen. Rel. Grav.*, 32:673–695.

Zalaletdinov, R. M. (1997). Averaging Problem in General Relativity, Macroscopic Gravity and Using Einstein's Equations in Cosmology. *Bull. Astron. Soc. India.*, 25:401–416. arXiv:9703016.

Zel'dovich, Y. B. (1968). The cosmological constant and the theory of elementary particles. *Sov. Phys. Usp*, 11(3):381–393.

Zibin, J. P., Moss, A., and Scott, D. (2007). The evolution of the Cosmic Microwave Background. *Phys. Rev. D.*, 76:12010. arXiv:0706.4482.

Zlatev, I., Wang, L., and Steinhardt, P. J. (1999). Quintessence, Cosmic Coincidence, and the Cosmological Constant. *Phys. Rev. Lett.*, 82:896–899. arXiv:9807002.